Masters Theses   Graduate School

8-2000

A study of the Earth return aerocapture for a manned Mars mission

William Donald Muth

Recommended Citation

To the Graduate Council:

I am submitting herewith a thesis written by William Donald Muth entitled "A study of the Earth return aerocapture for a manned Mars mission." I have examined the final electronic copy of this thesis for form and content and recommend that it be accepted in partial fulfillment of the requirements for the degree of Master of Science, with a major in Aerospace Engineering.

James Evans Lyne, Major Professor

We have read this thesis and recommend its acceptance:

Mancil W. Milligan, Rao V. Arimilli
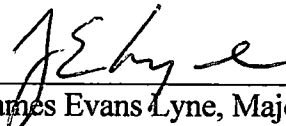
Accepted for the Council:

Carolyn R. Hodges

Vice Provost and Dean of the Graduate School

(Original signatures are on file with official student records.)

To the Graduate Council:

I am submitting herewith a thesis written by William Donald Muth entitled "A Study of the Earth Return Aerocapture for a Manned Mars Mission." I have examined the final copy of this thesis for form and content and recommend that it be accepted in partial fulfillment of the requirements for the degree of Master of Science, with a major in Aerospace Engineering.

Dr. James Evans Lyne, Major Professor

We have read this thesis and
recommend its acceptance:

Dr. Mancil W. Milligan

Dr. Rao V. Arimilli

Accepted for the Council:

Associate Vice Chancellor and
Dean of the Graduate School

A Study of the
Earth Return Aerocapture
for a Manned Mars Mission

A Thesis
Presented for the
Master of Science Degree

The University of Tennessee, Knoxville

William Donald Muth
August 2000

Dedication

This thesis is dedicated to my parents

Mr. William F. Muth

and

Mrs. Jeanette H. Muth

who have provided the support and encouragement that

made my education possible.

Acknowledgements

First, I would like to thank my major professor, Dr. Evans Lyne, for his support and advice throughout my career at the University of Tennessee. I would also like to thank the other committee members, Dr. Mancil Milligan and Dr. Rao Arimilli for their assistance in reviewing this thesis and for the knowledge that they passed on to me during my time at the University of Tennessee.

I am very grateful to Michelle Munk and NASA Langley Research Center for providing the financial support and technical guidance necessary to complete this research. I also would like to thank Larry Kos of NASA Marshall Space Flight Center and Gerald Lebeau of NASA Johnson Space Flight Center for providing information on various aspects of this research. I would like to give special thanks to Roman Jitts of North Carolina State University who was always willing to assist me on the usage of POST. I also wish to thank Christoph Hoffmann for his help in the final phases of the research.

Finally, I am very grateful to the Mechanical and Aerospace Engineering and Engineering Science department for supporting me financially and providing a wonderful staff and an extremely knowledgeable faculty during my stay in Knoxville.

Abstract

The current architecture being considered by NASA for a future manned Mars mission involves the use of an aerocapture procedure at both Mars and Earth arrival. The aerocapture will be used to decelerate and insert the vehicles into the desired orbits at the respective planets. The crew may return to Earth in a large, inflatable habitat known as the Transhab This Transhab would be complimented with an aeroshell, which will serve the dual purposes of providing protection from the intense heat of high-speed atmospheric flight and offer some lifting ability to the vehicle as well. The aeroshell has been dubbed the "Ellipsled" because of the characteristic shape. This thesis represents a preliminary study of the aerocapture of the Transhab/Ellipsled vehicle upon Earth return. Undershoot and overshoot boundaries have been examined as a function of entry velocity for a variety of constraining factors such as deceleration limits and vehicle ballistic coefficient. The effects of atmospheric dispersions have also been explored. In addition, a simple 180 degree roll maneuver has been implemented in the undershoot trajectories to help target the desired 407 km circular Earth orbit. Results show that the Transhab/Ellipsled vehicle has a nominal entry corridor width of 0.5 - 0.7 degrees for entry speeds ranging from 12.5 km/s to 14.5 km/s. In addition, entry corridor comparisons have been made between the Transhab/Ellipsled and a modified Apollo capsule which is also being considered for the Earth return vehicle. Future studies should focus on refining the heating rate analyses, off-nominal vehicle aerodynamics, winds, horizontal density waves, and changes in the vehicle trim angle of attack. Furthermore, a guidance algorithm should be implemented to optimize the overall trajectory and minimize inclination changes and post-aerocapture delta V needed to circularize the orbit.

Table of Contents

List of Tables

List of Figures

List of Symbols and Abbreviations

AOA   angle-of-attack

DRM   Design Reference Mission

ERV   Earth return vehicle

GAMMAI   initial entry angle

GEO   geosynchronous Earth orbit

IMLEO   initial mass in low Earth orbit

L/D   lift-to-drag ratio

LEO   low Earth orbit

MAV   Mars ascent vehicle

NASA   National Aeronautics and Space Administration

NTP   nuclear thermal propulsion

P2   POST weighted targeting function

POST   Program to Optimize Simulated Trajectories

3-DOF   three degrees-of-freedom

$T_{max\ g's}$ time of maximum deceleration

TMI   trans-Mars injection

TPS   thermal protection system

$T_{roll\ start}$ time to start roll maneuver

Greek Symbols

ΔV velocity increment

Chapter 1

Introduction

Section 1-1.   Mission Background

The last several years have brought about a renewed interest in Mars. The discovery of meteorites which may be of Martian origin and the success of missions such as Mars Pathfinder have fueled new research into a possible manned Mars mission that would take place in the near future [1, 2]. NASA is currently working from a plan called the Design Reference Mission (DRM) which details why, when, and how we will send men to Mars [3]. The original version of the DRM spoke of the possibility of landing the first men on Mars on or around 2009. However, most current research indicates that the first human landing will take place in the year 2014. The crew landing would occur approximately two years after two cargo flights place surface equipment and the Earth return vehicle (ERV) in orbit at Mars. Subsequent cargo and crew flights would depart for Mars at each opportunity occurring every 26 months. The DRM calls for each crew to use the systems launched during the previous opportunity which adds some degree of safety and risk management into the mission design.

The DRM calls for short Earth-to-Mars transit times of 180 days or less to minimize the crew's exposure to cosmic radiation and microgravity environments. The

DRM calls for a variety of new technologies to be used, one of which is nuclear thermal propulsion (NTP). The NTP system has a high specific impulse (I_{sp}) of approximately 925 seconds which makes it ideal for use in the trans-Mars injection (TMI) burn [4, 5]. Once on the surface of Mars, the crew of six astronauts would perform scientific and exploration duties for approximately 500 days. Another innovative technology to be employed during the mission is that of in-situ propellant production for the Mars ascent stage [3]. The in-situ propellant plant would split the carbon dioxide of the Martian atmosphere and then use hydrogen "seeds" brought from Earth to produce methane. Together, the methane and oxygen would provide an effective propellant and provide considerable mass savings for the mission. After the propellant has been manufactured, the crew would ascend to orbit in the Mars ascent vehicle (MAV) and then rendezvous with the orbiting ERV. The ERV would then depart from Mars orbit on a trajectory that would arrive at Earth in approximately 180 days.

Section 1-2.   Aerocapture Procedure

One of the most interesting new technologies that is being considered for use during the mission is that of the aerocapture procedure The term "aerocapture" refers to the maneuver used to capture the vehicle into orbit from a hyperbolic trajectory. On occasion, the terms "aerobraking" and "aeropass" are also encountered when studying aerocapture maneuvers. These terms are more general in that they refer to the use of atmospheric drag to change from one orbit to another (i.e. GEO to LEO).

The aerocapture strategy is being considered for use at both Mars and Earth arrival of the crewed vehicles An aerocapture is simply a process that uses atmospheric drag to dissipate energy from the hyperbolic arrival condition thereby allowing the vehicle to exit the atmosphere in the desired closed orbit. The idea of implementing an aerocapture procedure is based on the possibility of reducing the mission mass and thus reducing mission cost. Standard mission designs require large amounts of propellant to decelerate a vehicle upon Earth arrival. The propellant must therefore be launched into low Earth orbit (LEO) and carried throughout the mission duration The use of the aerobraking strategy could reduce or even eliminate the propellant needed. However, an aerocapture has the drawback that it subjects the vehicle to high heating rates and thus requires a heat shield to offer adequate protection to the crew. Therefore, one must weigh the propellant savings realized against the added mass of the heat shield when analyzing an aerocapture procedure. If the aerocapture allows the overall mission mass to be reduced, then it would in turn reduce the overall mission cost.

Figure 1-1 shows a comparison between the aerocapture and the typical direct entry scenarios that have been used in the past [6]. Several studies have focused on the Mars aerocapture of a proposed tri-conic vehicle [3, 7]. Jitts & Walberg of North Carolina State University have nearly completed some remarkable work on developing a blended control guidance algorithm to be used during the Mars aerocapture [7].

To be successful, the aerocapture must dissipate enough energy during the first pass through the atmosphere to capture into orbit [8]. Figure 1-2 displays what are known as undershoot and overshoot boundaries for the aerocapture [9]. The undershoot boundary is defined as the steepest atmospheric entry angle, while lifting full up, that the

3

Aerocapture - Orbit insertion via passage through atmosphere from interplanetary trajectory

Direct Entry - Descent to surface from interplanetary trajectory or orbit
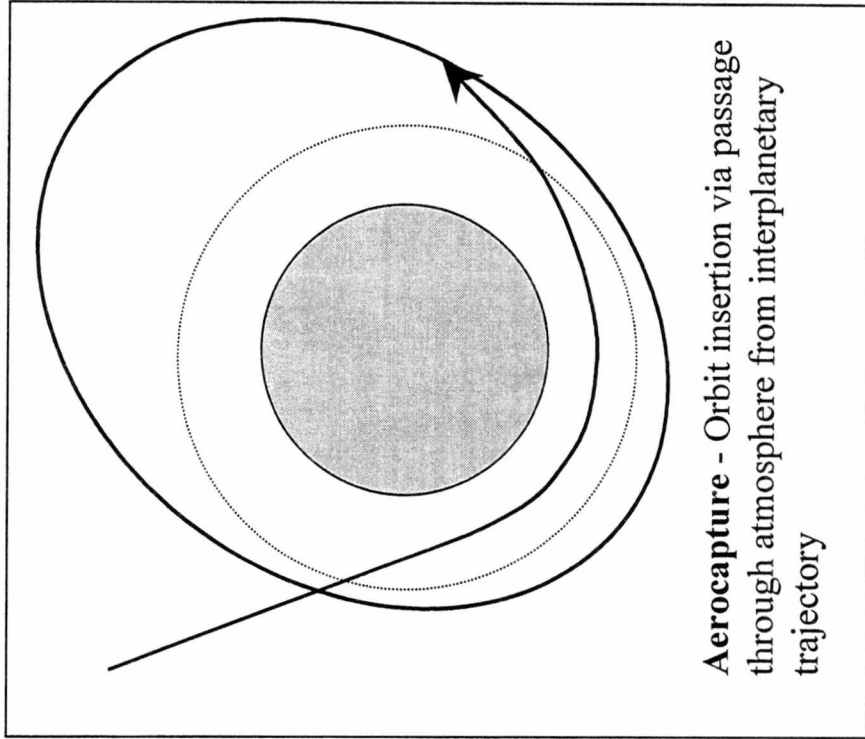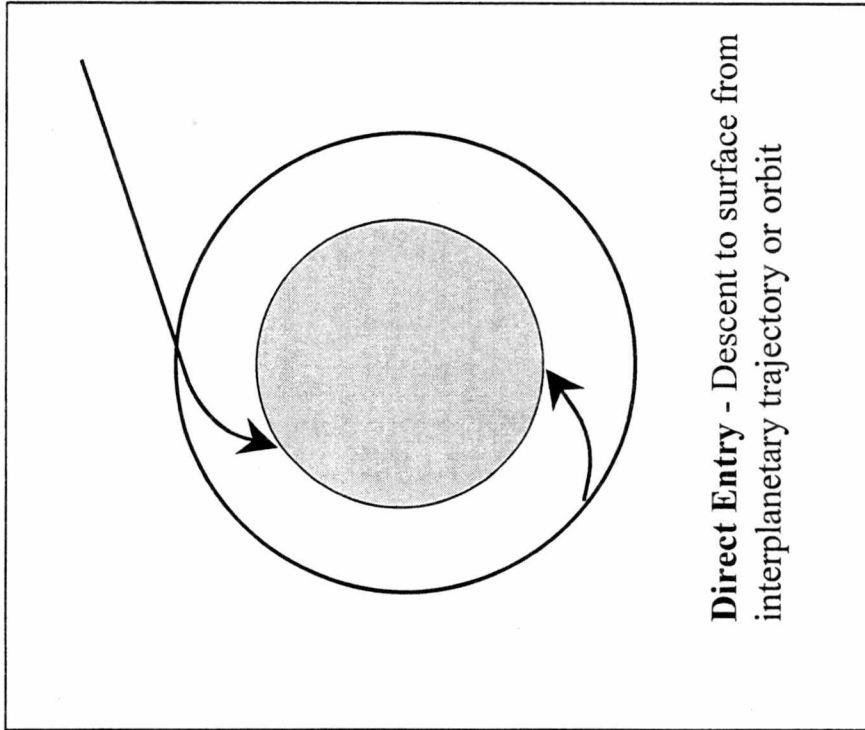
Figure 1-1. Diagram of Direct Entry and Aerocapture Scenarios
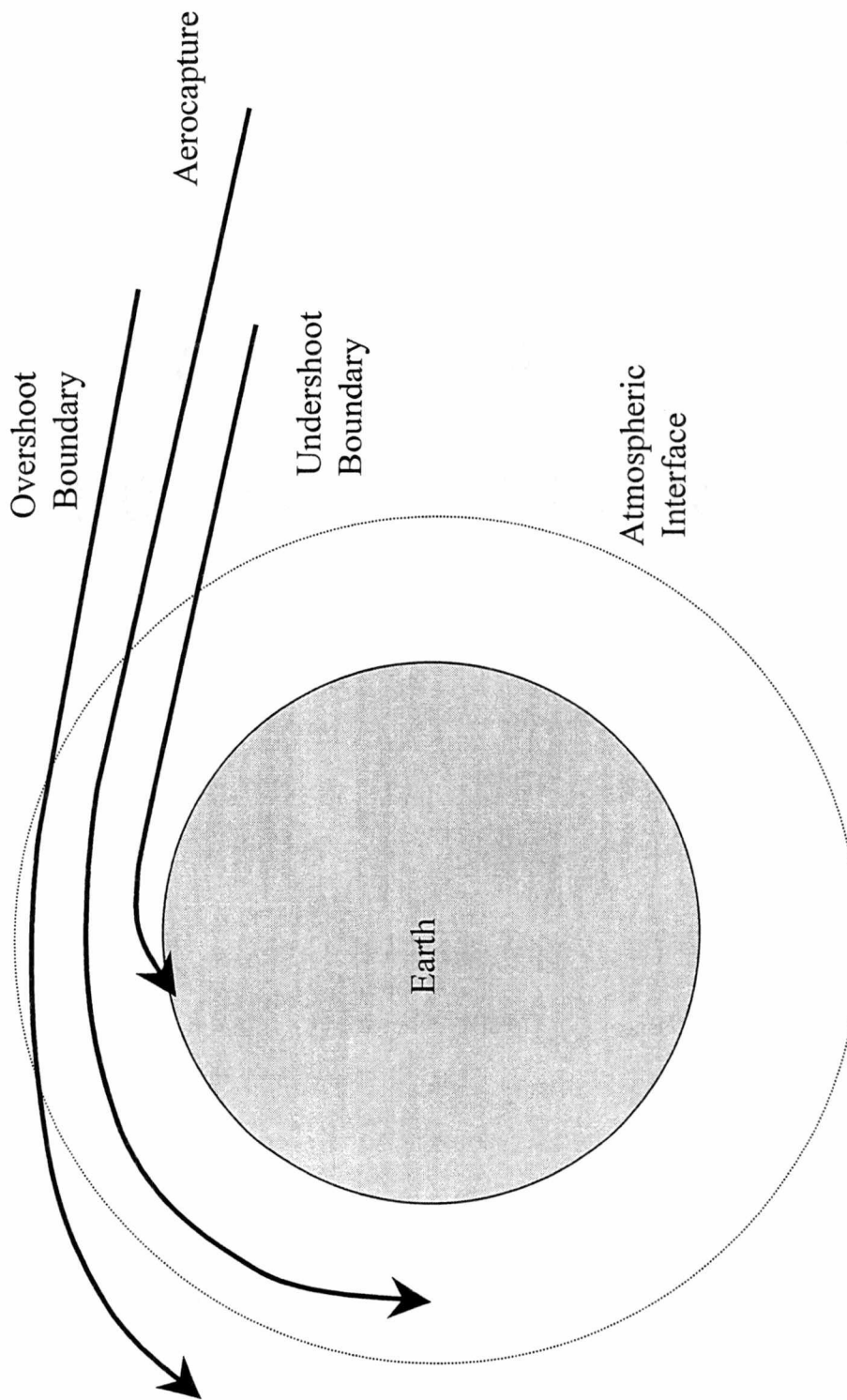
Figure 1-2. Diagram of Undershoot and Overshoot Boundaries

vehicle can remain under the imposed deceleration or heating limits and does not impact the surface. In the case of manned vehicles, such as the Transhab/Ellipsled, the undershoot boundary is often limited primarily by the maximum allowable deceleration. Entering the atmosphere at an angle steeper than the undershoot boundary will result in subjecting the vehicle to an excessive deceleration or heating load or cause the vehicle to hit the surface [10]. In contrast, the overshoot boundary is the shallowest entry angle, while lifting full down, that the vehicle can enter the atmosphere and still be able to capture into an acceptable orbit. If the vehicle enters at an angle shallower then the overshoot boundary, then it will continue in a hyperbolic trajectory away from the planet or capture into a longer period orbit than desired.

The area between the undershoot and overshoot boundaries is known as the entry corridor. The Transhab/Ellipsled, or any other vehicle attempting to perform an aerocapture, must enter the atmosphere at an entry angle contained within this corridor. Typically, there is a minimum allowable corridor width that will safely allow the vehicle guidance control system to target the desired orbit. There are a variety of other factors that may affect both the entry corridor width and the entry angles for the boundaries. The entry velocity and aerodynamic characteristics of the vehicle both play a significant role in determining the entry corridor. Imposed constraints such as the deceleration and heating limits can affect the corridor as well. In addition, natural phenomena such as winds and atmospheric uncertainties (dispersions) must be taken into account when determining the entry corridor. It should be noted that for certain vehicle configurations or entry conditions, an entry corridor might not exist. In other words, there may be no atmospheric trajectory that may be flown which will allow the vehicle to capture into the

desired orbit without exceeding the imposed limits on deceleration or other factors. It should also be noted that the idea of the entry corridor is not merely an artifact of aerocapture procedures. Rather, the entry corridor must be determined regardless of whether an aerocapture or direct entry is being performed. Entry corridors for a direct entry scenario are defined in basically the same manner as they would be for an aerocapture. However, because there is no desired orbit, entry corridors for a direct entry are usually limited by such factors as deceleration limits, heat loads, and the ability to target a desired point on the surface. Some previous studies have examined entry corridors and other aspects of both direct entry and aerocapture for various Earth return vehicles [11, 8]. However, no work has yet been carried out to analyze the entry corridor for the Transhab/Ellipsled vehicle

Section 1-3.   Objectives

The remainder of this document presents results of a preliminary study of the entry corridor for the Transhab/Ellipsled vehicle upon Earth return from a Mars mission. The primary objectives of this study are summarized as follows·

1   Determine the undershoot and overshoot boundaries and the corresponding entry corridor width for nominal entry conditions and vehicle aerodynamics for entry speeds ranging from 12.5 km/s to 14.5 km/s.

2. Determine the effects that off-nominal atmospheric conditions, deceleration limits, ballistic coefficients, and final target orbits have on the entry corridor.

3. Compare the nominal entry corridor of the Transhab/Ellipsled vehicle to that of the Apollo derived capsule which is also being considered for the crew return

4. Develop an optimized nominal trajectory that minimizes inclination change and ΔV needed to circularize the orbit to the desired 407 km orbit.

5. Perform initial studies on atmospheric heating rates and integrated heat loads experienced by the Transhab/Ellipsled vehicle.

Chapter 2

Vehicle Specifications

Section 2-1.   Transhab/Ellipsled Vehicle

The inflatable habitat which is being considered as a living and working environment for the Mars mission crew during the return trip to Earth is called the Transhab. The aerocapture procedure that the Transhab must perform will subject the vehicle to heating rates similar to those experienced by any other re-entry vehicle. Therefore, the Transhab will be protected from these high heating rates by a heat shield of some kind, probably of the ablator type [12]. The aerocapture also requires the vehicle to have some ability to be flown during the atmospheric trajectory portion of the aeropass procedure. The heat shield can be molded into almost any shape and form so it is possible to manufacture the heat shield in such a way as to provide some aerodynamic lifting ability for the vehicle The idea of combining the heat shield properties and aerodynamic characteristics yielded what is known as the aeroshell. From this point forward, the aeroshell will be referred to by the name NASA has given it - the "Ellipsled". Figure 2-1 shows a simple dimensioned diagram of the Transhab with Ellipsled aeroshell [13].

The Transhab/Ellipsled is a large vehicle with an expected mass of over 25,500 kg The reference area of the vehicle is 84.34 square meters, while the nose radius is 6.7

ELLIPSLED

TRANSHAB

9.7 m

9.45 m

16.8 m

5.2 m
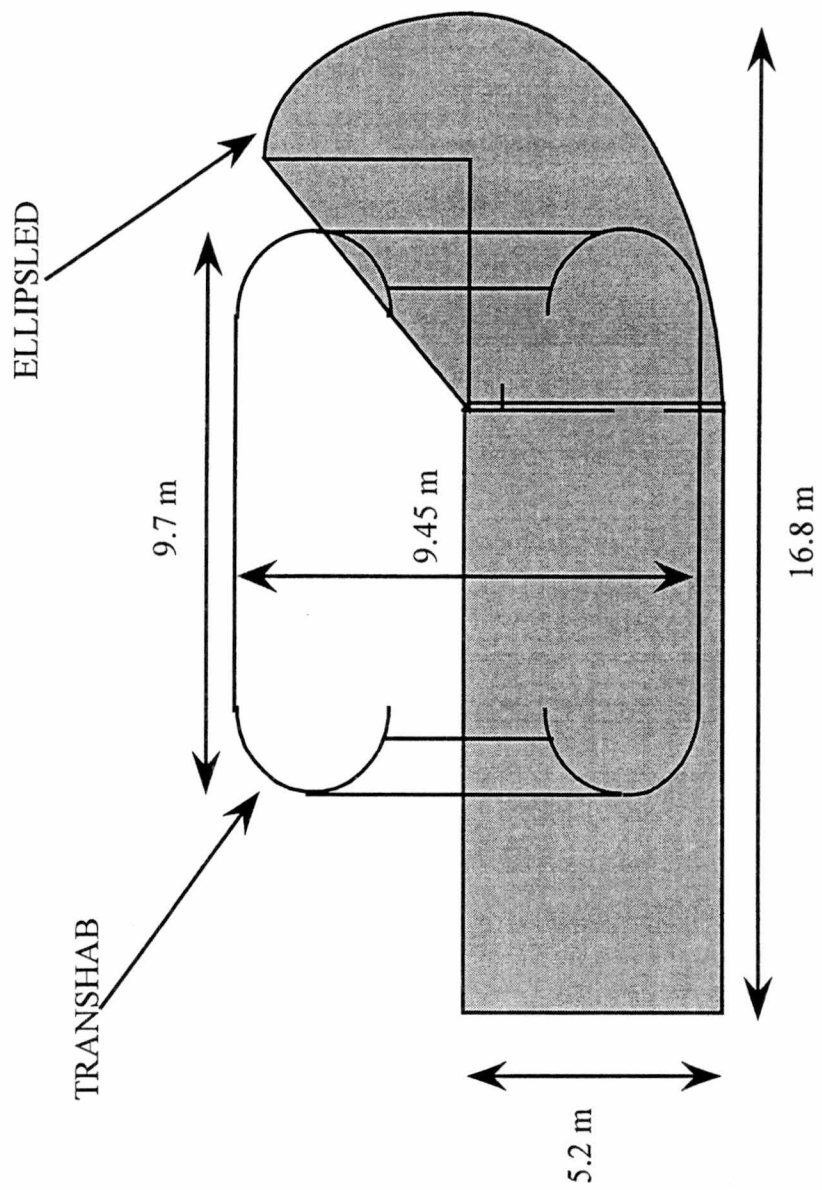
Figure 2-1. Diagram of the Transhab with Ellipsled Aeroshell

meters The Transhab portion of the vehicle has a mass of 14,522 kg The Ellipsled aeroshell has a mass of 3929 kg which translates into a mass fraction of 15.4%. The remaining 7053 kg is comprised of various data and communication equipment, batteries and solar arrays, radiator and thermal control system, and propulsion system components.

Table 2-1 below shows the aerodynamic characteristics of the Transhab/Ellipsled vehicle as determined by Gerald LeBeau of NASA Johnson Space Center. The aerodynamic characteristics were determined using Modified Newtonian theory in which all values are assumed constant at Mach numbers above 24. The table shows that the expected trim angle for the Transhab/Ellipsled is 45 degrees with a Lift-to-Drag ratio of 0.39. For comparison purposes, the Apollo style capsule, which has also been considered for the return vehicle, has a Lift-to-Drag ratio of approximately 0.3. Therefore, it appears that the Transhab/Ellipsled vehicle should have at least slightly better maneuverability than the Apollo style vehicle. The increased Lift-to-Drag ratio creates a wider entry corridor and gives the vehicle a greater ability to capture into the desired orbit

Section 2-2.   Apollo Derived Vehicle

In addition to the analysis for the Transhab/Ellipsled vehicle, a brief study on the Apollo derived capsule was also performed The Apollo derived Earth return vehicle is simply a scaled up version of the old Apollo capsules used during the lunar missions. The Apollo derived vehicle is being considered for use in direct entry scenarios, however this study analyzed the performance of the vehicle during aerocapture maneuvers. This

Table 2-1. Aerodynamic Characteristics of the Transhab/Ellipsled Vehicle

Mach Number	Trim Angle-of-Attack [deg]	Lift Coefficient	Drag Coefficient	L/D
2.0	37.12	0.6899	1.576	0.438
3.0	40.68	0.6317	1.5576	0.406
5.0	43.53	0.5658	1.5128	0.374
10.0	44.60	0.5476	1.4676	0.373
15.0	45.00	0.5493	1.4623	0.376
24 & higher	45.00	0.5636	1.4445	0.39

analysis was done primarily to allow easy comparison between the Apollo derived vehicle and the Transhab/Ellipsled vehicle.

The new Apollo derived vehicle was modified from the older version to accommodate six astronauts instead of the usual three. As a result, the vehicle has a mass of approximately 6500 kg, a reference length of 4.42 meters, and a surface area of 15.34 square meters. The coordinate system for the Apollo derived vehicle was altered from the original vehicle as well. As a result, the hypersonic trim angle of the Apollo derived vehicle is approximately 23 degrees as compared to the 157 degree hypersonic trim angle of the old Apollo capsules [14]. Figure 2-2 shows a sketch of the Apollo derived module and the new coordinate reference system. The aerodynamic coefficients for the Apollo derived vehicle are shown as a function of angle-of-attack in Table 2-2. Figure 2-3 is a plot of the data from Table 2-2. The points have been fitted using a polynomial regression line (trendline). The trendline equation is shown on the figure along with the R^2 value. The hypersonic values of the lift and drag coefficients were determined from the trendline equation by substituting the 23 degree angle-of-attack for the independent variable "x". The resulting lift coefficient was found to be 0.467 while the drag coefficient was 1.269. The C_L and C_D values were assumed to be constant because the vehicle never attained a Mach number less than Mach 24 during any portion of the trajectories analyzed in this research.
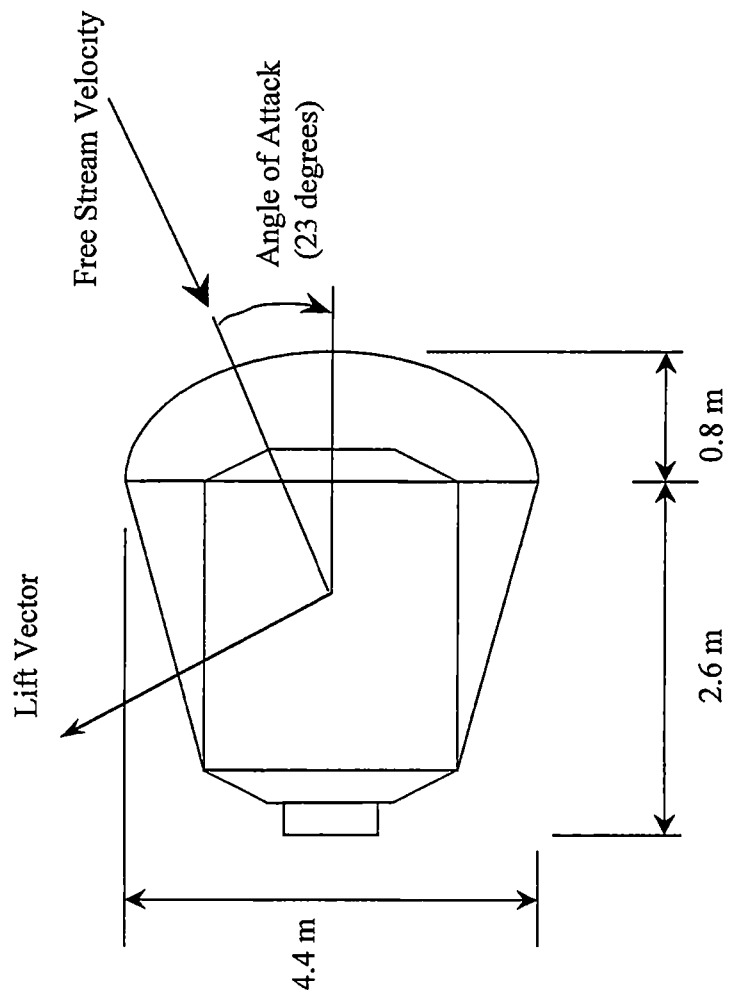
Figure 2-2. Diagram of the Apollo Derived Entry Vehicle
[Ref: Jim Masciarelli, Johnson Space Center]

Table 2-2. Aerodynamic Characteristics of the Apollo Derived Vehicle

Angle-of-Attack [deg]	Lift Coefficient	Drag Coefficient	L/D
0	0	1.60	0
5	0.12	1.59	0.075
10	0.23	1.54	0.149
15	0.33	1.46	0.226
20	0.41	1.36	0.301
25	0.49	1.25	0.392
30	0.53	1.10	0.482
35	0.55	0.96	0.572
40	0.54	0.83	0.651
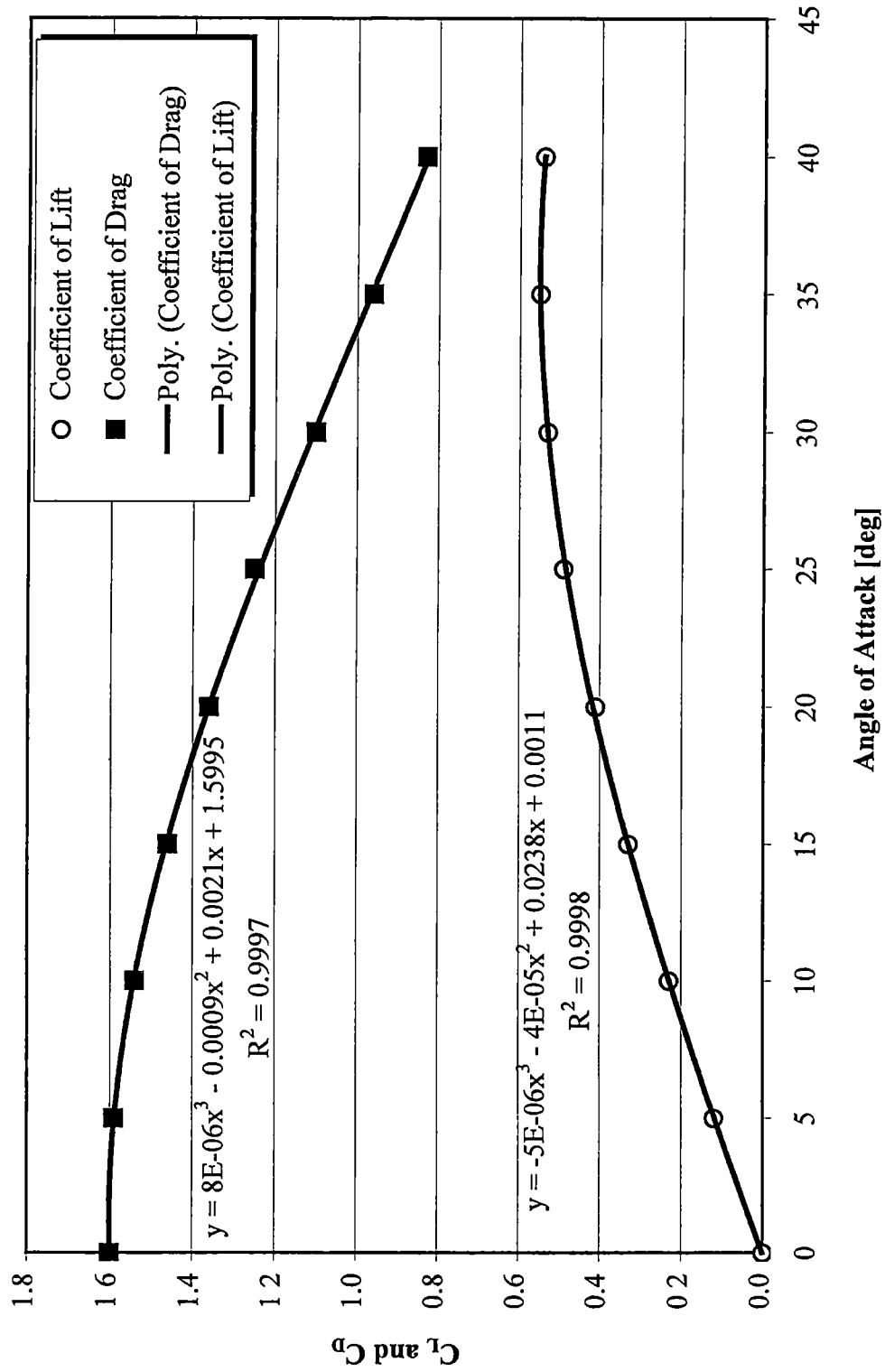
Figure 2-3. Curve Fits of Apollo Aerodynamic Characteristics

Chapter 3

Methodology

Section 3-1. Program to Optimize Simulated Trajectories

The results contained in this paper were obtained from running numerous computer simulations of the atmospheric trajectories. The simulations were performed using a computer code written by NASA in FORTRAN called the Program to Optimize Simulated Trajectories (POST) [15]. The program runs in a UNIX based environment and consists of an input deck, program files, and various output files. The input deck contains all of the user-defined variables for the trajectory simulations. The user may alter the vehicle configuration, entry condition, integration scheme, and various other simulation properties by making the appropriate changes to the POST input deck.

The POST version used for these studies was the three-degree of freedom (3-DOF) program. POST simulates the trajectories by representing the vehicle as a point mass and solving the appropriate equations of motion through numerical means. The program has a built in routine to achieve convergence in the solutions to meet the specified constraints. When POST is performing targeting or optimization routines, it uses default perturbation sizes. However, the user may adjust both the perturbation size and convergence criteria to meet any desired accuracy.

17

POST is a very robust simulation program and as such is extraordinarily complex. To achieve a complete proficiency with the program would require years of training and hands-on use of the program Table 3-1 lists some of the problems that POST may be used to solve [16] However, no matter how complex the problem may be, the user must follow the same basic steps to insure POST can perform an accurate simulation of the trajectory. The user first defines the vehicle characteristics and entry conditions in the input deck. This includes the vehicle aerodynamics, weight, reference area, entry speed, inclination, and other similar variables. (NOTE: POST does not have the ability to determine aerodynamic coefficients of a given vehicle, therefore the aerodynamic characteristics must be determined using another computer code or other means.) Secondly, the user defines the series of phases to take place in the trajectory. A phase may be any event that requires POST to perform a specific maneuver or do other calculations For instance, the time to begin a bank angle modulation or to perform a burn to circularize an orbit would be examples of phases (events). To completely define an event, the user must specify both the conditions that indicate when the event is to take place and any maneuvers to be performed during the event. The user can also use an event to change various program options such as integration scheme and time step The simulation can therefore be made as complex or as simple as the user desires through wise manipulation of the events POST requires a minimum of two events to run (an initial event and a termination event), but does not have a maximum limit on the number of events [15].

The next step is for the user to enter the appropriate guidance flags and program control array in the input deck POST is able to simulate a variety of atmospheric and

18

Table 3-1. Typical Applications of POST

(Ref Brauer *et al* , "POST Formulation Manual," Martin Marietta Corporation, Denver, CO, September 1990)

Type of Mission	Type of Vehicle	Optimization Variable	Typical Constraints	
			Equality	Inequality
Ascent to Near-Earth Orbit (2 - 20 mm cpu time)	Titan, Space Shuttle, Single Stage to Orbit (VTO and HTO)	Payload, Weight at Burnout, Propellant, Burntime, Ideal Velocity	Radius, Flight Path Angle, Velocity	Dynamic Pressure, Accelerations
Ascent to GeoSynch Orbit (3 - 50 mm cpu time	Titan, Space Shuttle/Upper Stage	Payload, Propellant	Apogee, Perigee, Inclination	Dynamic Pressure, Angle of Attack, Pitch Rates
Ascent Abort (2 - 5 mm cpu time)	Space Shuttle	Abort Interval	Landing Site Latitude and Longitude	Dynamic Pressure, Acceleration
ICBM Ballistic Trajectory (2 - 20 mm cpu time)	Titan, Minuteman, Peacekeeper	Payload, Miss Distance	Latitude, Longitude, Downrange, Crossrange	Reentry Flight Path Angle, Acceleration
Reentry (3 - 15 mm cpu time)	Space Shuttle, X-24C, Single Stage to Orbit	Heat Rate, Total Heat, Crossrange	Latitude, Longitude, Downrange, Crossrange	Heat Rate, Acceleration
ICBM Orbital Maneuvers (0 5 - 10 mm cpu time)	Titan, Transtage, Centaur,IUS, Solar-Electric Propulsion	Payload, Propellant, Ideal Velocity, Burntime	Latitude, Semimajor Axis, Eccentricity, Inclination, Argument of Perigee, Period	Reentry Attitude Angles, Perigee Altitude
Aircraft Performance (0 1 - 5 mm cpu time)	X-24B and C, Subsonic Jet Cruise, Hypersonic Aircraft	Mach, Cruise Time, Payload	Downrange, Crossrange, Dynamic Pressure, Mach, Altitude	Dynamic Pressure, Max Altitude Dynamic Pressure

orbital trajectories including launch and ascent trajectories, aerocapture maneuvers, orbital plane and altitude changes, planetary departures, etc. The ability of POST to simulate such a wide variety of trajectories comes from the proper usage of the guidance and program flags available to the user. The guidance flags, called IGUID(#) in POST, control such things as the type of coordinate system to be used and how the angles in that system will be defined. The program control array, named NPC(#) in POST, contains various flags which allow the user to specify such things as the integration scheme to be used, planetary characteristics such as oblateness and atmospheric models, and propulsion methods to be used.

Finally, if it is desired that POST simulate the trajectory and perform a targeting routine, then the user must define the trajectory constraints and vehicle controls in the input deck. Controls are such variables as entry angle, bank angle, angle-of-attack, time to begin an event, and ΔV magnitude to name a few. Constraints on the other hand may include deceleration limit, perigee and apogee altitude, inclination, energy, and orbital period. Once the user has completed the input of controls and constraints, POST may attempt to simulate the trajectory. When POST completes the calculations and projects the trajectory, the user may look at the output files to check that the constraints were met. The "P2" weighting function, which is shown in the output deck, allows the user to know how close the trajectory is to the specified constraints A P2 value of less than one indicates that all of the constraints have been satisfied within the user-defined tolerances. On the other hand, a P2 value of greater than one shows that at least one constraint was not met satisfactorily. In that case, the user must then go back and correct any errors and

examine the perturbation sizes and/or convergence criteria. Usually, the perturbation sizes need to be adjusted for a converged solution (P2 less than one) to be obtained.

In addition, if POST is to optimize the trajectory then the user must also define the optimization variable POST is capable of optimizing a trajectory with respect to one user-defined variable, but cannot optimize any trajectory until a targeted solution is found. POST performs the targeting/optimization process by perturbing the control variables to meet the imposed constraints and then either minimizes or maximizes (depending on the user's needs) the optimization variable. For optimization to be successful, usually one more control variable than constraint is required.

Section 3-2.   Aerocapture Simulations

After the basics of POST are understood, one can begin to attempt to model the desired trajectory The construction of the input deck requires the proper addition of the various program options to select the correct integration scheme, guidance controls, and the input method for the aerodynamic characteristics. For the simulations performed in this study, a fourth order Runga-Kutta integration technique was chosen for the atmospheric portion of the trajectories In addition, the integration time step was set at one second to achieve good accuracy during the atmospheric flight portion of the trajectory. In later simulations in which orbital maneuvers will be performed, the integration scheme should be changed to an Encke method once the vehicle exits the atmosphere. The angle-of-attack, bank angle, and angle of side slip were all defined as third order polynomial functions of time The constant term of the polynomials were

21

input at the beginning of each simulation. The higher order terms were left as the default values of zero The aerodynamic coefficients, provided by Gerald LeBeau, were entered as tables in which the independent variable was Mach number and the dependent variables were the coefficients of lift and drag.

Once the program options were set correctly, the trajectory constraints and entry conditions needed to be input. The entry velocities were input as inertial velocities at an initial altitude of 121,900 meters above the oblate planet. All entries were assumed to be due east and equatorial in nature as well. The Earth's atmosphere was modeled using the 1976 U.S. Standard Atmosphere. The effects of winds and horizontal density waves were not considered. The Earth was modeled as an oblate planet with the proper harmonic values in the gravity potential function.

The constraints imposed during these simulations were as follows. First, a 5-g deceleration limit for the aerocapture is generally accepted as appropriate for the Earth return procedure. Therefore, regardless of the method used to obtain the solutions, the maximum deceleration was not allowed to exceed 5-g during any trajectory. NASA has also prescribed the target orbit for the Earth aerocapture to be a 407 km circular orbit The first simulations that were performed only targeted this orbit in the overshoot trajectories. Later, a bank angle modulation scheme was implemented to help target the 407 km circular orbit in the undershoot trajectories as well. The bank angle modulation would be performed using thrusters on the Transhab/Ellipsled vehicle. The large mass of the vehicle greatly limits the ability of the thrusters to roll the craft over. Thus, studies were performed for two different roll rates. The first study was completed for a roll rate of 10 degrees per second while the second study was limited to 5 degrees per second. The

target orbit should also retain the same inclination as the initial trajectories because any unexpected inclination change would have to be corrected with propulsive methods that add to overall mission cost. Although the first simulations ignored inclination change, later simulations limited inclination change to try to reduce the post-aerocapture ΔV and the corresponding propellant mass. Heating rates and integrated heat loads are extremely important in the analysis of aerocapture procedures, however no constraint was placed on atmospheric heating rates or integrated heat loads in the simulations performed during this research Heating rates and integrated heat loads were calculated for selected entries and the results will be shown later in this document.

Chapter 4

Transhab/Ellipsled Analysis and Results

Section 4-1. Entry Corridor

The first problem to be addressed by this research was the determination of the entry corridor for the Transhab/Ellipsled vehicle under nominal atmospheric conditions as modeled by the 1976 U.S. Standard Atmosphere table. The simulation also used the nominal vehicle aerodynamic characteristics as shown in Table 2-1. The initial angle-of-attack was set at 45 degrees while the coefficients of lift and drag were input to POST as a function of Mach number. All of the simulations performed used inertial entry velocities ranging from 12.5 km/s to 14.5 km/s As mentioned earlier, all trajectories were assumed to be due east, equatorial entries. In addition, the nature of the aerocapture trajectory does not allow the Mach number of the vehicle to drop below 24 Therefore, the aerodynamic coefficients for the hypersonic trajectories analyzed in this paper are essentially constant.

4-1.1   Undershoot Boundary

To define the entry corridor, it was necessary to find the undershoot and overshoot boundaries for the range of entry speeds. The undershoot trajectories required that the vehicle hold a zero degree bank angle and thus maintain full lift up. The only constraint placed on the undershoot trajectories during this study was that of the maximum 5-g deceleration. Determining the undershoot boundaries with this one simple constraint was relatively easy and only required an accuracy to three decimal places in the entry angle. While the exit conditions for the two lower entry velocities were highly elliptical in nature, the remaining entry velocities resulted in hyperbolic trajectories. Although these hyperbolic trajectories are not useful they nevertheless indicate the undershoot bounds as defined by the 5-g constraint without the 407 km final orbit targeting requirement. Table 4-1 summarizes the exit conditions for the undershoot trajectories over the range of entry speeds studied.

4-1.2   Overshoot Boundary

On the other hand, the overshoot trajectories required the vehicle to hold a bank angle of 180 degrees, thus providing full lift down. The only constraint that applied to the overshoot trajectories was that of the target orbit. After completing the first few entry speeds, it became obvious that it would be extremely difficult to target a 407 km circular orbit using only the aeropass procedure. It was then decided to try to target an apoapse

Table 4-1. Exit Conditions for the Untargeted Undershoot Boundary

Entry Speed	Entry Angle	Apoapse Altitude	Periapse Altitude	Period	Exit Inclination	G-Max	Time to 407 km
[km/s]	[deg]	[km]	[km]	[min]	[deg]	[g's]	[s]
12 5	-6.363	65500.00	63.17	1284.73	6.03E-05	5.000	326.50
12 6	-6.375	90557.04	63.90	1948.58	5.87E-05	5.000	320.96
13.0	-6.418	hyperbolic	66.38	infinite	5.29E-05	4.997	301.04
13.5	-6.463	hyperbolic	68.80	infinite	4.71E-05	4.997	280.29
14.0	-6.500	hyperbolic	70.71	infinite	4.22E-05	4.998	262.90
14 5	-6.530	hyperbolic	72.30	infinite	3.82E-05	5.001	248.00

26

altitude since an elliptical orbit with an apoapse altitude of 407 km would be a good estimate of the target orbit and help minimize the ΔV needed to circularize the orbit later. However, the extreme accuracy needed in the entry angle to target the 407 km apoapse soon became a problem. After determining the overshoot entry angles to twelve decimal places, the resulting mean apoapse altitude was about 418 km. It was concluded that in the interests of time management, this mean apoapse was a reasonable approximation of the desired apoapse of 407 km. It is important to note that the mean apoapse is defined as the altitude above the mean radius of the Earth The mean radius of the Earth is in turn defined as the average of the polar and equatorial radii. Table 4-2 shows the exit conditions for the overshoot trajectories.

Also, notice the differences in maximum deceleration experienced by the vehicle. In all cases, the undershoot trajectories experienced no more than a 5-g deceleration. The overshoot boundaries experienced much lower deceleration loads, ranging from 2.4-g to 3.8-g. Figure 4-1 shows the altitude versus time and g-load versus time profiles for the undershoot trajectory at an entry speed of 13.5 km/s, while Figure 4-2 shows the same information for the overshoot trajectory at an entry speed of 13.5 km/s.

4-1.3 Entry Corridor Width

Some of the data from Tables 4-1 and 4-2 have been translated to graphical form in Figure 4-3 which shows the entry angles versus entry speed for both the undershoot and overshoot boundaries. As mentioned earlier, the area between the undershoot and

27

Table 4-2. Exit Conditions for the Overshoot Boundary

Entry Speed [km/s]	Entry Angle [deg]	Apoapse Altitude [km]	Periapse Altitude [km]	Period [min]	Exit Inclination [deg]	G-Max [g's]	Time to 407 km [s]
12 5	-5 341691881600	417 691	115 698	89 627	4 04E-04	2 458	3139 258
12.6	-5 373350804000	417 900	115 690	89 630	4.07E-04	2 527	3097.680
13.0	-5.491541150500	417 694	115.697	89.627	4 04E-04	2 813	3141.534
13.5	-5 622541324900	417 692	115.697	89.627	4 03E-04	3 184	3150.629
14.0	-5 737859415800	417 692	115 697	89 627	4 03E-04	3 570	3156.367
14 5	-5.839992795200	417.698	115 696	89 627	4 03E-04	3 971	3156 531
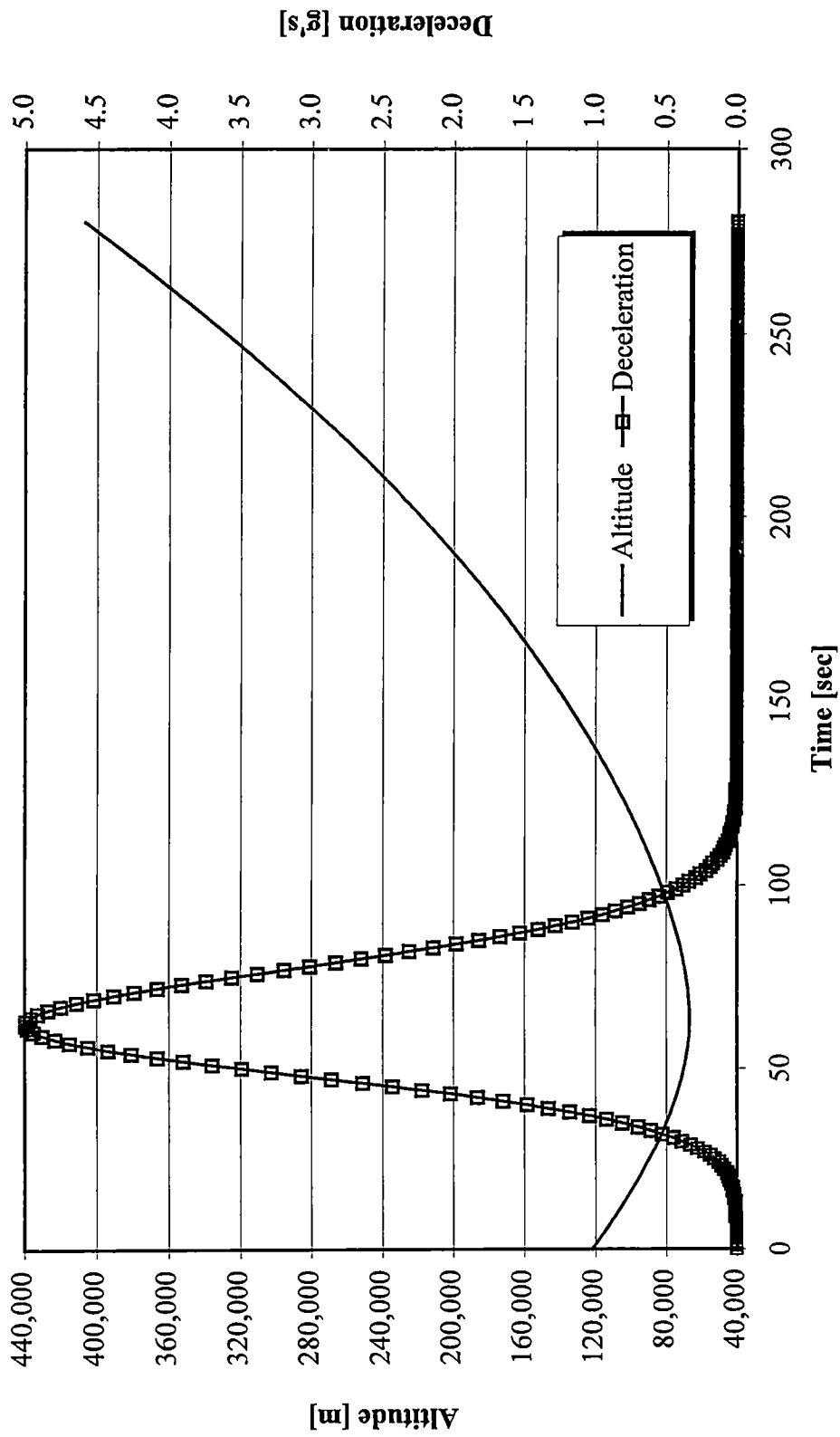
28

Figure 4-1. Altitude and Deceleration History for Untargeted Undershoot Trajectory
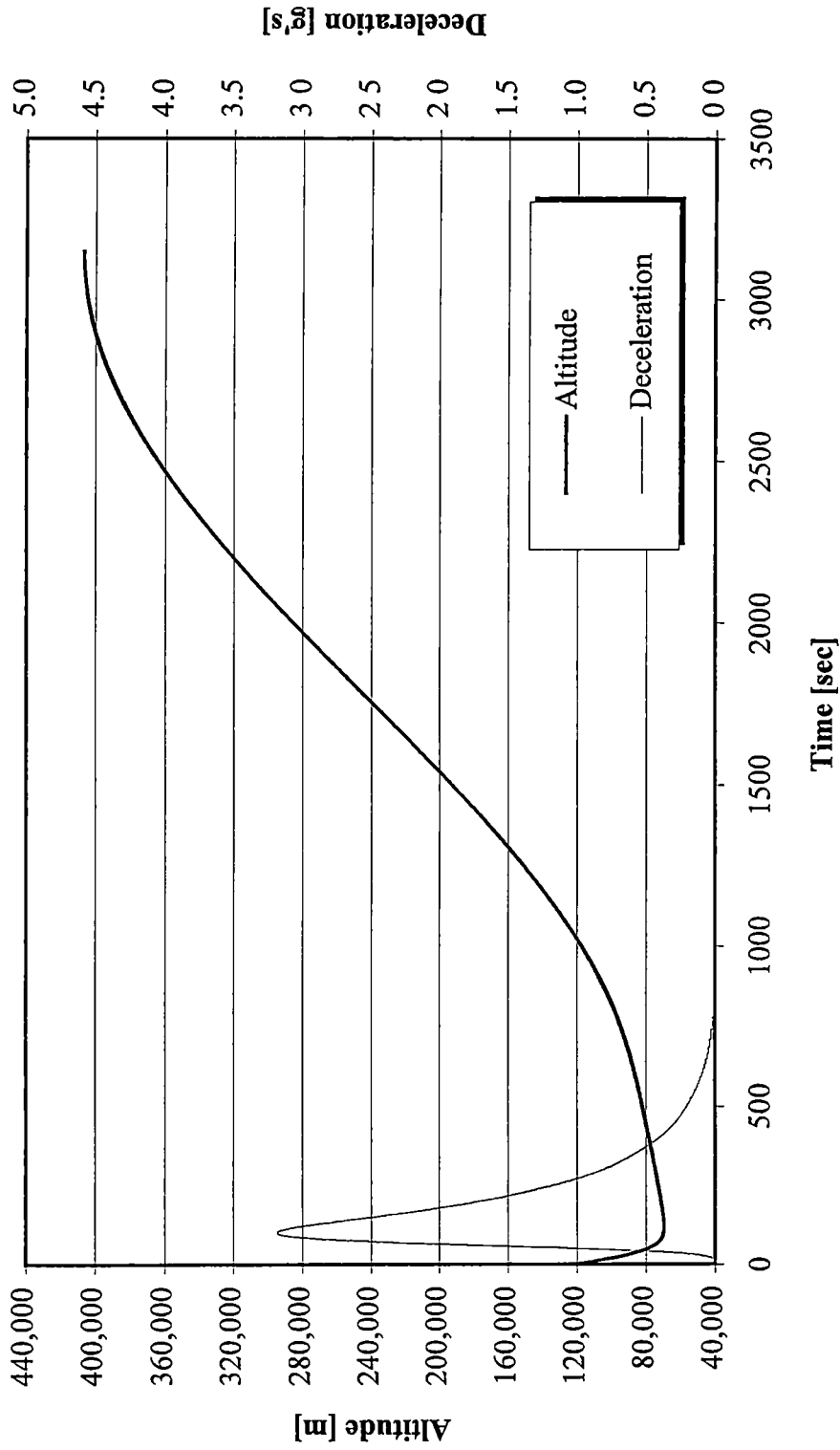
Nominal Atmosphere   Entry Speed = 13.5 km/s   AOA = 45 deg   Transhab/Ellipsled Vehicle

Figure 4-2. Altitude and Deceleration History for Overshoot Boundary
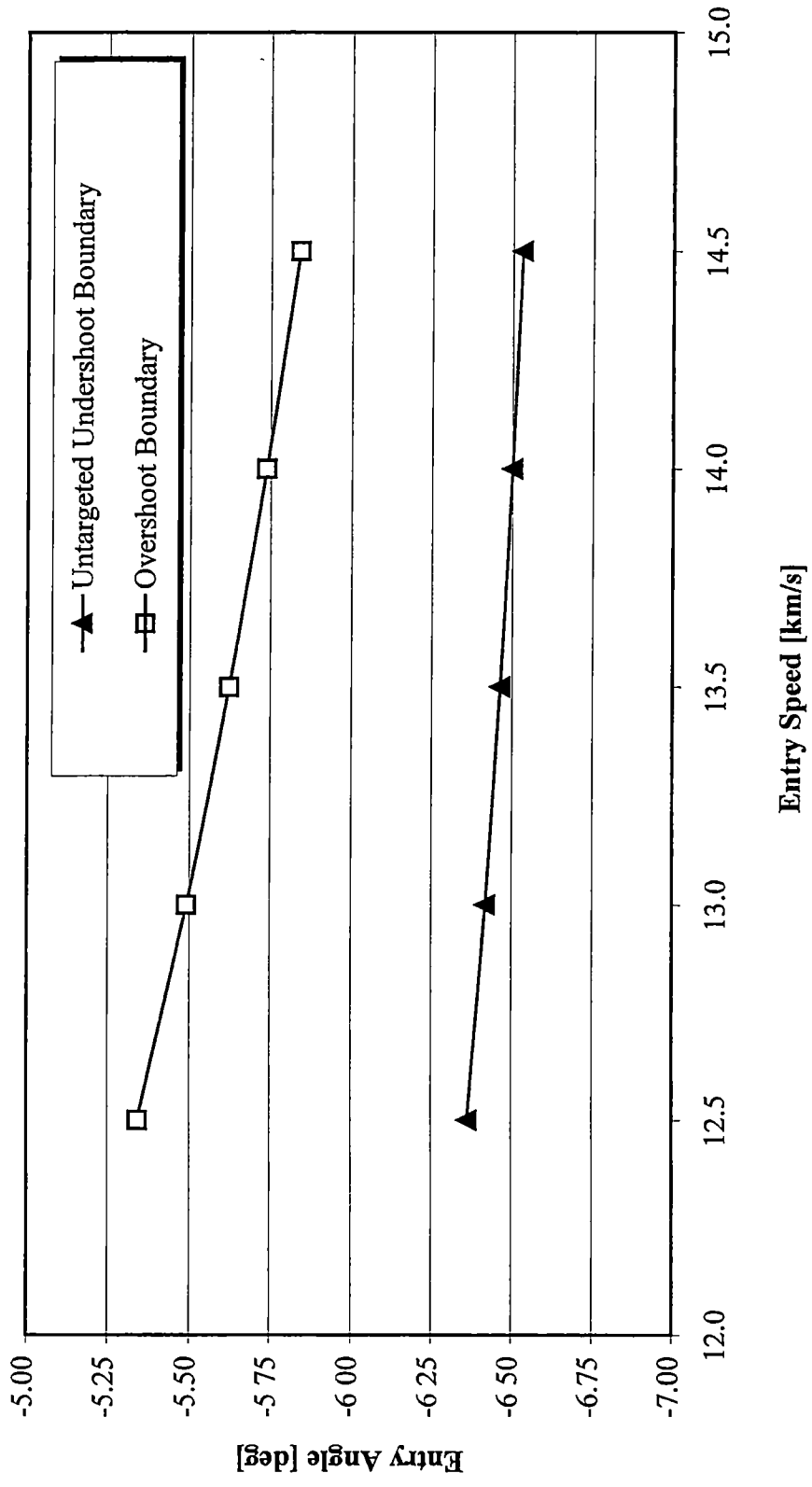
Nominal Atmosphere   Entry Speed = 13.5 km/s   AOA = 45 deg   Transhab/Ellipsled Vehicle

Figure 4-3. Corridor Boundaries for the Transhab/Ellipsled Vehicle

Nominal Atmosphere   5 G Deceleration Limit   AOA = 45 deg   No Undershoot Targeting

overshoot boundaries is known as the entry corridor. Figure 4-4 details the entry corridor width as a function of entry speed for the Transhab/Ellipsled vehicle as determined in this first study. Figure 4-4 shows that the entry corridor width ranges from a maximum of 1 065 degrees at an entry speed of 12.5 km/s to a minimum of 0.743 degrees occurring at an entry speed of 14.5 km/s. NASA typically requires entry corridors to be a minimum of 0.5-0.7 degrees wide to insure that the navigation systems can safely target the nominal trajectory [17]. The results from this initial study seem to indicate that the entry corridor meets the 0.5 - 0.7 degree requirement throughout the range of entry speeds and under nominal conditions.

Section 4-2.   Bank Angle Modulation Schemes

The previous two chapters detailed the procedures and results of the first undershoot and overshoot boundary analyses completed for the Transhab/Ellipsled vehicle. While the overshoot boundary trajectories resulted in elliptical orbits, the undershoot boundary trajectories ended mainly in hyperbolic trajectories. For the aerocapture to be a success, the vehicle must be able to capture into the desired orbit regardless of the angle at which the vehicle enters the atmosphere. Therefore, some additional control has to be incorporated into the POST simulations to allow the vehicle to capture into the desired orbit when entering at the undershoot entry angles. The control most often used to target a particular orbit is that of bank angle.
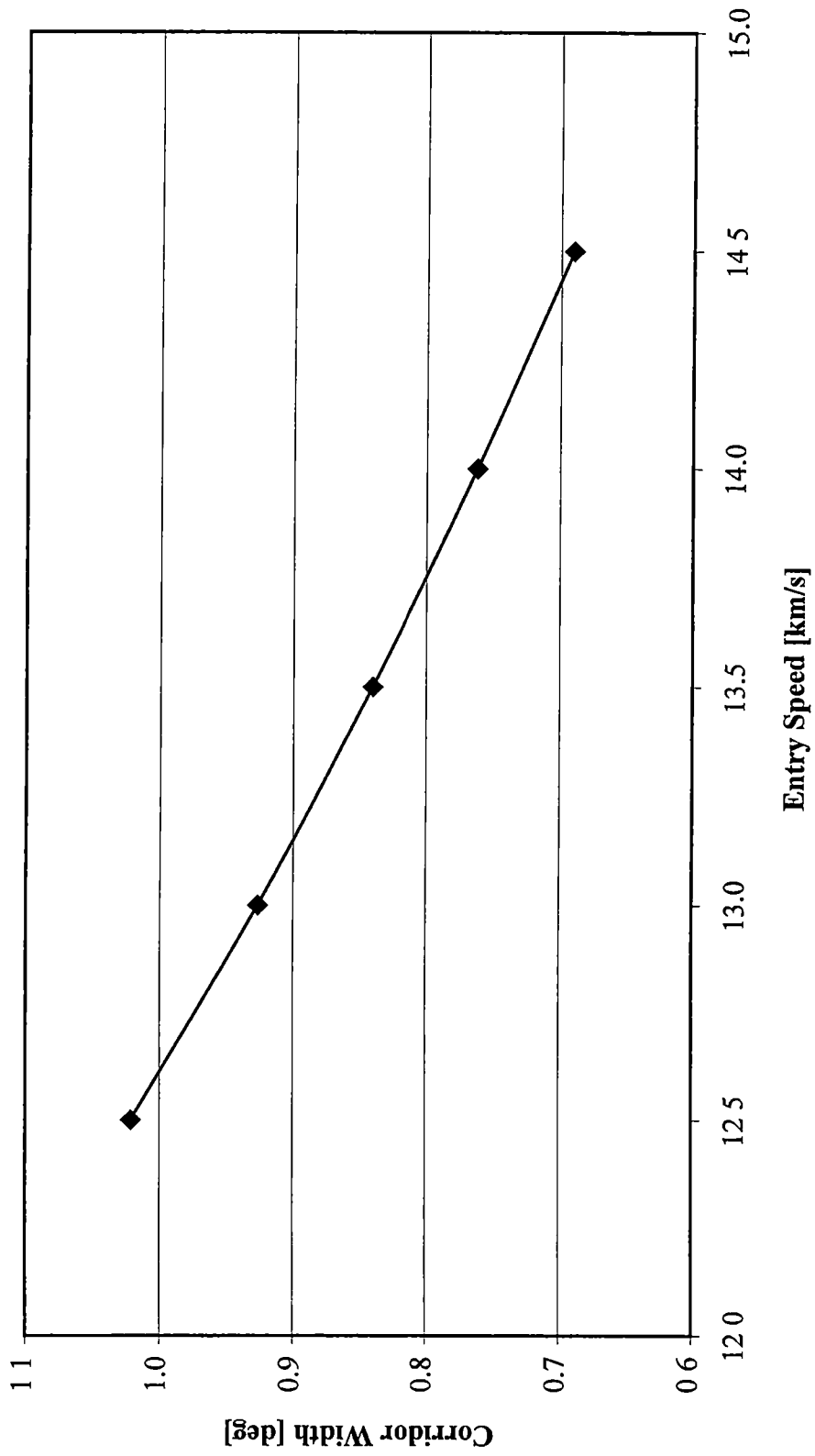
Figure 4-4. Entry Corridor Width for the Transhab/Ellipsled Vehicle

Nominal Atmosphere   5 G Deceleration Limit   AOA = 45 deg   No Undershoot Targeting

4-2.1 Constant Bank Angle

The first method used to target the desired orbit in the undershoot trajectories was to implement a constant, but non-zero, bank angle throughout the trajectory. The 5-g deceleration constraint was left in place and all other entry conditions were left the same as that for the first entry corridor study. Namely, all the cases assumed a due east equatorial entry, an oblate planet, and nominal atmospheric density. The POST targeting routine was utilized in this undershoot trajectory study to determine the constant bank angle necessary to target the 407 km orbit. The initial guesses for the entry angle were those corresponding to the untargeted undershoot boundary trajectories, while the initial guesses for the bank angle were set to approximately 75 degrees. POST then began the simulations and perturbed the controls as necessary to target the 407 km apoapse and maintain the 5-g deceleration limit. The simulations were complete when POST obtained a P2 value of less than one which indicated that all of the constraints had been satisfied within the given tolerances

The bank angles required to target the orbit ranged from 100 to 130 degrees depending on the entry speed of the vehicle. The resulting trajectories had apoapse altitudes of approximately 420 km and maximum decelerations of nearly 5-g. Table 4-3 shows the exit conditions for the undershoot trajectories using the fixed bank angle scheme. Notice that the entry angles are significantly shallower than those found for the untargeted undershoot boundaries in Section 4-1.1. Also note the large exit inclinations resulting from the implementation of a constant bank angle targeting scheme. The implications of large inclination changes such as these will be discussed later.

34

Table 4-3. Undershoot Exit Conditions Using a Fixed Bank Angle Targeting Scheme

Entry Speed [km/s]	Entry Angle [deg]	Bank Angle [deg]	Period [min]	Apoapse Altitude [km]	Perrapse Altitude [km]	Exit Inclination [deg]	Max g's [g's]	Time to 407 km [s]
12.5	-5.801123079414	100.655	89.109	418.190	64.055	9.817	4.9940	2260.407
13.0	-5.854629989200	108.393	89.306	418.750	82.898	10.260	5.0012	2399.006
13.5	-5.900056241729	116.386	89.425	418.094	95.342	10.392	4.9832	2587.049
14.0	-5.944336555267	124.375	89.501	418.112	102.849	10.196	5.0000	2716.886
14.5	-5.980161574997	133.536	89.554	418.142	108.027	9.473	5.0007	2837.190

Figure 4-5 shows the changes to the undershoot angle caused by implementing the constant bank angle. The fixed bank angle causes the entry angles to be reduced by nearly 0.6 degrees which accounts for more than half the width of the entry corridor. Figure 4-5 also shows the corridor as defined by the standard overshoot boundary and the undershoot boundary using a fixed bank angle targeting scheme. When compared to Figure 4-3, it is clear the use of a fixed bank angle closes the corridor significantly. The large reduction in the entry corridor width is shown explicitly in Figure 4-6 The conclusion to be drawn from this analysis is that while using a fixed bank does allow the vehicle to target the desired orbit, it also results in an entry corridor much too narrow for practical use. Therefore, a more complex method of targeting the desired orbit must be used to insure that the minimum corridor width of 0.5 - 0.7 degrees is achieved

4-2.2   Roll Maneuvers

The previous section revealed that the use of a fixed bank to target the desired orbit resulted in an entry corridor of insufficient width Therefore, it was decided that a more complex bank angle modulation scheme was needed in order to target the orbit and maintain the corridor width The simulation was thus altered to include a 180 degree roll maneuver By rolling the vehicle over 180 degrees it should be possible to target the elliptical orbit, limit the maximum deceleration to 5-g, and maximize the corridor width simultaneously.

The only other constraint that was considered for this analysis was that of the maximum roll rate. In practice, the vehicle would perform a roll maneuver by firing thrusters to both initiate the roll and then to stop the roll at the appropriate bank
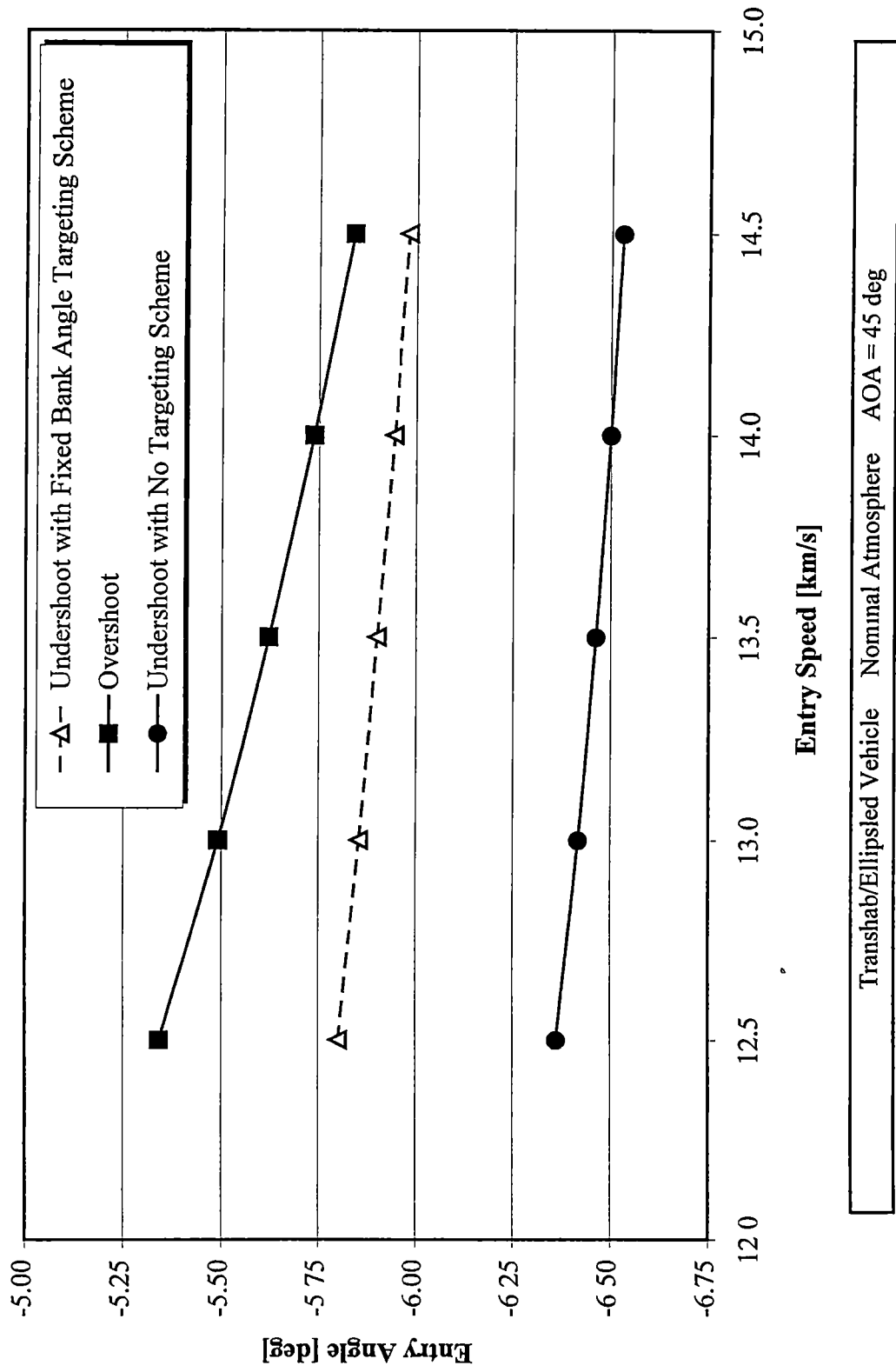
Figure 4-5. Effect of Fixed Bank Angle Targeting Scheme on Corridor Boundaries
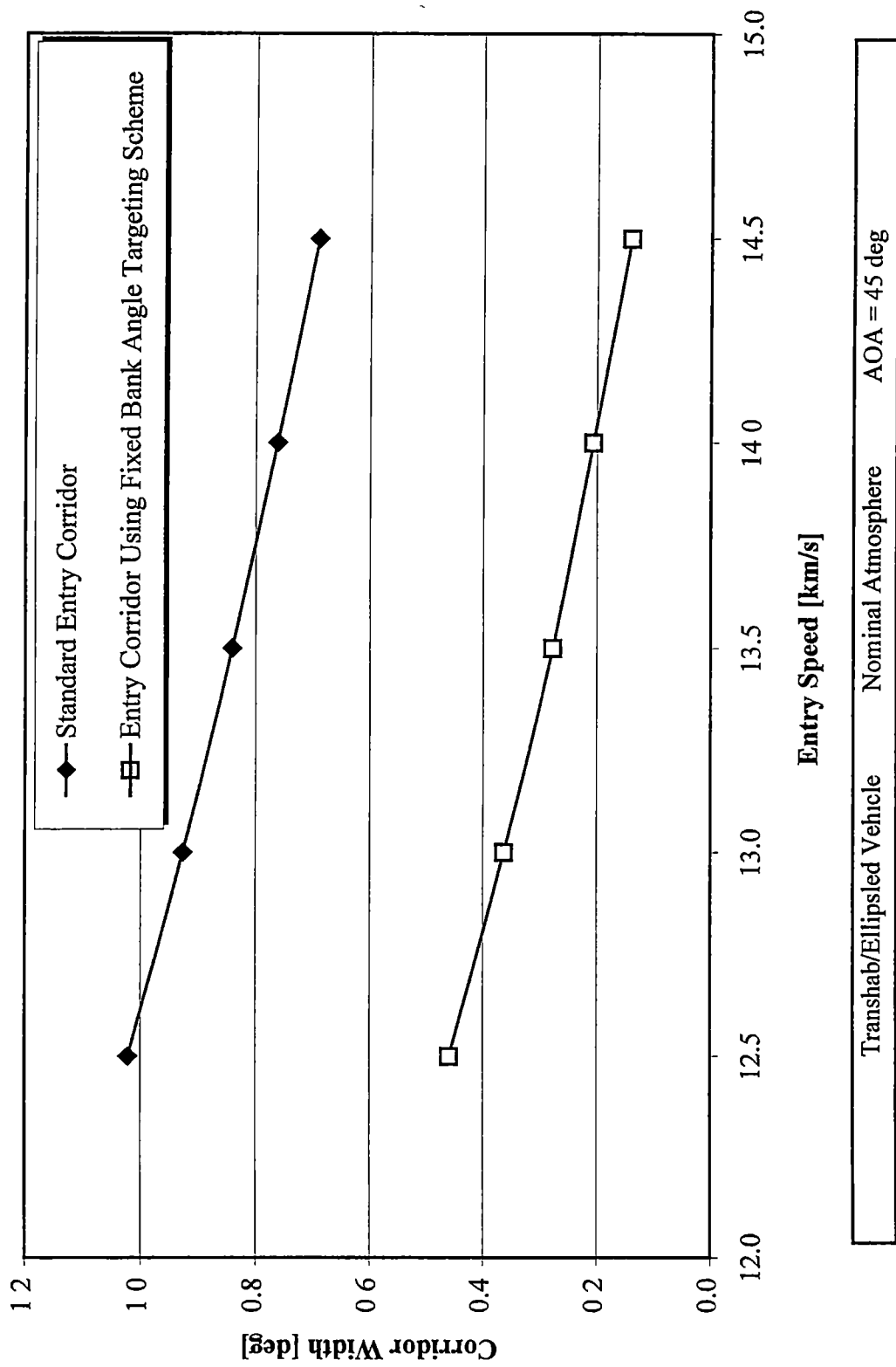
Figure 4-6. Effect of a Fixed Bank Angle Targeting Scheme on Entry Corridor Width

Transhab/Ellipsled Vehicle   Nominal Atmosphere   AOA = 45 deg

angle. The size of the thrusters available and the vehicle mass determines what maximum roll rate that can be achieved by the vehicle The initial assumption was that the vehicle could perform a maneuver at a roll rate of no more than ten degrees per second. However, after further consultation with NASA colleagues, it was determined that a five degrees per second roll rate was a more realistic estimate of the thruster abilities. For comparison purposes, analyses were completed using both 5 'and 10 deg/s roll rate limits, and the results are shown hereafter.

This study once again employed the POST targeting subroutine to obtain the undershoot boundaries. First, for a given entry speed, the initial guess for the entry angle was assumed to be that of the untargeted undershoot boundary. Next, additional events were incorporated into the POST input deck. These events allowed POST to choose the best time to begin the roll maneuver and specified when the roll maneuver was to end. Initially, the roll rate was set to 10 deg/s, which resulted in a total roll time of 18 seconds. Later, the roll rate was set to 5 deg/s, yielding a roll maneuver lasting 36 seconds. To obtain an initial guess of when to begin the roll, the trajectory files from the untargeted undershoot boundaries were examined to locate the time of peak deceleration. The initial guesses for the time to begin the roll were set to a few seconds before the time of peak deceleration. Once the input deck modifications were complete, POST was allowed to perform the simulations and project the trajectories. POST altered the time to begin the roll and the entry angle as needed to target the orbit and insure that the deceleration never exceeded 5-g. When POST had obtained a P2 value under one, the simulations were complete and the data was recorded. It may be of some interest to note here that it is possible to perform the same targeting scheme through a manual iterative procedure.

However, the time spent by the user performing such a procedure can be many times longer than the time POST spends doing the same functions. A typical manual procedure may take between 120 and 150 iterations to obtain a solution. This translates into one to two hours of work usually In contrast, POST can obtain nearly identical solutions, with the help of the user, in about 15-20 minutes. Therefore, it is in the best interest of the user to become familiar with the targeting/optimization routines that POST offers as early as possible.

10 Degrees Per Second Roll Rate Study

Table 4-4 reveals the results of the study when the roll rate is limited to 10 deg/s. The first result to be pointed out is that the entry angles, especially at the higher entry speeds, were slightly shallower than those for the nominal undershoot trajectories. In Table 4-4, the "$T_{max\ g's}$" column designates the time of peak deceleration in the nominal undershoot trajectories Notice that the time to begin the roll maneuver always occurs before the time of peak deceleration Another important result is that the roll maneuver must be started earlier as entry speed increases in order to target the 407 km circular orbit. Finally, note that the apoapse altitudes, periapse altitudes, and orbital periods are significantly different from the untargeted undershoot trajectories found in Section 4-1.1. This simple fact indicates that the roll maneuver achieved the goal of eliminating the hyperbolic exits found with the untargeted undershoot cases.

Figure 4-7 displays a deceleration comparison of the undershoot trajectories at an entry speed of 13.5 km/s. The figure shows that implementing a roll maneuver with a roll

40

Table 4-4. Exit Conditions for the Undershoot Boundary using a 180 Degree Roll Maneuver (10 deg/s Roll Rate)

| Entry Speed | Entry Angle | $T_{roll\ start}$ | $T_{max\ g's}$ | Period | Apoapse Altitude | Periapse Altitude |
[km/s]	[deg]	[s]	[s]	[min]	[km]	[km]
12.5	-6.363283	67.704190	67.70	89.655	420.59	115.51
13.0	-6.418388	62.518740	65.00	89.641	419.19	115.60
13.5	-6.462841	57.843632	62.50	89.663	421.48	115.47
14 0	-6.496209	53.561173	60.50	89.661	421.26	115.48
14 5	-6.518249	49.564803	59.00	89.646	419.64	115.58
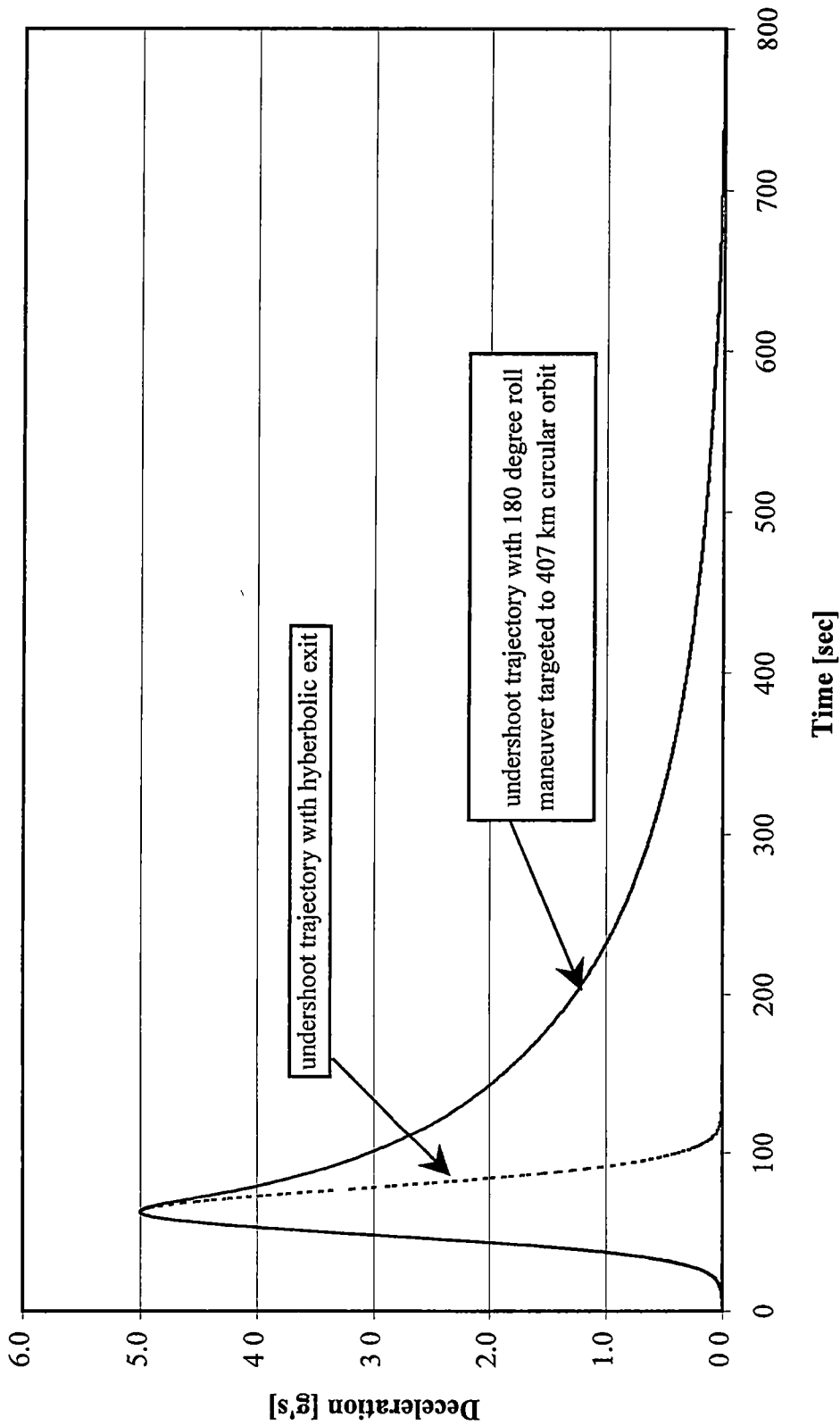
Figure 4-7. Deceleration History Comparison of Undershoot Trajectories

undershoot trajectory with hyberbolic exit

undershoot trajectory with 180 degree roll maneuver targeted to 407 km circular orbit

Entry Speed = 13 5 km/s   Roll Rate = 10 deg/s   Nominal Atmosphere

Time [sec]

Deceleration [g's]

rate of 10 deg/s exposes the vehicle to a more prolonged deceleration pulse, but does not exceed the imposed 5-g limit. This prolonged deceleration pulse is required for the vehicle to reach its target orbit. Figure 4-8 shows a comparison of altitude history for the same undershoot trajectories detailed in Figure 4-7. Note that the addition of the roll maneuver causes the vehicle to take over 3000 seconds to reach an altitude of 407 km. Of that time, approximately 1000 seconds are spent in atmospheric flight. This is important because the time spent in atmospheric flight will affect the integrated heat loads to which the vehicle is subjected. The heating characteristics in turn will determine the thermal protection system (TPS) needed for the aerocapture to be successful. The matter of atmospheric heating will be examined later in Section 4-6.

Table 4-4 also shows the high degree of accuracy needed in the time at which to begin the roll for this simple, single-roll targeting scheme. This indicates that the exit conditions are highly sensitive to the time at which the roll maneuver is begun. Figure 4-9 shows the effects on the orbital period of beginning the roll maneuver too late. Notice that only a small delay in beginning the roll maneuver (ΔTime) results in a very large error in orbital period. The guidance system would have to be extremely accurate in order to handle this sensitivity problem. This indicates the impracticality of such a single-roll targeting scheme with no subsequent maneuvers for trajectory correction.

5 Degrees Per Second Roll Rate Study

After further consideration, it was decided that a roll rate of 10 deg/s might exceed the abilities of the thrusters on the Transhab/Ellipsled vehicle. Therefore, another
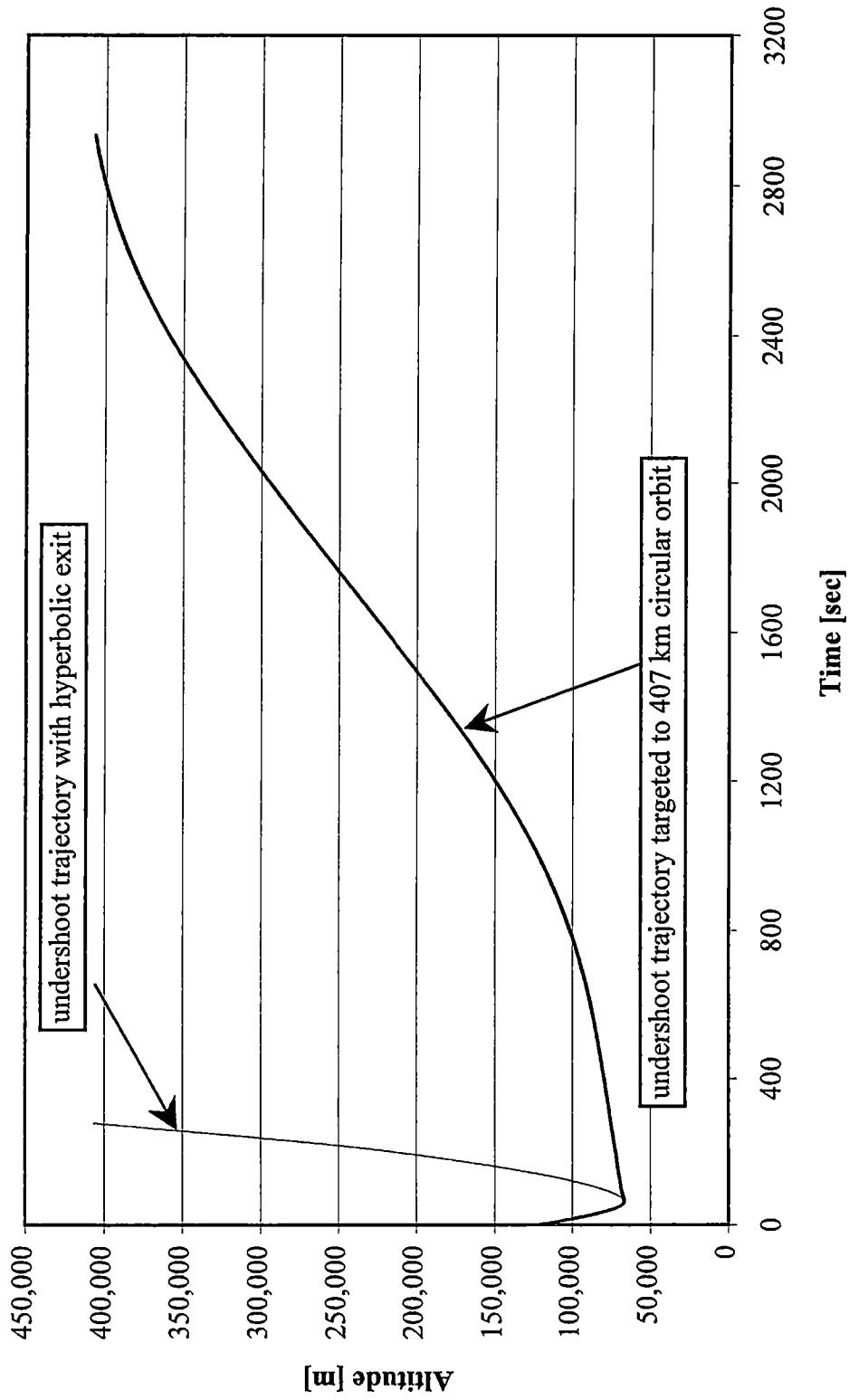
Figure 4-8. Altitude History Comparison of Undershoot Trajectories
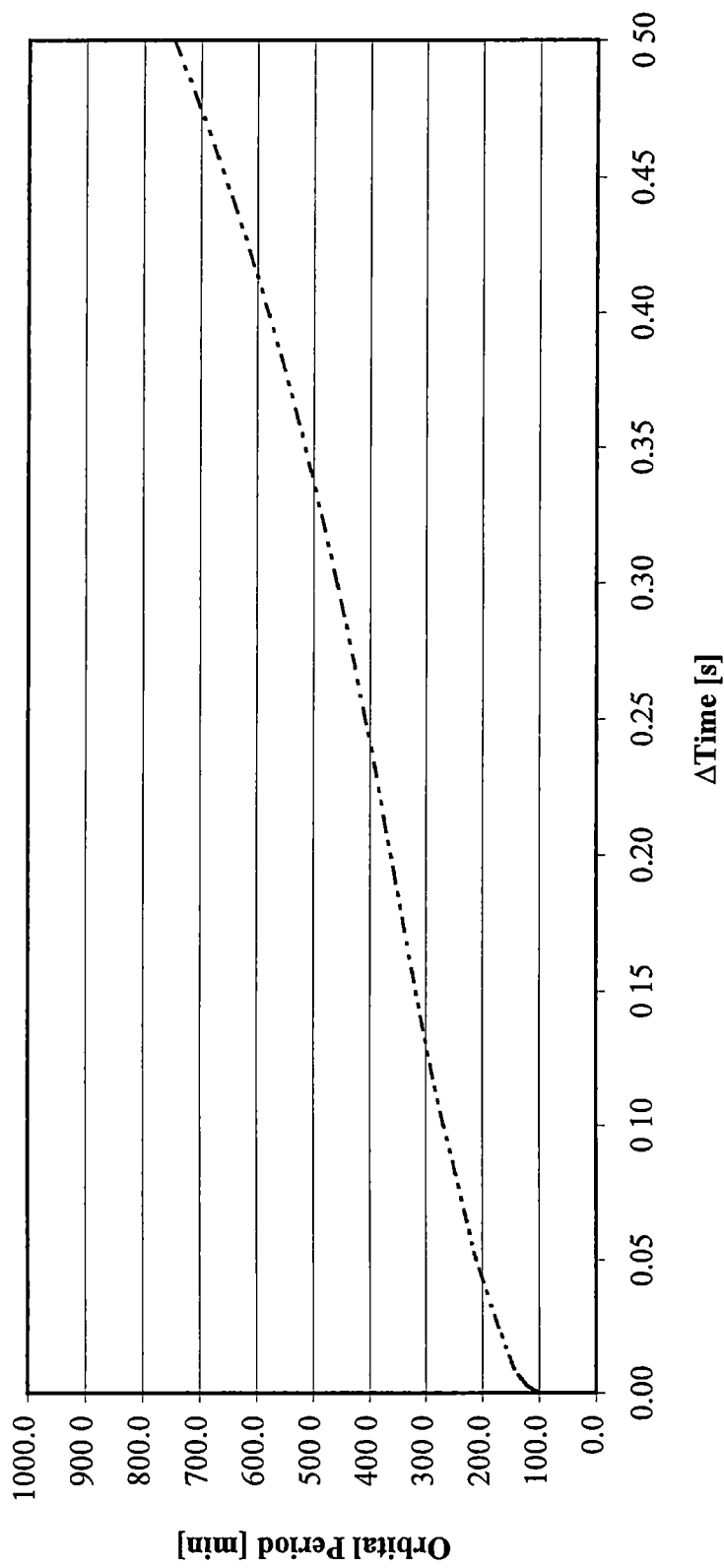
Transhab/Ellipsled Vehicle   Entry Speed = 13 5 km/s   Roll Rate = 10 deg/s   Nominal Atmosphere

Chart labels:
- Altitude [m] (y-axis): 0, 50,000, 100,000, 150,000, 200,000, 250,000, 300,000, 350,000, 400,000, 450,000
- Time [sec] (x-axis): 0, 400, 800, 1200, 1600, 2000, 2400, 2800, 3200
- undershoot trajectory with hyperbolic exit
- undershoot trajectory targeted to 407 km circular orbit

Figure 4-9. Effect of Delay in Roll Start on Orbital Period

Transhab/Ellipsled Vehicle   Entry Speed = 13.5 km/s   Roll Rate = 10 deg/s   Nominal Atmosphere

study was begun that limited the roll rate of the vehicle to 5 deg/s. The same procedure that was used in the 10 deg/s roll rate study was implemented in this study.

Table 4-5 is the summary of the exit conditions for the undershoot trajectory with the 5 deg/s roll rate incorporated. Once again, notice that the exit conditions are basically the same as those that were found for the 10 deg/s roll rate case. The entry angles for these cases are slightly different than those for the nominal entry corridor as expected based on the results of the 10 deg/s roll rate analysis described above. Like Table 4-4, the "$T_{max\ g's}$" column of Table 4-5 indicates the time of peak deceleration in the nominal undershoot trajectories This reference is used to compare the time at which the roll maneuver is begun for each trajectory. The only significant difference between the two $T_{roll\ start}$ columns of Tables 4-4 and 4-5 is that the 5 deg/s roll was started much earlier than the 10 deg/s roll maneuver. Figure 4-10 is a plot of the altitude versus time and deceleration versus time histories for the undershoot trajectory at a 13.5 km/s entry speed. The similarities between the altitude and deceleration histories of Figure 4-10 and those shown in Figures 4-7 and 4-8 should be clear. The deceleration never exceeded 5-g, and the time to reach an altitude of 407 km was approximately 3000 seconds. Once again the orbital period was extremely sensitive to the time at which the roll maneuver was begun. Figure 4-11 diagrams how the orbital period was affected even by very small delays (delta time) in the starting the 5 deg/s roll maneuver.

As shown in this chapter, the addition of a 180 degree bank angle change allows the desired orbit to be targeted in the undershoot trajectories without exceeding the 5-g deceleration limit. The roll rate limit, while extremely important to the physical design of the vehicle, does not significantly affect the corridor width. Figure 4-12 reveals how the

Table 4-5. Exit Conditions for the Undershoot Boundary using a 180 Degree Roll Maneuver (5 deg/s Roll Rate)

Entry Speed [km/s]	Entry Angle [deg]	$T_{roll\ start}$ [s]	$T_{max\ g's}$ [s]	Period [min]	Apoapse Altitude [km]	Periapse Altitude [km]	Inclination [deg]
12.5	-6.360070	59.788775	68.50	89.667	421.93	115.42	1.7698
13 0	-6.409175	54 456613	66.00	89.636	418.62	115.62	1.7500
13.5	-6.444471	49.569893	64.00	89.645	419.56	115.57	1.7033
14.0	-6.466216	44.988339	62.50	89.658	420.95	115.49	1.6286
14.5	-6.473655	40.562254	62.50	89.662	421 37	115.47	1.5213

Figure 4-10. Altitude and Deceleration History of Undershoot Trajectory using a 5 deg/s Targeting Roll Maneuver

Transhab/Ellipsled Vehicle   Entry Speed = 13.5 km/s   Roll Rate = 5 deg/s   Nomnal Atmosphere

Figure 4-11. Effect of Delaying Roll Maneuver on Orbital Period
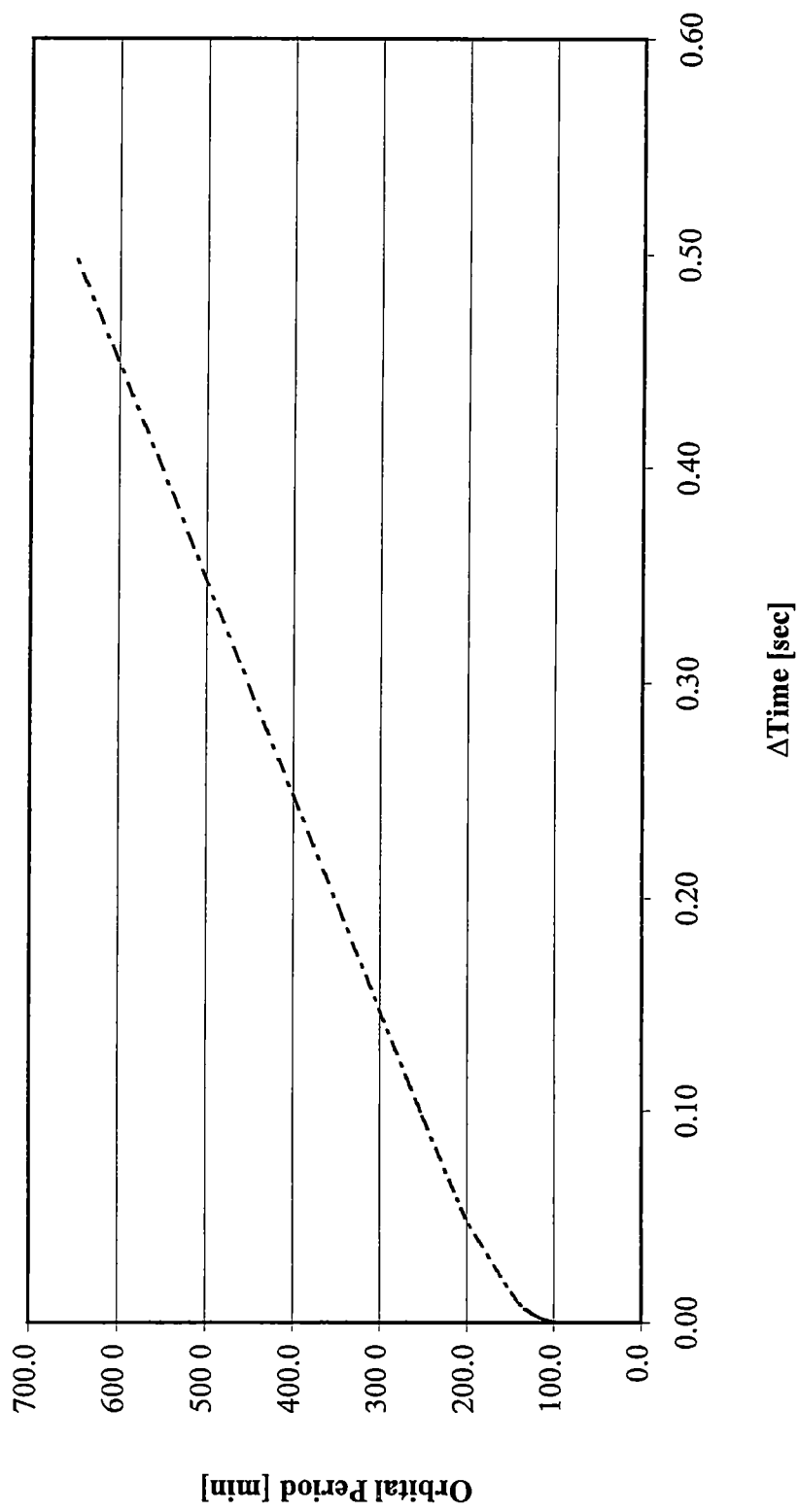
Transhab/Ellipsled Vehicle   Entry Speed = 13.5 km/s   Roll Rate = 5 deg/s   Nominal Atmosphere
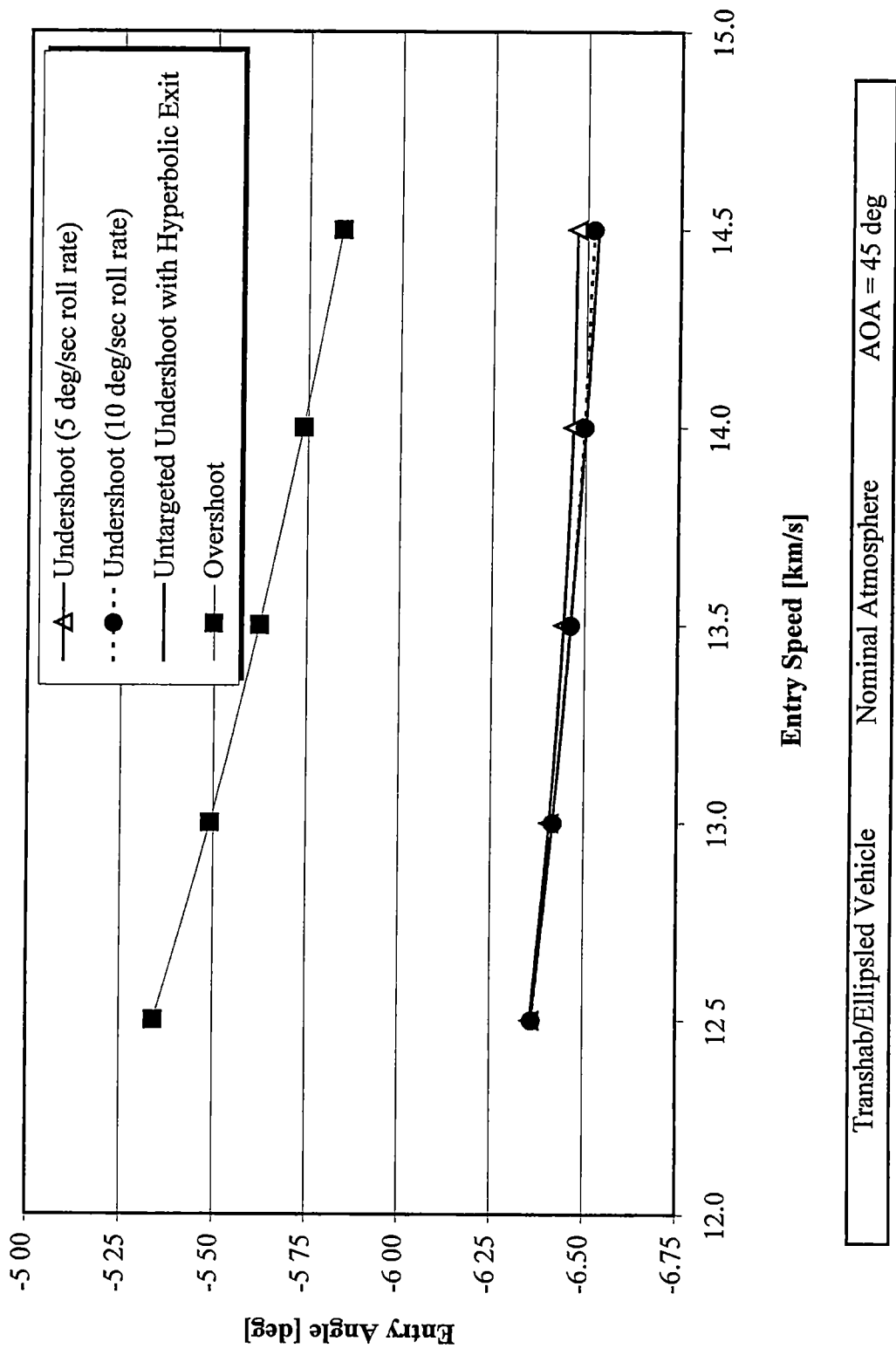
Figure 4-12. Changes in Undershoot Boundary Due to Roll Rate Limits

implementation of the roll maneuver affects the undershoot boundary. Notice that there is relatively little difference between the undershoot boundary as defined by the 10 deg/s roll rate and the 5 deg/s roll rate. Figure 4-13 shows exactly how small the effect of choosing a roll rate is to entry corridor width.
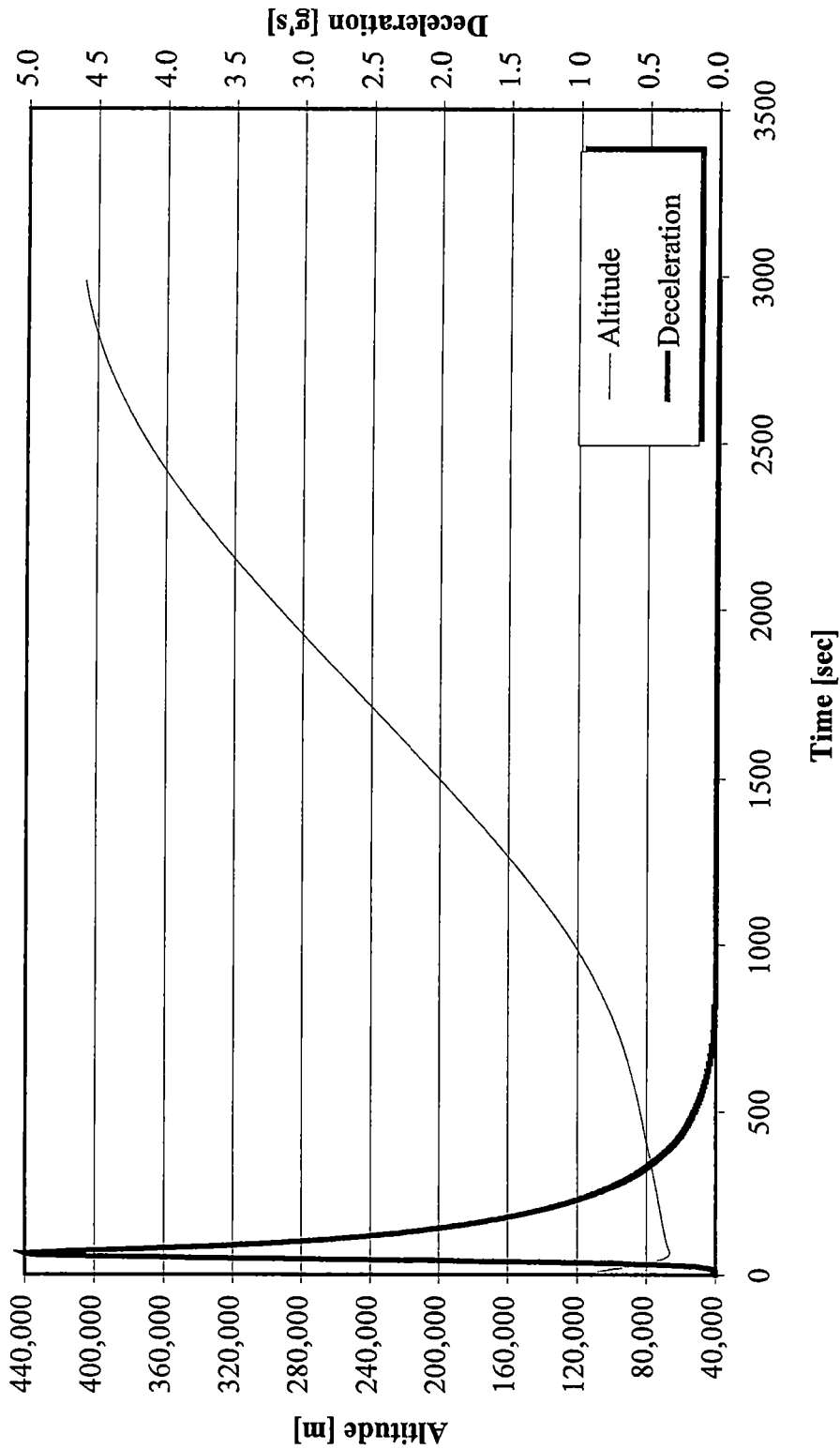
Section 4-3.   Atmospheric Dispersions

After the nominal entry corridor was determined in the previous study, it was necessary to examine off-nominal entry conditions Although nominal atmospheric conditions represent the environment during the standard Earth day, there is at least the possibility of the Transhab/Ellipsled vehicle returning to Earth when the atmosphere has a slightly higher or lower density than normal. The present models for the atmosphere of Earth are very good when compared to the models for other planets Atmospheric dispersions can cause significant modeling problems for planets such as Mars where there is significantly greater uncertainty in atmospheric density profiles [18]. This atmospheric uncertainty was one of the major obstacles that Jits & Walberg [7] had to overcome in their study of the Mars aerocapture of the triconic vehicle

The undershoot and overshoot boundaries for any aerocapture can be significantly influenced by the density profile encountered by the vehicle. This is due to the fact that the aerocapture relies on aerodynamic forces to dissipate energy and target a prescribed orbit. Aerodynamic forces, such as lift and drag, are of course a function of the density of the atmosphere as well as the aerodynamic characteristics of the vehicle. As a result, both
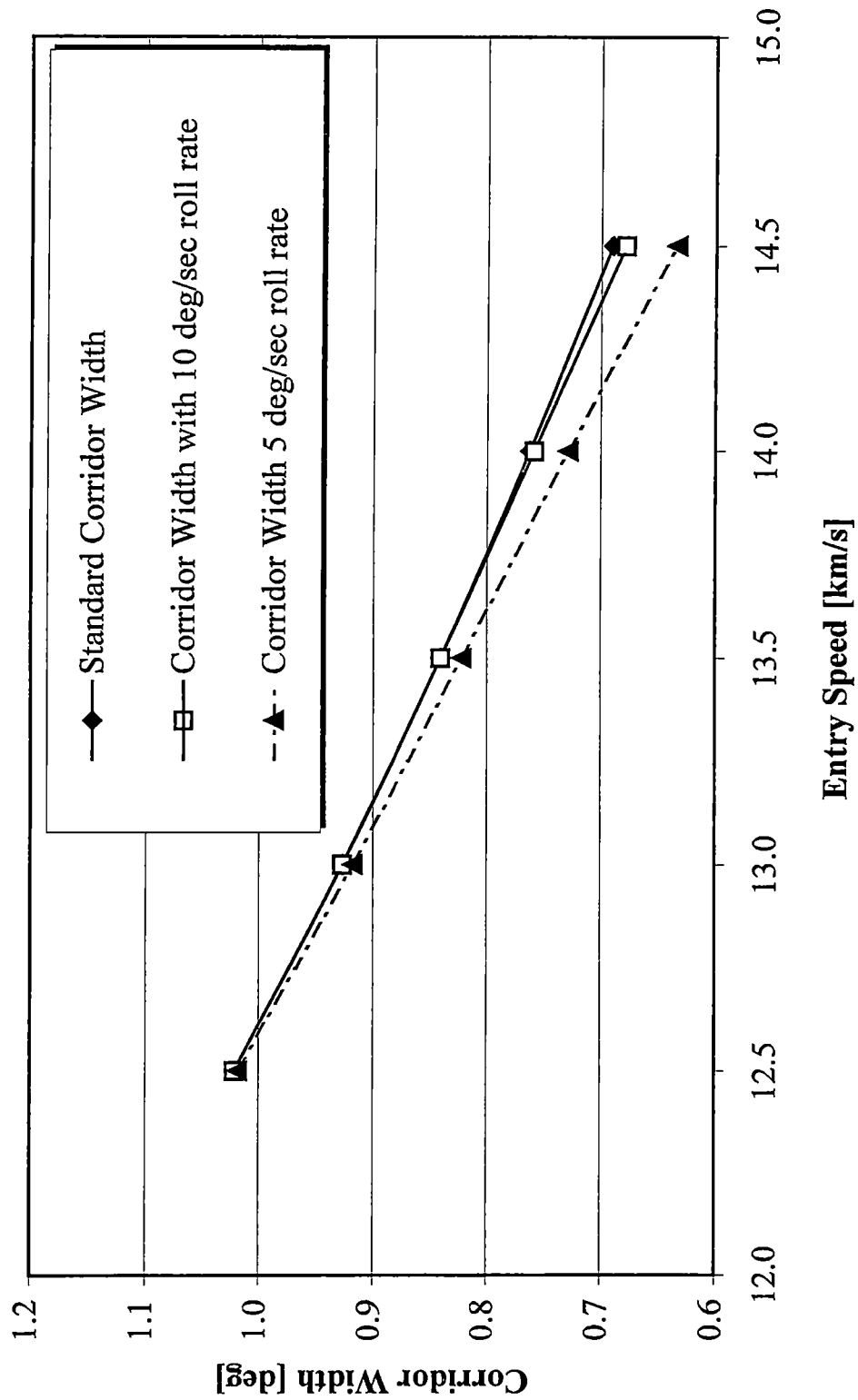
Figure 4-13. Changes in Entry Corridor Width Due to Roll Rate Limits

Transhab/Ellipsled Vehicle   Nominal Atmosphere   AOA = 45 deg

the width and location of the entry corridor may be affected by differences in the atmospheric density.

4-3.1 Dispersion Modeling

Atmospheric dispersions can be modeled in a variety of ways including sinusoidal functions, random density tables, or simple high-density/low-density extremes. For the purposes of this preliminary study, it was decided that modeling the dispersions with a 30% uncertainty in atmospheric density was sufficient. Thus, either a constant high density (130% of nominal atmosphere) or low density (70% of nominal atmosphere) atmosphere was used in place of the nominal atmospheric density profile given by the 1976 U.S. Standard Atmosphere. No other factors such as horizontal density gradients or winds were considered in this study.

4-3.2 Analysis

The off-nominal atmospheric densities were incorporated in POST by the use of a density multiplier table [15]. The density multiplier table simply takes the density model already in use by POST and multiplies each density by a user specified decimal percent change in density. The resulting table represents a high or low-density profile of the magnitude desired by the user.

A procedure similar to that described in the previous chapter was used to find the undershoot and overshoot boundaries using the off-nominal atmospheric conditions.

53

Once the density multiplier was set in the density table, the bank angle was set according to the boundary to be determined. The undershoot boundaries began with a constant bank angle of zero degrees while the overshoot boundaries used a constant bank angle of 180 degrees. Next, the entry speed was set and the entry angle varied. The undershoot boundaries were found using both the 5-g deceleration limit and a 180 degree roll maneuver to target the desired 407 km orbit. The overshoot boundaries on the other hand were determined by holding the bank angle equal to 180 degrees and targeting the apoapse altitude to be nearly 407 km.

Tables 4-6 and 4-7 below show the exit conditions for the undershoot and overshoot boundaries for the low-density atmosphere. Notice that the exit conditions are very similar to those of the entry corridor boundaries found in the last section.

Tables 4-8 and 4-9 show the respective exit conditions for the high-density atmosphere model. Again, notice the similarity between the exit conditions for the high-density model to those of the nominal and low-density models. This close similarity indicates the target orbit is nearly identical for all cases.

Figure 4-14 is a plot of the data from Tables 4-6 through 4-9 The summary shown in Figure 4-14 indicates that the undershoot and overshoot boundaries are indeed shifted to new locations by the changes in atmospheric density. The entry corridor widths for all three density models are displayed graphically in Figure 4-15. It is clear from looking at the figure that although the corridors may be shifted to different locations, the corridor widths are relatively unaffected by the dispersions in atmospheric density. It is important to note however that a 30% uncertainty in atmospheric density would require that the entry corridor be defined by the high-density undershoot boundary and the

Table 4-6. Undershoot Trajectory Exit Conditions for a 70% Nominal Atmosphere

Entry Speed [km/s]	Entry Angle [deg]	Troll [sec]	Apoapse Altitude [km]	Periapse Altitude [km]	Period [min]	Exit Inclination [deg]	G-Max [g's]	Time to 407 km [s]
12 5	-6 506879195000	61 73115129000	421 909	113.185	89 6440	1 7677	4 9991	2871 363
13 0	-6.55949636385000	56.27917860000	420 211	113 296	89 6280	1 7512	5 0001	2940 759
13 5	-6 59738563000	51 28983041000	419 461	113 342	89 6210	1.7066	5 0000	2984.545
14 0	-6 621309916000	46 61827738000	420 373	113 291	89 6300	1.6339	4.9999	2971.995
14.5	-6 631222037441	42 12368555381	418 578	113 395	89 6130	1.5297	4.9999	3049.854

Table 4-7. Overshoot Trajectory Exit Conditions for a 70% Nominal Atmosphere

Entry Speed [km/s]	Entry Angle [deg]	Troll [sec]	Apoapse Altitude [km]	Periapse Altitude [km]	Period [min]	Exit Inclination [deg]	G-Max [g's]	Time to 407 km [s]
12 5	-5 478969577	N/A	419 626	113 356	89.6230	4.11E-04	2.4442	3007 187
13 0	-5 6320167328	N/A	418 393	113 426	89 6110	4 08E-04	2 7984	3065.731
13 5	-5 7660471767	N/A	421 855	113.225	89 6440	4 13E-04	3.1678	2960.432
14 0	-5 8840318568	N/A	419 796	113 344	89 6250	4 11E-04	3.5523	3020.647
14 5	-5.9885274234	N/A	420.360	113.311	89 6300	4 11E-04	3.9518	3008 971

Table 4-8.   Undershoot Trajectory Exit Conditions for a 130% Nominal Atmosphere

Entry Speed [km/s]	Entry Angle [deg]	Troll [sec]	Apoapse Altitude [km]	Periapse Altitude [km]	Period [min]	Exit Inclination [deg]	G-Max [g's]	Time to 407 km [s]
12 5	-6 252300709751	58 367151720150	419 621	117 148	89 661	1 77052182	5 0000	2938 836
13 0	-6 299419836406	53 125790260340	419 452	117 167	89 660	1 74931225	5 0000	2970 266
13 5	-6 332764954979	48.315017955210	418 002	117 252	89.646	1 70063945	5.0000	3061 920
14 0	-6 352836799203	43.798454312050	420.392	117.116	89 669	1 62439581	4 9999	2976 008
14 5	-6 358539057335	39 422628384170	420 040	117.138	89.665	1 51439363	5 0000	2999 459

Table 4-9.   Overshoot Trajectory Exit Conditions for a 130% Nominal Atmosphere

Entry Speed [km/s]	Entry Angle [deg]	Troll [sec]	Apoapse Altitude [km]	Periapse Altitude [km]	Period [min]	Exit Inclination [deg]	G-Max [g's]	Time to 407 km [s]
12 5	-5 241549427416	N/A	418 885	117 224	89 655	4 10E-04	2 4676	3037 684
13.0	-5 388790713730	N/A	419.931	117 162	89 664	4.11E-04	2 8260	3007 094
13.5	-5 517550043719	N/A	420.154	117 149	89.667	4 11E-04	3.1982	3006 877
14 0	-5 630906394130	N/A	418 577	117.241	89 652	4 07E-04	3.5850	3071 658
14 5	-5 731309109900	N/A	419.209	117.204	89.577	4 10E-04	3 9870	3049 772
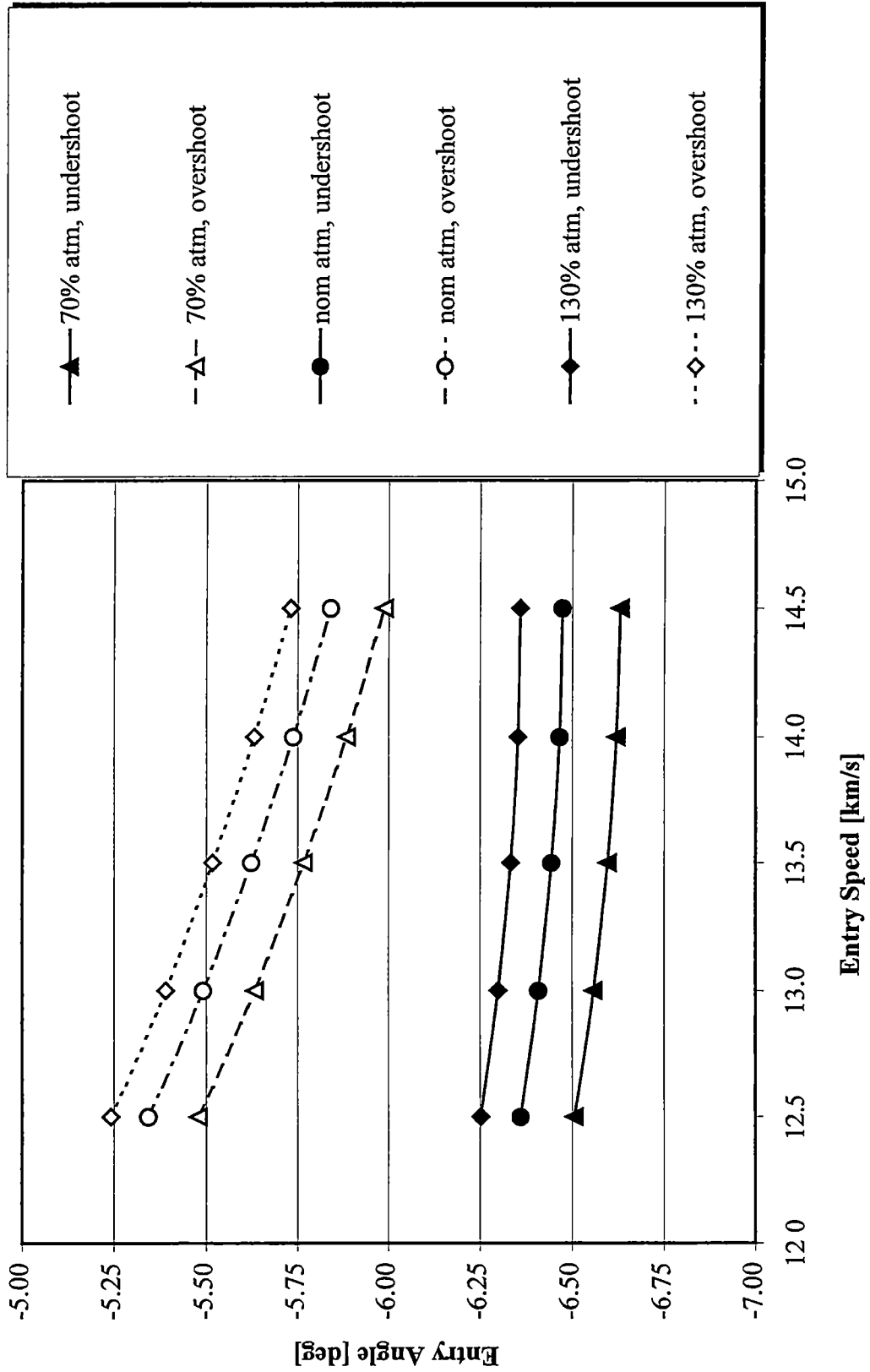
Figure 4-14. Effect of Atmospheric Dispersions on Undershoot and Overshoot Boundaries
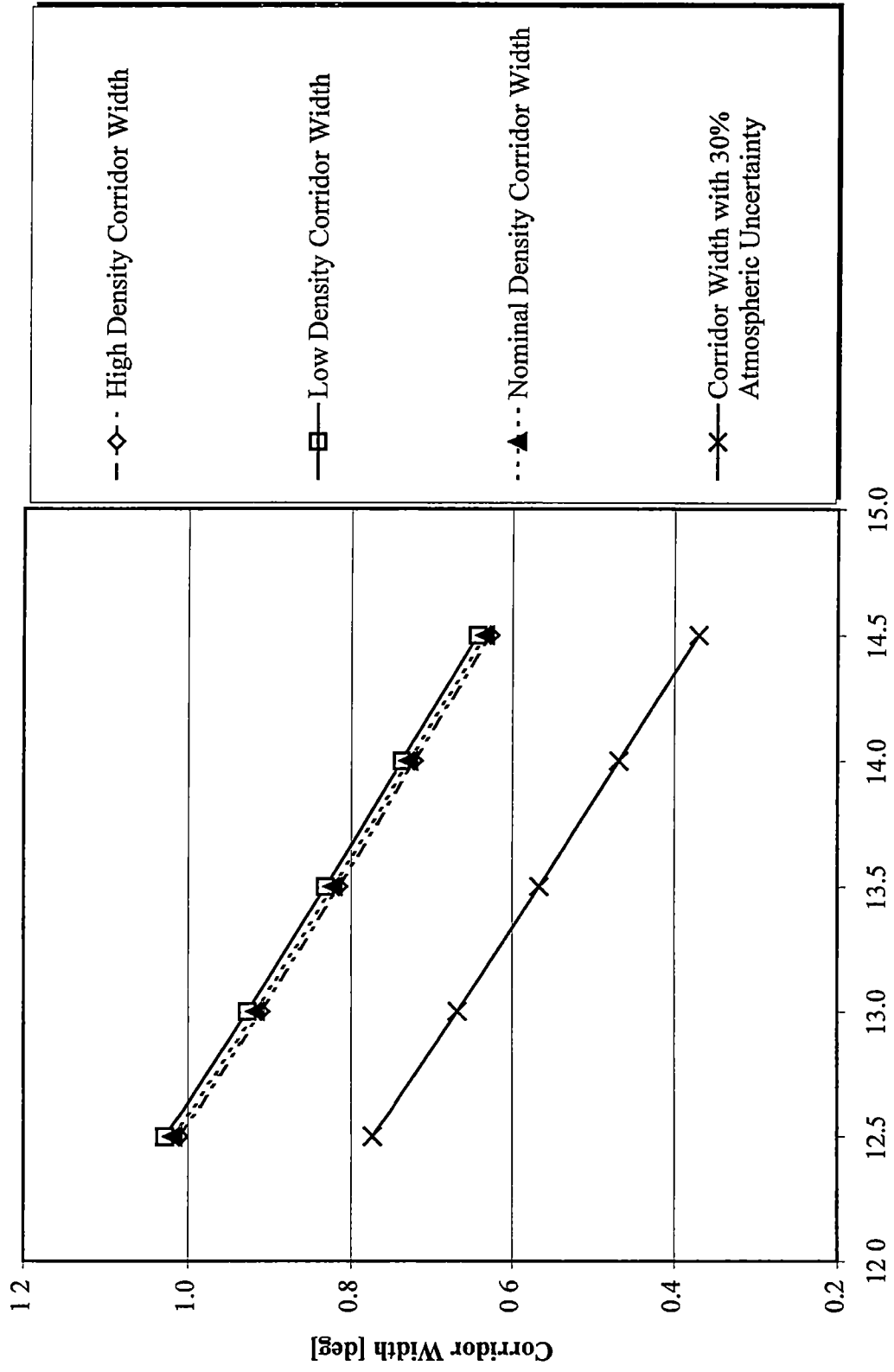
Figure 4-15. Effects of Atmospheric Dispersions on Entry Corridor Width

overshoot boundary of the low-density case. The overall result (also shown in Figure 4-15) is a narrower corridor than with a nominal density profile. This compounds the problems for the vehicle guidance system because the corridor must be wide enough to allow for vehicle aerodynamic and entry angle dispersions as well as the uncertainties in atmospheric density.

Section 4-4.   Deceleration Limit Study

As explained earlier, the crew returning to Earth will have been exposed to extended periods of low gravity on the Martian surface and zero gravity during the interplanetary transits. Therefore, the crew will have been physically deconditioned and may not have to ability to withstand high deceleration loads. The DRM typically calls for a 5-g constraint to be placed on all Earth return scenarios. However, in certain circumstances such as an aborted Mars landing, the crew may be subjected to extremely long periods of zero gravity without the benefit of living in the 3/8-g environment of Mars for 500 days. Therefore, it is possible that even the 5-g deceleration limit is not conservative enough to insure the safety of the crew under all contingencies. In accordance with this idea, a study was initiated to explore the effects on entry corridor width of a more stringent deceleration limit. Specifically, a 3 5-g deceleration limit was imposed on the Earth return aerocapture trajectories and the resulting entry corridor was examined

This study was carried out in the exact same manner as the study for the corridor with the 180 degree roll maneuver The roll rate was limited to 5 deg/s for the undershoot

trajectories, while the overshoot trajectories did not implement any type of bank angle modulation. The only constraint that was altered was that of the maximum deceleration which was allowed to be only 3.5-g instead of 5-g as before. The vehicle was still assumed to be entering in a due east equatorial fashion, and the oblate planet and nominal atmospheric models were still in place The undershoot and overshoot boundaries were determined in the same manner as before, and the resulting corridor width documented.

Table 4-10 shows the resulting exit conditions for both the undershoot and overshoot trajectories with the 3 5-g limit imposed. The exit conditions for the lower entry speeds are essentially the same as those found in the previous studies. In contrast, the higher entry speed cases resulted in vastly different exit conditions. The overshoot trajectories for entry speeds of 14.0 and 14.5 km/s did not allow for targeting of the nearly 407 km circular orbit. Instead, the 14.0 km/s entry speed case ended in a highly elliptical orbit while the 14.5 km/s entry speed case ended in a hyperbolic exit trajectory. The 14.0 km/s and 14.5 km/s overshoot trajectories had maximum decelerations of 3.5-g. The fact that the high-speed overshoot trajectories (which usually experience the lowest deceleration pulses) were limited by the maximum deceleration of 3.5-g indicates that the entry corridor has closed. Accordingly, POST was unable to target the constraints for the undershoot trajectories for the 14.0 km/s and 14.5 km/s entry speeds.

Figure 4-16 shows the undershoot and overshoot boundaries as defined in this study. Figure 4-16 shows that for entry speeds of 14 0 - 14.5 km/s, no undershoot boundary could be found (the corridor has closed) Figure 4-17 quantifies how the entry corridor narrows as entry speed is increased while the deceleration limit is set to 3.5-g. The corridor width quickly decreases to less than 0.5 degrees at an entry speed of 13.5

Table 4-10. Exit Conditions with 3.5-g Deceleration Limit Imposed

Undershoot Trajectories

Entry Speed [km/s]	Entry Angle [deg]	Troll [sec]	P2	Apoapse Altitude [km]	Periapse Altitude [km]	Period [min]	Exit Inclination [deg]	G-Max [g's]	Time to 407 km [s]
12 5	-6.033368958	56 8781670800	0 8741	421 022	115 491	89 659	1.2983	3.5002	2931 253
13 0	-6 081783411	50 4746174400	0 7210	419 780	115 565	89 647	1.2121	3 5001	2985 131
13 5	-6 095028584	43 8989134200	0 9414	421 439	115 471	89 663	1 0578	3 5012	2955 384
14 0	**** Corridor Closes ****								
14 5	**** Corridor Closes ****								

Overshoot Trajectories

Entry Speed [km/s]	Entry Angle [deg]	Troll [sec]	P2	Apoapse Altitude [km]	Periapse Altitude [km]	Period [mn]	Exit Inclination [deg]	G-Max [g's]	Time to 407 km [s]
12 5	-5 341691882	N/A	N/A	417 691	115 698	89 627	4 04E-04	2 458	3139 258
13 0	-5 491541151	N/A	N/A	417.694	115 697	89 627	4 04E-04	2 813	3141 534
13 5	-5 622541325	N/A	N/A	417 692	115 697	89 627	4 03E-04	3 184	3150 629
14 0	-5 735145516	N/A	0 2734	51059 466	87 166	946 684	8 48E-05	3 505	470 210
14 5	-5 818718468	N/A	0 8102	hyperbolic	85 982	hyperbolic	5.57E-05	3 509	345 244
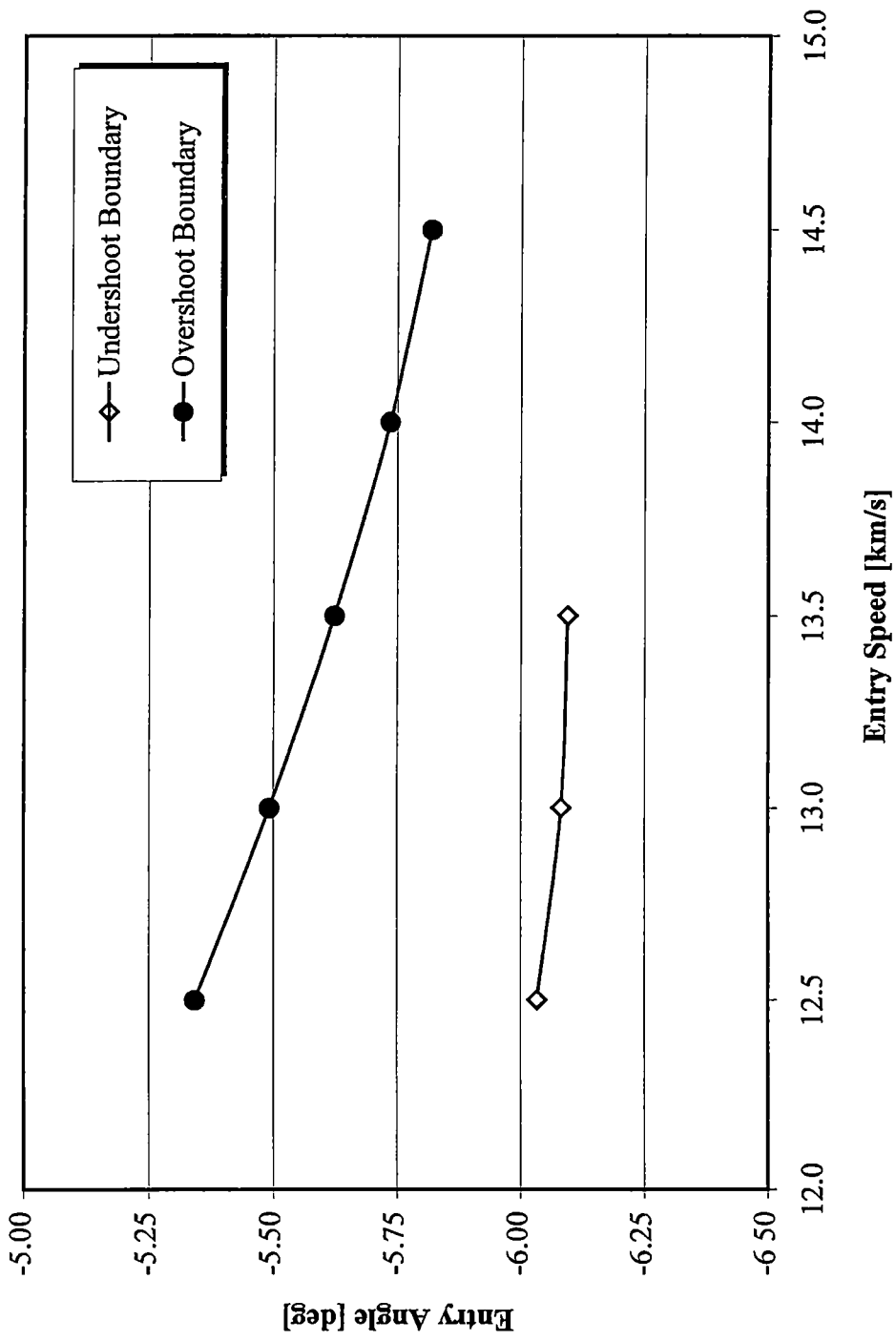
Figure 4-16. Corridor Boundaries Due to a 3.5-g Deceleration Limit
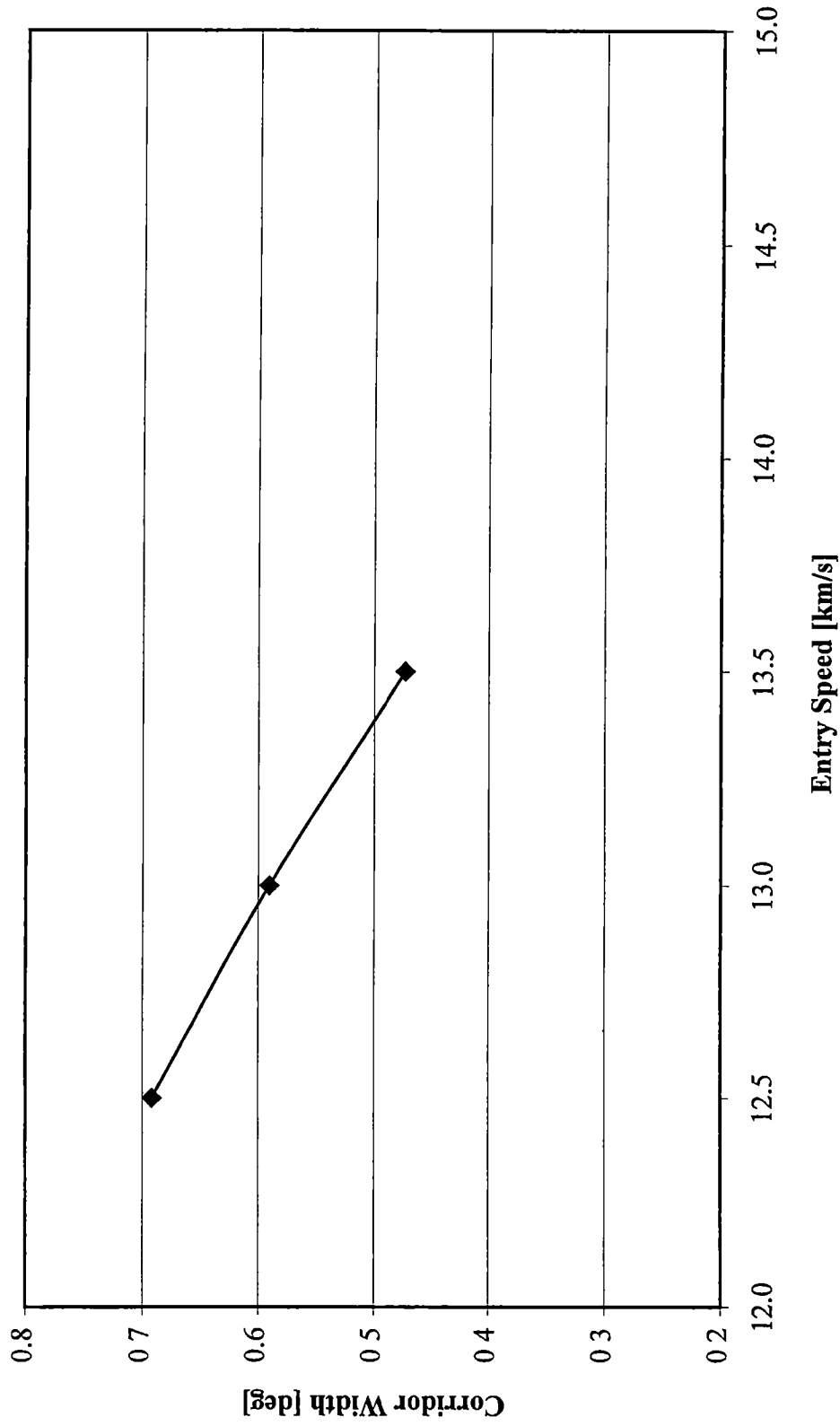
Transhab/Ellipsled Vehicle   Nominal Atmosphere   AOA = 45 deg/s   Roll Rate = 5 deg/s

Figure 4-17. Entry Corridor Width Due to a 3.5-g Deceleration Limit

Transhab/Ellipsled Vehicle   Nominal Atmosphere   AOA = 45 deg/s   Roll Rate = 5 deg/s

km/s. At entry speeds greater than 13.5 km/s the corridor is non-existent. This indicates that if a 3.5-g deceleration limit is indeed required, the Transhab/Ellipsled vehicle will be able to complete the aerocapture safely only at speeds up to 13.5 km/s.

Section 4-5.   Ballistic Coefficient Study

In addition to factors such as atmospheric density and deceleration limits, other parameters may affect the location and width of the entry corridor. The parameter known as ballistic coefficient is an example of this. The ballistic coefficient is defined in equation (1) as [19]:

$$\frac{m}{C_d \bullet A} \qquad (1)$$

where: m = mass of vehicle [kg]

C_d = coefficient of drag [dimensionless]

A = reference area of vehicle [m^2]

The ballistic coefficient reflects how far into the atmosphere a body must pass to decelerate a given amount. The ballistic coefficient, using the standard vehicle properties and aerodynamics, was calculated to be 216.4 kg/m^2.

Changes to the vehicle mass, reference area, or coefficient of drag will lead to changes in the ballistic coefficient. The simplest way to analyze the effects of ballistic coefficient on the entry corridor is to control the ballistic coefficient by adjusting the vehicle mass. It is also of interest to note that during actual mission planning, the vehicle mass often varies significantly as the design goes from the early to final stages. Therefore, the vehicle mass was altered to allow the vehicle to have a ballistic coefficient of 50%, 75%, 100%, 150%, and 200% of the nominal value of 216.4 kg/m^2. Table 4-11 shows the values of the ballistic coefficient used for this study. Table 4-11 also details how the vehicle mass was changed to affect the ballistic coefficient. Alternatively, modifying the CD or reference area can change the ballistic coefficient as well. However, this would involve a reshaping and resizing of the Transhab/Ellipsled and such a vehicle modification is beyond the scope of this study.

In the interest of time, this study only included three entry speeds: 12.5, 13.5, and 14.5 km/s. For all cases, the vehicle being analyzed was the Transhab/Ellipsled vehicle with the nominal aerodynamics discussed earlier in this thesis. As before, all entries were assumed to be due east, equatorial entries and the atmosphere was modeled as the 1976 U.S. Standard Atmosphere. The 5-g deceleration limit was imposed on these simulations The undershoot and overshoot boundaries were found by allowing POST to perform a targeting routine on the trajectories. The undershoot boundaries were found with the implementation of a 180 degree roll maneuver performed at a roll rate of 5 deg/s. The implementation of the bank angle change helped in targeting the desired 407 km apoapse altitude. The overshoot boundaries were obtained using the POST targeting routine as

Table 4-11. Summary of Ballistic Coefficients and Corresponding Vehicle Mass

Ballistic Coefficient [kg/m^2]	Coefficient of Drag [dimensionless]	Vehicle Reference Area [m^2]	Vehicle Mass [kg]
104.661	1.4445	84.348528	12752.05
156 991	1.4445	84.348528	19128 01
209 321	1.4445	84.348528	25503.97
313.981	1.4445	84.348528	38255.90
418.642	1.4445	84.348528	51007.95

well. The only constraint placed on the overshoot boundaries was that of the apoapse altitude.

Figure 4-18 shows corridor width as a function of entry speed for the range of ballistic coefficients studied. As Figure 4-18 clearly shows, ballistic coefficient has only a minimal influence over entry corridor width for the Ellipsled vehicle. Figure 4-19 shows the information in another way by plotting entry corridor width versus ballistic coefficient for the range of entry speeds analyzed. Again, it should be obvious that a relatively large change in ballistic coefficient causes very small changes in corridor width. While ballistic coefficient appears to have little affect on entry corridor *width*, there may be a more significant affect on the location of the corridors as defined by the undershoot and overshoot boundaries. Figure 4-20 explains this idea. Figure 4-20 shows the undershoot and overshoot boundaries plotted as a function of ballistic coefficient for the range of entry speeds considered in this study. The figure reveals that ballistic coefficient significantly changes the location of both the undershoot and overshoot boundaries. This relates well to the large displacements of the entry corridors due to atmospheric dispersions previously discussed. The location of the entry corridor in itself is not a concern of major importance as long as the guidance system can navigate the vehicle safely through the corridor. Therefore, while this study has revealed changes in the location of the entry corridor due to ballistic coefficient, the corridor remains relatively unchanged from a width standpoint.
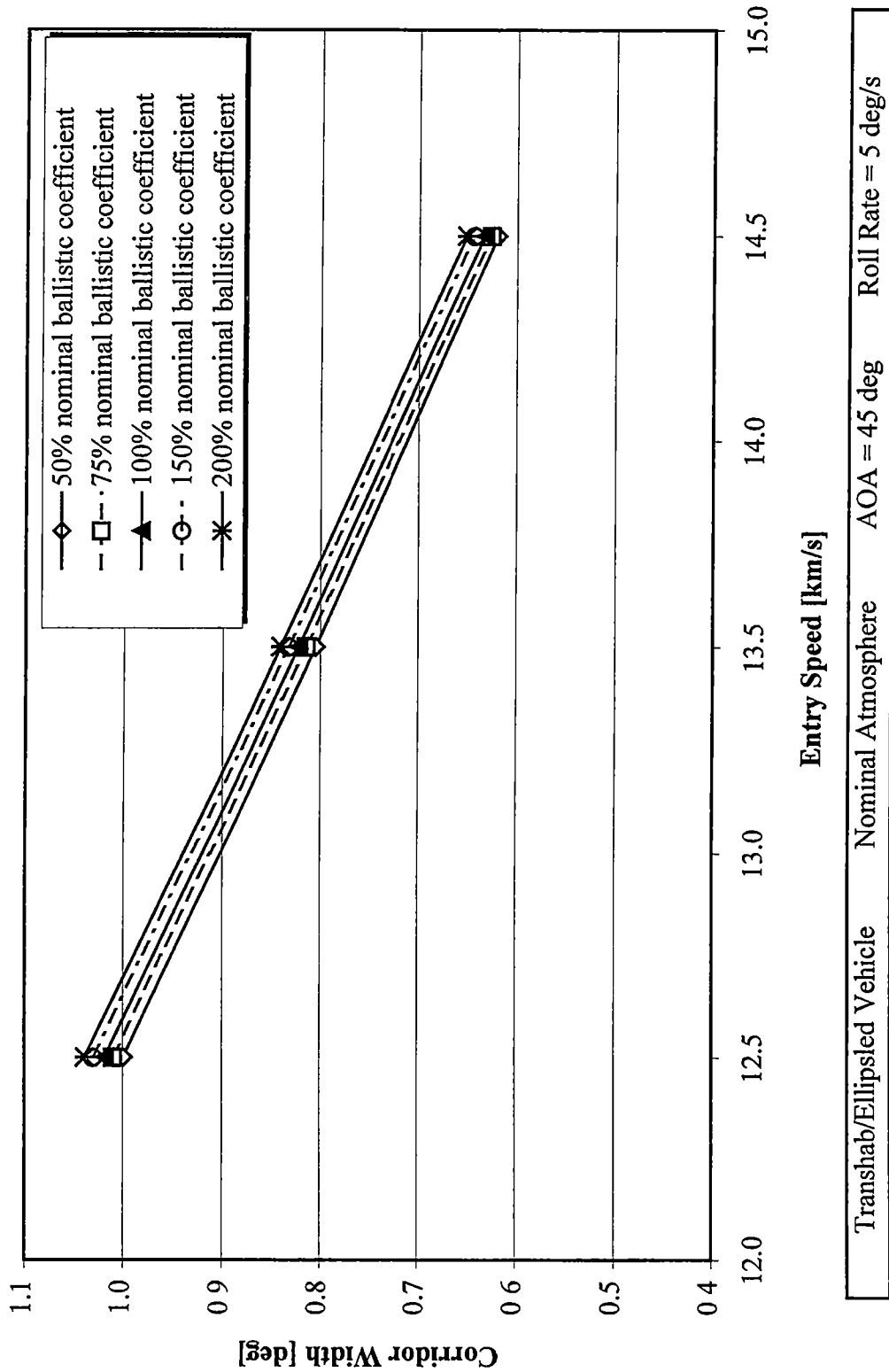
Figure 4-18. Entry Corridor Width as a Function of Entry Speed and Ballistic Coefficient

Figure 4-19. Entry Corridor Width vs. Ballistic Coefficient
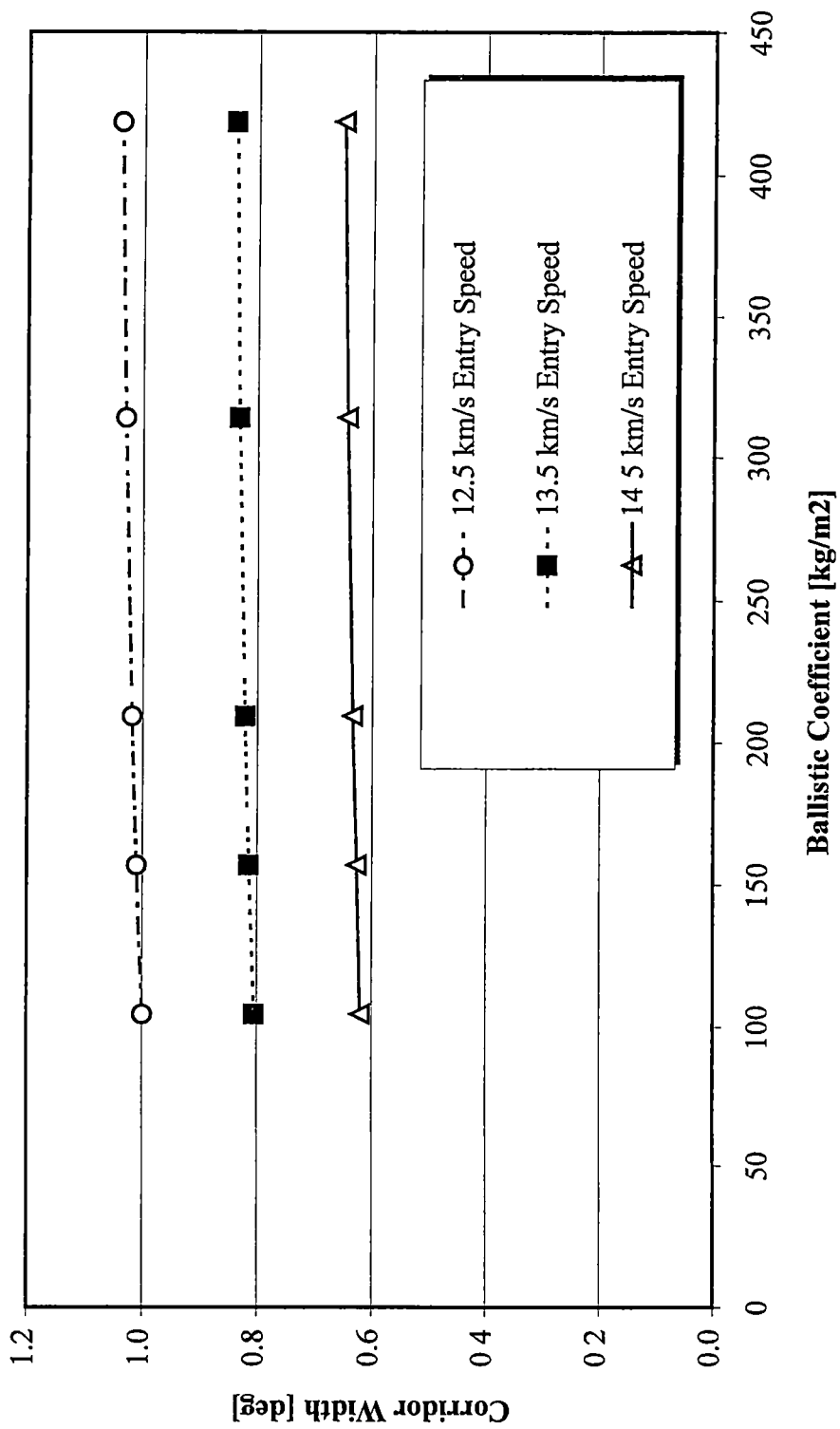
Transhab/Ellipsled Vehicle   Nominal Atmosphere   AOA = 45 deg   Roll Rate = 5 deg/s
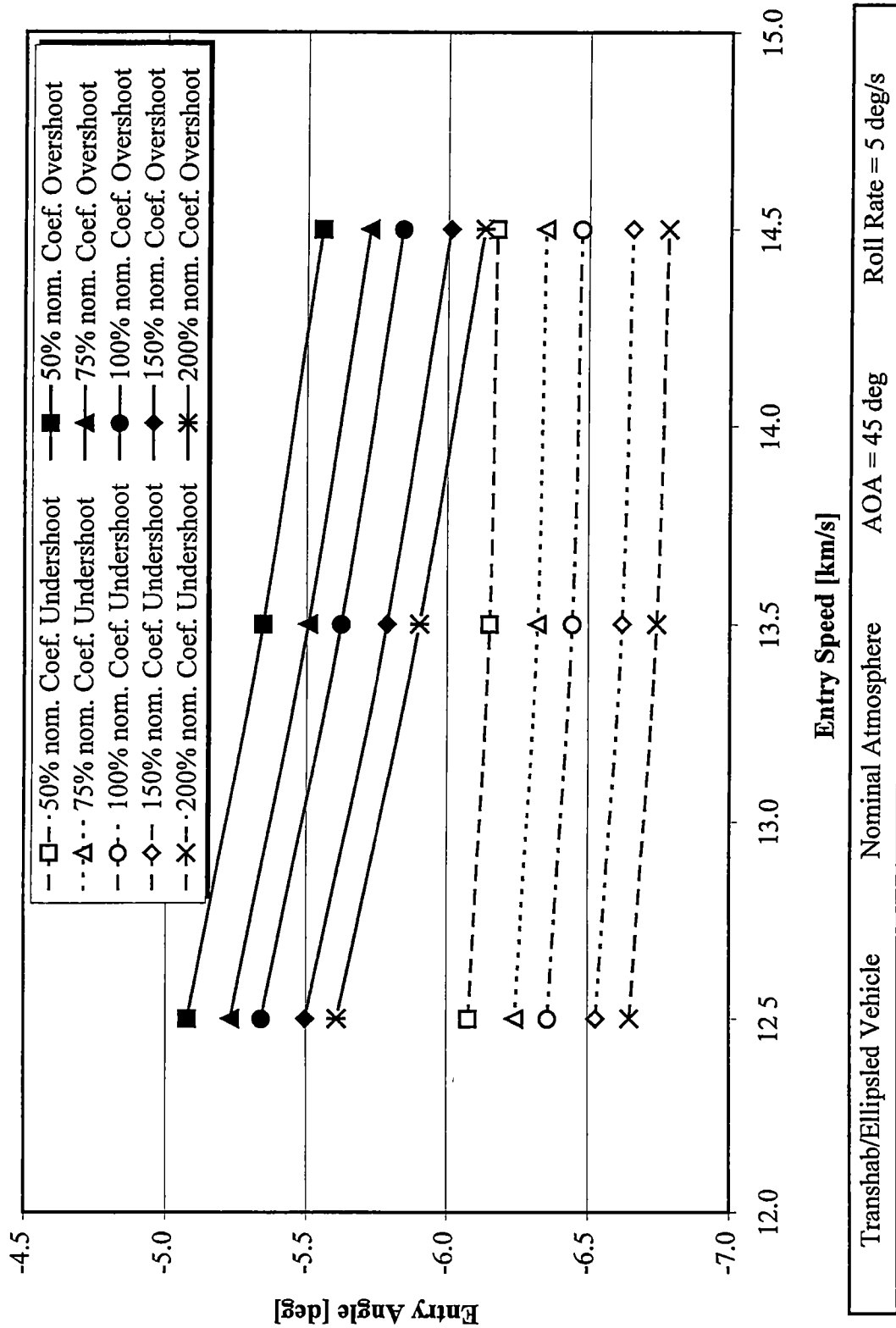
Figure 4-20. Corridor Boundaries as a Function of Ballistic Coefficient

Transhab/Ellipsled Vehicle   Nominal Atmosphere   AOA = 45 deg   Roll Rate = 5 deg/s

Section 4-6. Heating Rate Analysis

As mentioned earlier, the atmospheric heating rates experienced by any entry vehicle may be a constraining factor in mission design and planning. First, atmospheric heating must be taken into account because of the inherent dangers to the crew. Secondly, atmospheric heating often requires a considerable mass to be allocated to thermal protection systems (TPS). Estimating atmospheric heating rates and total integrated heat loads allows the mission planner to determine the type of TPS needed and the mission mass that must be devoted to the TPS.

For entry speeds below about 11 km/s, convection plays the dominant role in the total heating rate experienced by the vehicle. However, for very high speed entries such as those analyzed in this paper, radiative heating effects become significant and sometimes become the dominant form of heating. Therefore, this section will address the issue of both convective and radiative heating effects. Only the stagnation point heating was analyzed; no centerline or off-centerline heating effects were considered in this analysis. In addition, an estimate of the total integrated heat load on stagnation point was made.

The heating analysis discussed in this section was performed only for the Transhab/Ellipsled vehicle and used the nominal atmospheric density profile to examine both the undershoot and overshoot trajectories. The calculations used the cold wall assumption, effectively causing the predicted heating rates to be conservative in nature In flight, the driving temperature gradient would be smaller, thereby reducing the actual heating rates to some degree. In addition, the undershoot trajectories analyzed here

included the 5 deg/s roll maneuever to target the 407 km circular orbit. The other constraints, such as the 5-g deceleration limit, remained in place as well.

4-6.1 Radiative Heating Rates

The radiative heating effects experienced by the Transhab/Ellipsled vehicle were calculated using a bi-variant table lookup procedure in POST. The data needed to create the bi-variant heating rate table in POST was taken from Sutton *et al* [20]. First, heating rates were interpolated from the data for a nose radius of 6.7 meters. Next, the heating rates were input to POST as a function of both density and atmospheric relative velocity. A zero heating rate was specified at extremely low densities (altitudes above 84 km) and speeds below 9 km/s to insure that POST did not extrapolate heating rates incorrectly. The implementation of these modifications had no significant effect on the maximum stagnation point heating rate or the total integrated heat load. POST was then able to interpolate or extrapolate as necessary to find the heating rate at each time step throughout the trajectory.

Figure 4-21 shows the results of the radiative heating analysis. The figure clearly indicates the maximum radiative heating rates experienced by the Transhab/Ellipsled vehicle as a function of entry speed. As a comparison, the Apollo capsules experienced total heating rates ranging from 300 - 500 W/cm^2 [11]. Clearly, the Transhab/Ellipsled vehicle experiences significantly higher heating rates merely from radiative heat transfer. This is primarily due to the higher entry speeds the Transhab/Ellipsled vehicle
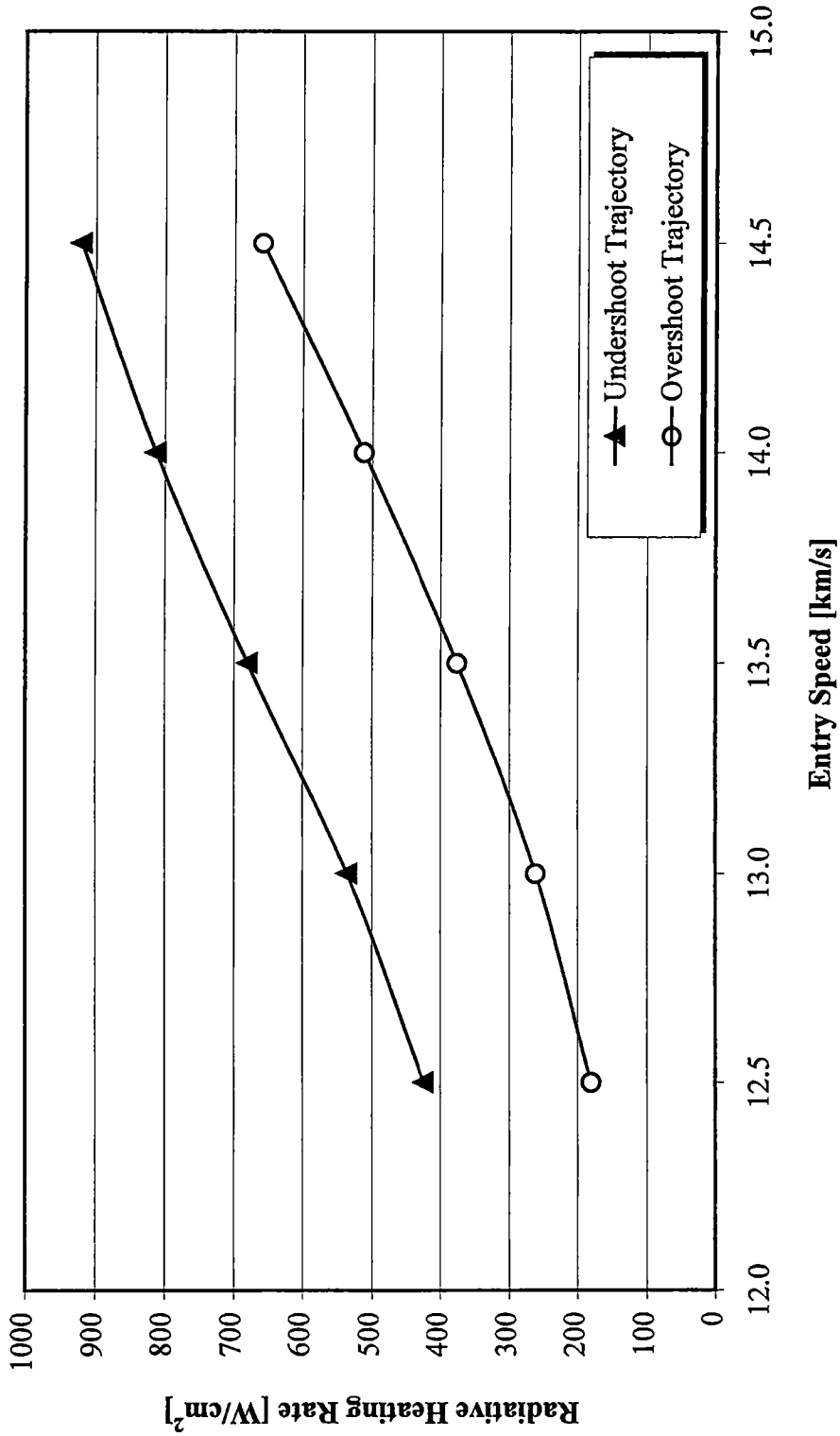
Figure 4-21. Maximum Stagnation Point Radiative Heating Rates on the Transhab/Ellipsled Vehicle

experiences. A secondary factor in the heating rates is the large nose radius of the vehicle.

4-6.2 Chapman Convective Heating Rates

As stated earlier, convetive heating is often the dominant form of aerodynamic heating for vehicles entering the atmosphere at 11 km/s or less. Even though radiative heating is the dominant form of heating for the Transhab/Ellipsled vehicle, convective heating nevertheless will contribute significantly to the total heating rate and integrated heat load.

To analyze the effects of convective heating on the Transhab/Ellipsled vehicle, a POST subroutine was called upon in the input deck. POST has a built-in routine to calculate laminar, convective heating rates at the stagnation point of the vehicle using the Chapman heating rate equation (2) shown below [16].

$$q'' = \frac{17600}{\sqrt{r_n}} \left(\frac{\rho}{\rho_{SL}} \right)^{1/2} \left(\frac{V_A}{26000} \right)^{3.15} \left(10^{-4} \right) \qquad (2)$$

where: q'' = laminar convective stagnation point heating rate [W/cm^2]

r_n = nose radius of the vehicle or body [m]

ρ = local atmospheric density [kg/m^3]

74

ρ_{SL} = sea level atmospheric density [kg/m³]

V_A = atmospheric relative velocity [m/s]

The Chapman heating rates were thus calculated in POST and output along with the other trajectory parameters such as altitude, velocity, time, etc. Figure 4-22 shows the results of the convective heating analysis. The maximum Chapman heating rates experienced by the Transhab/Ellipsled vehicle are shown as a function of entry speed for both the undershoot and overshoot trajectories. Again, note that only the nominal atmospheric density model was considered.

Now that both the convective and radiative heating effects have been discussed separately, it is possible to look at the overall heating rate experienced by the vehicle. Figure 4-23 shows the maximum convective, radiative, and total heating rates experiences by the Transhab/Ellipsled vehicle over the range of entry speeds considered. As Figures 4-21 and 4-22 showed, the maximum heating rates occur during the undershoot trajectory. Thus, only the undershoot heating rates have been plotted in Figure 4-23. The figure makes it clear that while the radiative heating is the dominant form of heat transfer, the convective heating contributes approximately 25 % of the total heating rate.

Figure 4-24 is a plot of the radiative, convective, and total heating rates as a function of time for the 13.5 km/s entry speed undershoot cases. The overall effects of the two modes of heat transfer remains clear The radiative heating effects dominate by supplying about 75% of the total heat pulse. The total peak stagnation point heating rates range from 280 W/cm² to 1124 W/cm² for the Transhab/Ellipsled vehicle.
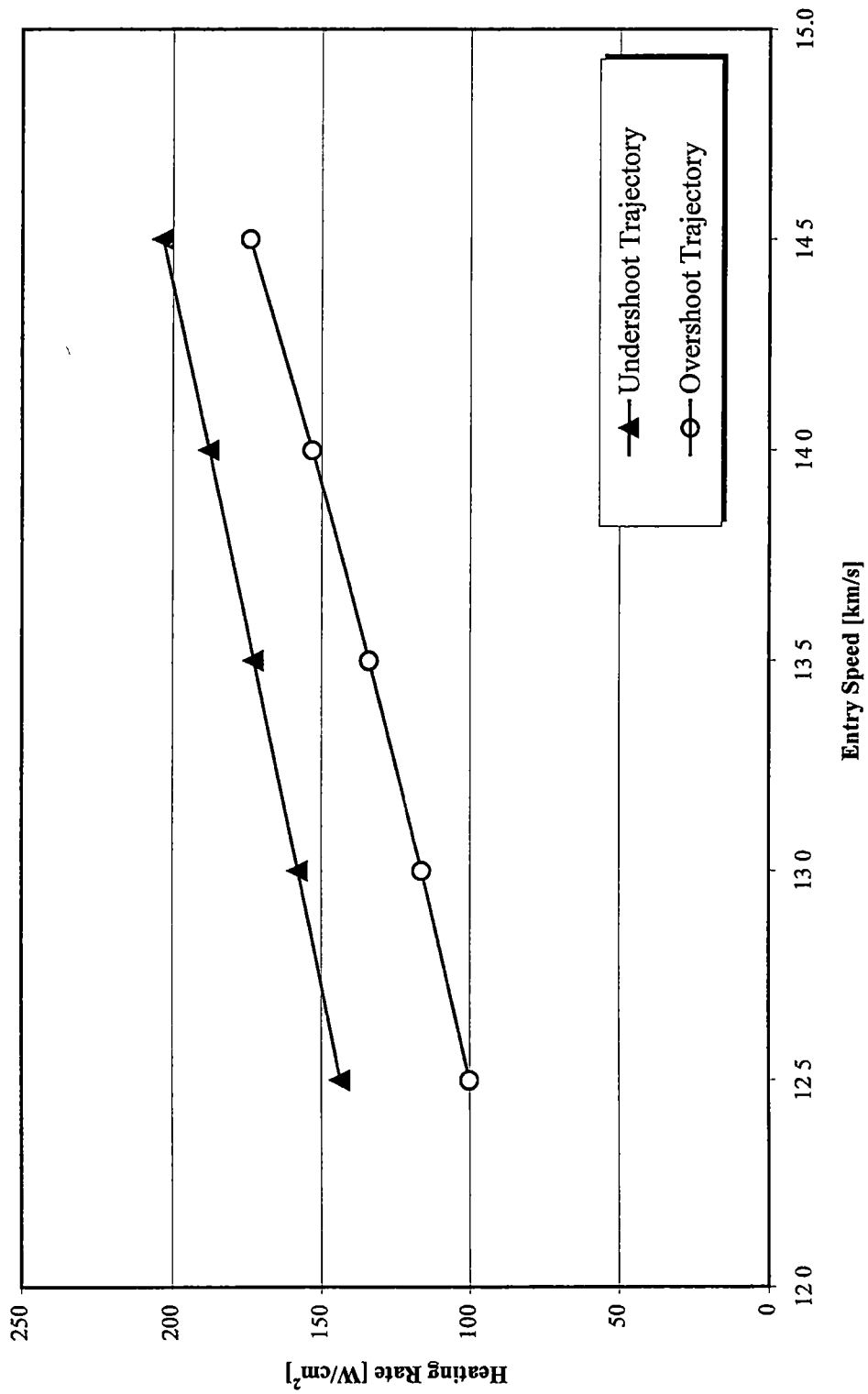
Figure 4-22. Maximum Stagnation Point Chapman Convective Heating Rates
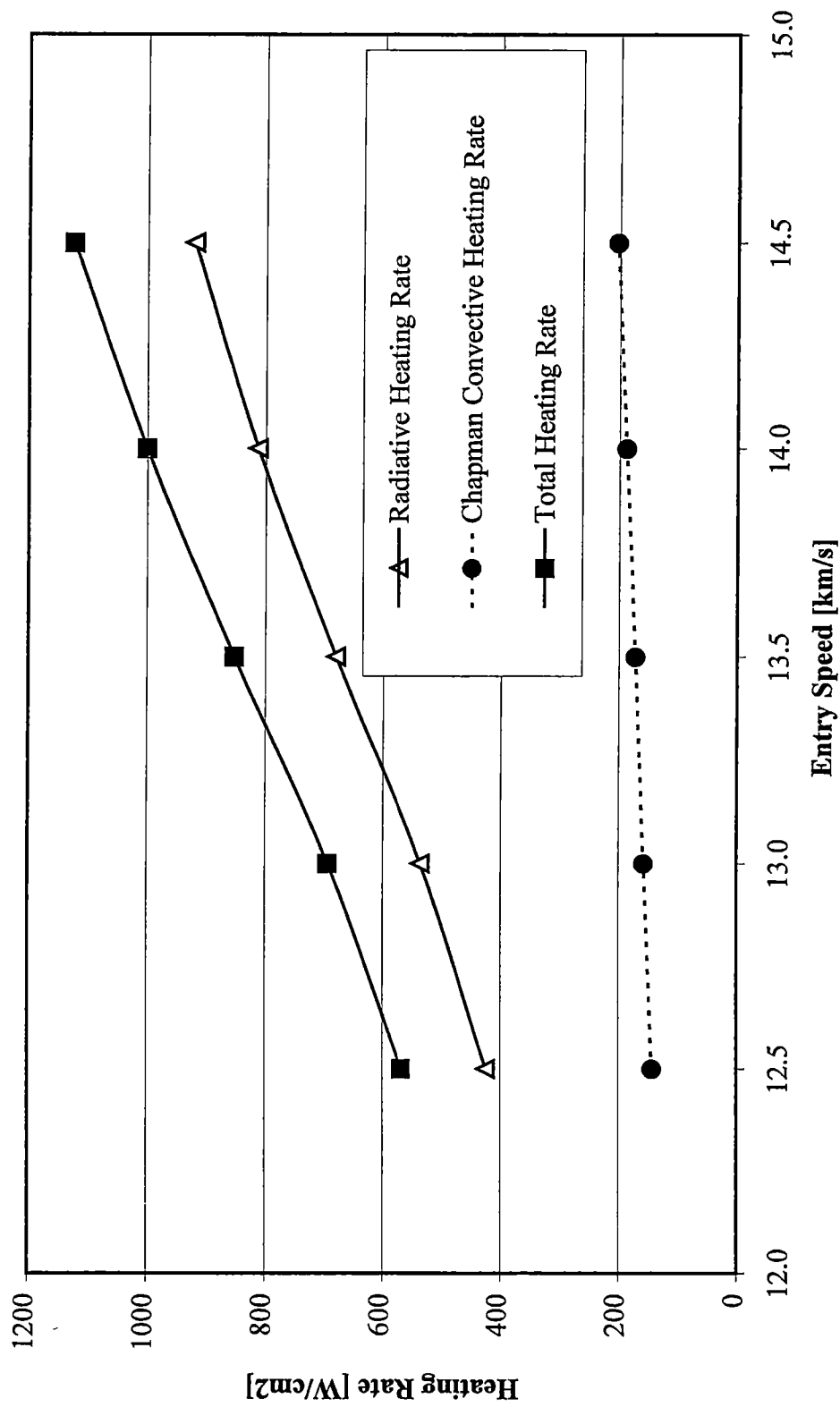
Figure 4-23. Maximum Stagnation Point Heating Rates Experienced by the Transhab/Ellipsled Vehicle
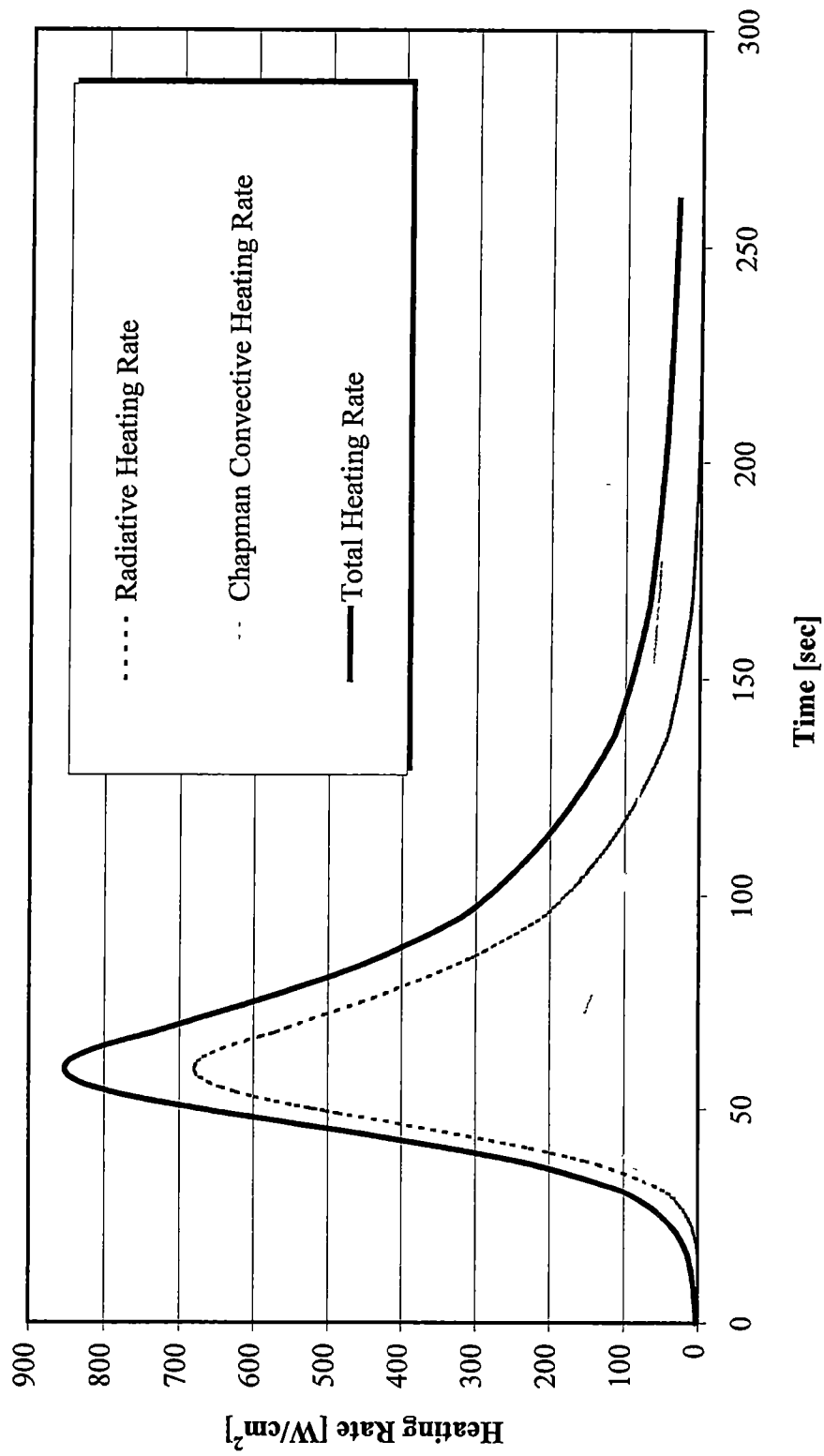
Figure 4-24. Heat Pulses for the 13.5 km/s Entry Speed Undershoot Trajectory

Transhab/Ellipsled Vehicle   Nominal Atmosphere   AOA = 45 deg   Roll Rate = 5 deg/s

Heating rates of this magnitude far exceed the limits of currently available radiatively cooled materials such as Space Shuttle tiles and will almost certainly require the TPS to be of the ablator family [12]. Ablating heat shields have been made from a variety of materials including graphite, carbon-phenolic, phenolic-nylon, silica-phenolic, silicone elastomers, and ceramics [12].

4-6.3 Total Integrated Heat Loads

The heating rates analyzed in the previous two sections are extremely important for the selection of the type of TPS to be used on the vehicle. However, merely selecting the proper TPS is not enough. The TPS must also be "sized". Sizing involves the determination of the amount, usually denoted by thickness, of a given TPS that is required to protect the vehicle. The primary factor that affects the sizing of the TPS is the total integrated heat load.

The total integrated heat load is calculated by simply integrating the heating rate pulse over the time of the trajectory. The total heat load quantifies the total amount of heat that the vehicle must "absorb" during the trajectory. Some vehicles may experience extremely high heating rates for short periods of time. This type of trajectory can yield relatively low total heat loads even thought the maximum heating rate may be very high. On the other hand, some vehicles may experience relatively low heating rates over a very long period of time. In those cases, the total integrated heat loads can be quite large even though the heating rates are very modest in size. Therefore, an analysis of both heating

rate and total heat load are needed for a complete TPS design. While this paper does not go into the TPS sizing, some estimates of the total heat load were made.

First, the radiative and convective heating rates were determined as explained in the previous sections. Next the total heating rates were calculated using a spreadsheet. Finally, the total heating rate was integrated over the atmospheric flight portion of the trajectories. Figure 4-25 shows the total heat loads experienced by the Transhab/Ellipsled vehicle over the range of entry speeds.

Section 4-7.   Inclination Minimization and Orbit Circularization

The resulting orbits from the many simulations completed during this research were meant to approximate the desired 407 km circular orbit. The first step in this approximation was to target an apoapse altitude of nearly 407 km. A tolerance of +/- 15 km for the apoapse constraint was deemed suitable for this preliminary study. The results shown thus far in this paper should offer adequate evidence that the apoapse was targeted in this manner. The resulting orbits typically had periapse altitude of around 115 km and orbital periods of approximately 89.6 minutes.

While the apoapse and periapse altitudes were nearly identical for all the simulations, the inclination changes ranged from 0 to 1.75 degrees depending on the type of trajectory being flown and whether or not a roll maneuver of some kind was implemented. For the untargeted undershoot boundaries and all of the overshoot boundaries, the exit inclinations were very small because no roll maneuver was performed. However, in the undershoot trajectories where a roll maneuver was

Figure 4-25. Total Integrated Stagnation Point Heat Loads for the Transhab/Ellipsled Vehicle
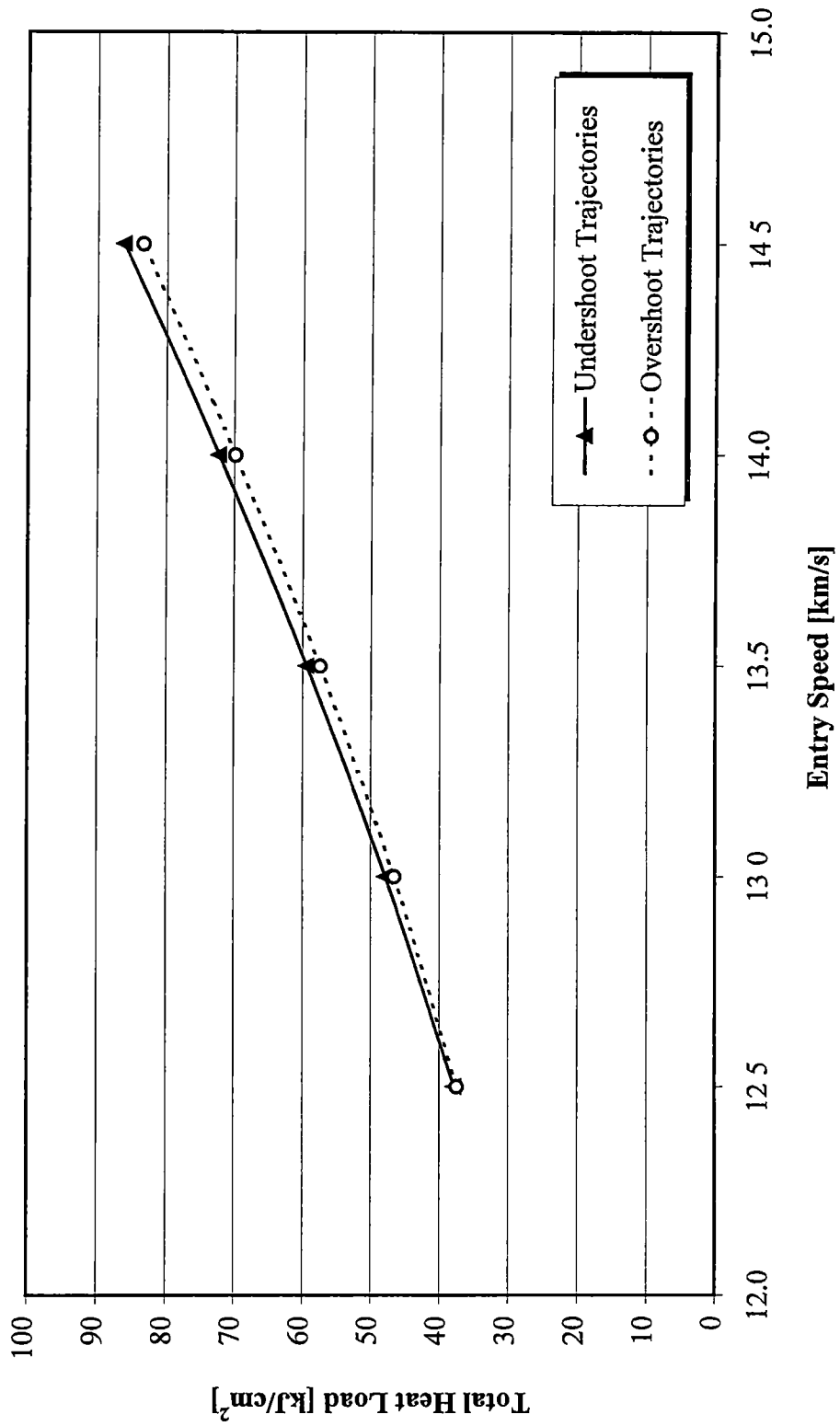
Transhab/Ellipsled Vehicle   Roll Rate Limit = 5 deg/s   Nominal Atmosphere   AOA = 45 deg

incorporated, exit inclinations were on the order of 1.5 – 2.0 degrees. The reason for such large inclinations is that the lift vector rolls with the vehicle, thus pulling the vehicle away from the original inclination

The studies detailed previously in the document show that the Transhab/Ellipsled vehicle appears to be suitable for use during the aerocapture procedure for the range of entry speeds considered. However, proper mission planning requires a "bigger picture" view. Thus it was decided to examine the problems that the inclination change and orbit circularization may have on the overall mission design. Specifically, the propellant required for these two maneuvers is of major importance. These two factors will be addressed separately in the following sections.

4-7.1 Inclination Minimization

The inclination changes seen previously in Table 4-5 are due to the lift vector changing direction while the vehicle is performing the roll maneuver needed to target the desired orbit. Changes in orbital inclination are usually very undesirable because of the large cost required to correct them. The large inclination change can be corrected in two ways. First, the guidance system could implement some sort of roll reversal which would help minimize the inclination change. This is usually the preferred method because it is assumed that the propellant requirements for such a maneuver are less than for the traditional means of correcting inclination. The second option is to perform propulsive burns after the vehicle has left the atmospheric flight portion of the trajectory. Sometimes, the roll reversal technique simply cannot eliminate the inclination change while still targeting the desired orbit and meeting other constraints. In those cases, a

propulsive burn of some kind is necessary which adds to overall mission mass and weight estimates. A thorough analysis should reveal which of these two methods, or perhaps a combination of the two methods, provide the largest mass savings. Using propulsive means to change inclination is often very costly. Equation (3) below shows the velocity increment (ΔV) needed to change the inclination propulsively by Δi degrees [21].

$$\Delta V = 2V \sin \frac{\Delta i}{2} \tag{3}$$

where: ΔV = velocity increment to change inclination [m/s]

V = circular velocity [m/s]

Δi = inclination change [deg]

Thus, to correct for an inclination change of approximately 1.5 degrees at a speed of 7.5 km/s, a velocity increment of about 200 m/s would be required. When coupled with the ΔV needed to circularize the orbit, the overall propellant mass may become prohibitively large if the inclination is minimized in this way.

Therefore, it was determined that use of bank angle modulations might offer the best solution to the inclination problem because such a technique may require less propellant than conventional solutions. Thus, if the inclination change could be corrected for by the simple use of lift vector control through bank angle modulations, the total

83

propellant usage might be reduced. Of course, an investigation into the propellant requirements for the roll maneuvers would be needed to verify this theory.

The approach used to minimize inclination change was one that allowed POST to determine the times and magnitudes of the bank angle modulations. Several events were added to the POST input deck that allowed the program to select the initial bank angle, time to begin each roll, the roll rate, and the time to pause between roll maneuvers This architecture allowed POST a lot of freedom to target the orbit and meet the other constraints. The constraints that were imposed were similar to those used earlier (specifically the constraints were a roll rate limit of 6 deg/s, a deceleration limit of 5-g, and a target apoapse altitude of approximately 407 km). The roll rate limit was increased from 5 deg/s to 6 deg/s to make the inclination change minimization easier for POST. It should be noted that a small increase in roll rate limit would require a slight sizing adjustment to the thrusters, but sizing changes of this magnitude are normal in mission design work. An additional constraint on periapse altitude was incorporated into the simulation as well. This constraint forced the periapse altitude to be greater than 30 km. The addition of this constraint was necessary to make sure that the inclination minimization did not take place at the expense a higher ΔV to raise the periapse. If the periapse is lowered, then the ΔV needed to raise the lower periapse could outweigh the ΔV saved by minimizing the inclination change. The simulations maintained the other basic entry conditions used in previous studies such as nominal atmospheric profile, due east equatorial entries, and nominal vehicle aerodynamics. However, to examine the possibility of reducing the inclination, the simulations were performed for mid-corridor trajectories Mid-corridor trajectories were chosen because they offer the most flexibility

for POST to target the desired orbit while maintaining a small inclination change. Choosing a mid-corridor trajectory is also relevant for the fact that the "nominal trajectory" flown by most entry vehicles is typically near the mid-corridor point. Table 4-12 shows the resulting exit conditions for the 12.5 km/s trajectory with and without the inclination minimization routine in place. Clearly, the inclination listed for the mid-corridor case is much smaller than the 1.75 degree inclination that was obtained in the undershoot studies. The inclination change for the mid-corridor trajectory is about 0 4 degrees which requires a ΔV of 54 m/s to correct. This is approximately 25% of the ΔV needed to correct the inclinations from earlier undershoot simulations. Further work should be done to examine the possibility of reducing the inclination change at the higher entry speed cases.

4-7.2 Orbit Circularization

The previous section demonstrated that inclination changes may cause significant increases in ΔV required to correct the post-aerocapture orbit. Similarly, the ΔV needed to circularize the orbit after the aerocapture can add a large propellant requirement to the mission design. Therefore, the ΔV needed to circularize the orbits found in these studies was calculated. The orbit circularization maneuver was assumed to take place in two phases. First, a propulsive burn would be performed to raise the periapse out of the atmosphere to an altitude of 407 km. This burn would be done at the apoapse. Next, a burn at the periapse would be required to correct the apoapse altitude to 407 km. Both of

85

Table 4-12. Exit Conditions for Various 12.5 km/s Entry Speed Trajectories

Type of Trajectory	Entry Angle [deg]	Apoapse Altitude [km]	Periapse Altitude [km]	Period [min]	Exit Inclination [deg]	G-Max [g's]	Time to 407 km [s]
Undershoot	-6 360070138485	421 93	115 42	89 667	1.7698	4.9999	2874 481
Overshoot	-5 341691881600	417 691	115 698	89 627	4 04E-04	2 458	3139.258
Mid-Corridor	-5.842374087987	418.986	115.469	89 6380	0.3998	2 9816	3001 701

86

these maneuvers were done using the efficient Hohmann transfer method. The Hohmann transfer method basically requires the orbital velocities to be known at the position of the vehicle in the current orbit and in the target orbit. The energy equation (4) shown below describes all orbits [21].

$$E = \frac{V^2}{2} - \frac{\mu}{r} = -\frac{\mu}{2a} \qquad (4)$$

where: E = energy of the orbit [km^2/s^2]

V = velocity [km/s]

μ = gravitational parameter [for Earth μ = 3.989x10^{11} km^3/s^2]

r = orbital radius [km]

a = semi-major axis [km]

The above equation can be solved for velocity which results in the following equation:

$$V^2 = \mu \left(\frac{2}{r} - \frac{1}{a} \right) \qquad (5)$$

The velocity equation above can be used to calculate the velocity of the vehicle at any given point in the orbit. This in turn allows the ΔV's needed to transfer between orbits to

be calculated. Once the ΔV's were obtained, the propellant mass for each burn was calculated using a form of the rocket equation (6) as shown below [22]:

$$\Delta V = I_{sp}\, g\, \ln\left(\frac{m_o}{m}\right) \qquad (6)$$

where: I_{sp} = specific impulse of the engine [sec]

g = acceleration due to gravity [for Earth $g = 9.80665$ m/s^2]

m_o = initial mass of the vehicle [kg]

m = final mass of the vehicle [kg]

For the propellant calculations in this paper, calculations for specific impulses (I_{sp}) of 320, 370, and 445 seconds were completed. By solving the rocket equation for the final mass, the propellant needed for the ΔV can be determined by simply subtracting the final mass from the initial mass.

Table 4-13 shows a summary of the ΔV's needed to circularize the orbit and the propellant requirements as well. Table 4-13 also shows the ΔV and propellant needed to return the inclination to zero degrees. From the three maneuvers summarized in Table 4-13, it is obvious that the propulsive burn needed to change the inclination typically requires the largest ΔV, and subsequently, the most propellant. In fact, this one maneuver accounts for approximately 70% of the total ΔV and propellant needed to correct the orbit

Table 4-13 Typical ΔV and Propellant Requirements to Correct Orbit

Type of Trajectory	Apoapse Altitude [km]	Periapse Altitude [km]	Exit Inclination [deg]	ΔV to Raise Periapse [m/s]	ΔV to Correct Apoapse [m/s]	ΔV to Correct Inclination [m/s]	Total ΔV for Orbital Correction [m/s]
undershoot (12 5 km/s)	421 930	115 420	1 7698	84 602	-4 212	236 830	325 643
overshoot (12 5 km/s)	417 691	115 698	4 04E-04	84 533	-3 017	0 054	87 604
mid-corridor (12 5 km/s)	418 986	115 469	0 3998	84 597	-3 382	53 502	141 481

Propellant Required

Type of Trajectory	I_{sp} = 320 sec [kg]	I_{sp} = 370 sec [kg]	I_{sp} = 445 sec [kg]
undershoot (12 5 km/s)	2514	2189	1834
overshoot (12 5 km/s)	702	608	507
mid-corridor (12 5 km/s)	1124	975	814

89

when no inclination change minimization is performed. However, in mid-corridor trajectories, the exit inclinations change much less. For the 12.5 km/s entry speed mid-corridor case in which the inclination was minimized, the ΔV needed to correct the inclination was only about 25% of the total ΔV. In pure overshoot trajectories, inclination change is essentially zero and does not add to the total ΔV significantly.

Second in importance is the ΔV needed to raise the periapse out of the atmosphere. The ΔV required to raise the periapse to a 407 km altitude from a 115 km altitude is approximately 85 m/s. It may be possible to reduce the total ΔV even more if the periapse could be raised by some bank angle modulation method. Both the inclination and periapse corrections could possibly be done using bank angle modulations. The reduction of the ΔV associated with these two orbital corrections could drastically cut the total propellant usage if the bank angle modulations do not require an excessive amount of propellant.

Chapter 5

Apollo Comparison

A short study was deemed necessary to investigate the benefits, or drawbacks, of using the Transhab/Ellipsled vehicle over the Apollo derived vehicle. For the Apollo comparison, undershoot and overshoot boundaries were determined and the resulting corridors documented. The Apollo derived vehicle is described in more detail in Chapter 2; however some brief comments should be made here. First of all, the vehicle was assumed to have constant angle-of-attack and aerodynamic coefficients for all of the simulations presented here. Similarly, all simulations were carried out using the nominal density profile as described by the 1976 U.S. Standard Atmosphere table. All entries were assumed to be due east and equatorial in nature as well.

The undershoot boundaries were determined using a 180 degree bank angle change to target the desired orbit. The roll rate for the bank angle changes was set to 5 deg/s for all cases A maximum 5-g deceleration was the limiting factor imposed on the undershoot boundaries The overshoot boundaries were found by targeting the desired orbit as was done in the Transhab/Ellipsled studies. By defining the boundaries in these ways, an easy comparison can be made between the two vehicles from an entry corridor perspective. In the Apollo cases, the simulations were once again completed using the POST projected gradient targeting routine The use of the projected gradient algorithm

decreased solution time, while achieving the same or better accuracy than any manual iterative scheme could obtain.

Table 5-1 summarizes the exit conditions for the undershoot trajectories of the Apollo derived vehicle. Notice that the orbital parameters, such as apoapse and periapse altitude, are virtually the same as those found for the Transhab/Ellipsled vehicle. The similarities indicate that the same orbit is being targeting for both vehicles. Table 5-2 is the corresponding data from the overshoot trajectories. Again note that the exit conditions are nearly the same for both vehicles regardless of the boundary in question. Figure 5-1 is a plot of entry angle as a function of entry speed for both the undershoot and overshoot boundaries. Figure 5-2 shows the entry corridor width versus entry speed for the Apollo derived vehicle. The trends in the boundary plot of Figure 5-1 and the corridor width plot of Figure 5-2 correspond nicely to those shown previously for the Transhab/Ellipsled vehicle. However, there is a significant reduction in corridor width for the Apollo derived vehicle, especially at higher entry speeds. The entry corridor width drops to 0.7 degrees at an entry speed of 14 0 km/s At an entry speed of 14.5 km/s, the entry corridor width is only 0.6 degrees. Such a small corridor may be inadequate for the guidance system to safely navigate the vehicle. Therefore, the Apollo derived vehicle may not be suitable if entry speeds in excess of 14.0 km/s are expected

Finally, note the large exit inclinations shown for the undershoot trajectories in Table 5-1. The inclination change problems that were discussed for the Transhab/Ellipsled vehicle are also common to the Apollo derived vehicle The inclination change should be able to be minimized using the same procedure that was described for use with the Transhab/Ellipsled vehicle.

Table 5-1. Undershoot Exit Conditions for the Apollo Derived Vehicle

Entry Speed	Undershoot Angle	Troll	Apoapse Altitude	Periapse Altitude	Period	Inclination	G_{max}	T_{gmax}	Time to 407 km
[km/s]	[deg]	[sec]	[km]	[km]	[min]	[deg]	[g's]	[sec]	[sec]
12.5	-6 53467430	62 8687	421 01	111 49	89 6181	1 69123	4 99999	71.5	2850 62
13.0	-6 58959643	57 1758	418 72	111 65	89.5965	1 67414	4.99999	68 5	2951 07
13 5	-6 62949645	51 9744	419 12	111 63	89 6000	1.62825	4 99999	66 5	2953 23
14.0	-6 65461878	47 0996	417 72	111.71	89 5869	1 55221	5 00000	65 5	3064 76
14 5	-6 66401603	42 3738	418 35	111.68	89 593	1.44145	5.00101	64 5	3016 91

Table 5-2. Overshoot Exit Conditions for the Apollo Derived Vehicle

Entry Speed	Overshoot Angle	Troll	Apoapse Altitude	Periapse Altitude	Period	Inclination	G_{max}	T_{gmax}	Time to 407 km
[km/s]	[deg]	[sec]	[km]	[km]	[min]	[deg]	[g's]	[sec]	[sec]
12.5	-5 54174834	N/A	419 918	111 609	89 608	0	2 51390	113 0	2953.80
13 0	-5 69689415	N/A	419 762	111.615	89 607	0	2.87960	106 5	2964.88
13.5	-5 83253056	N/A	419 896	111 606	89 608	0	3 26110	101 5	2966.20
14 0	-5 95193446	N/A	419 834	111 609	89 607	0	3 65830	96 5	2973 23
14 5	-6 05769240	N/A	419 934	111 603	89 608	0	4 07096	92 0	2974 76

93
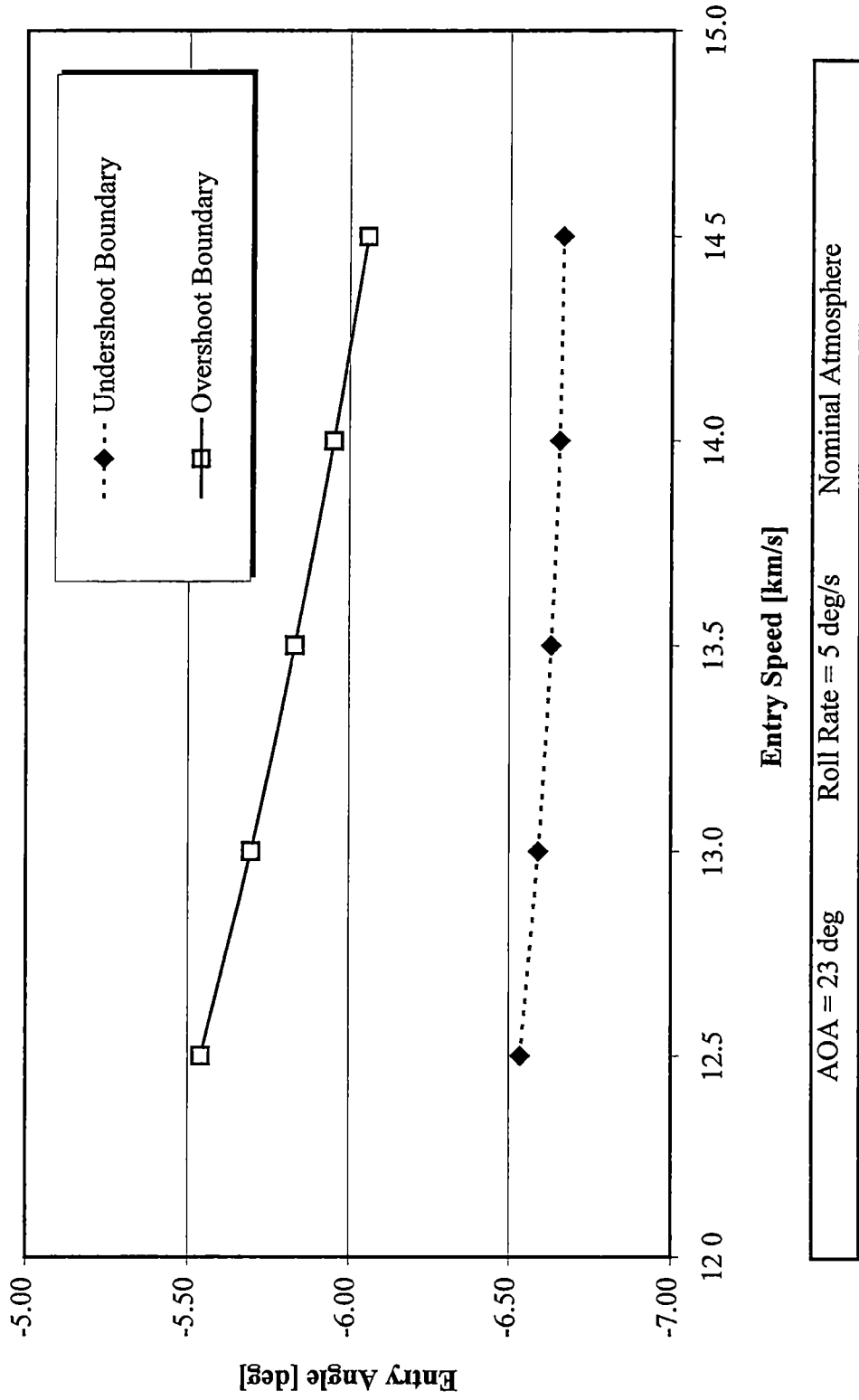
Figure 5-1. Undershoot and Overshoot Boundaries for the Apollo Derived Vehicle
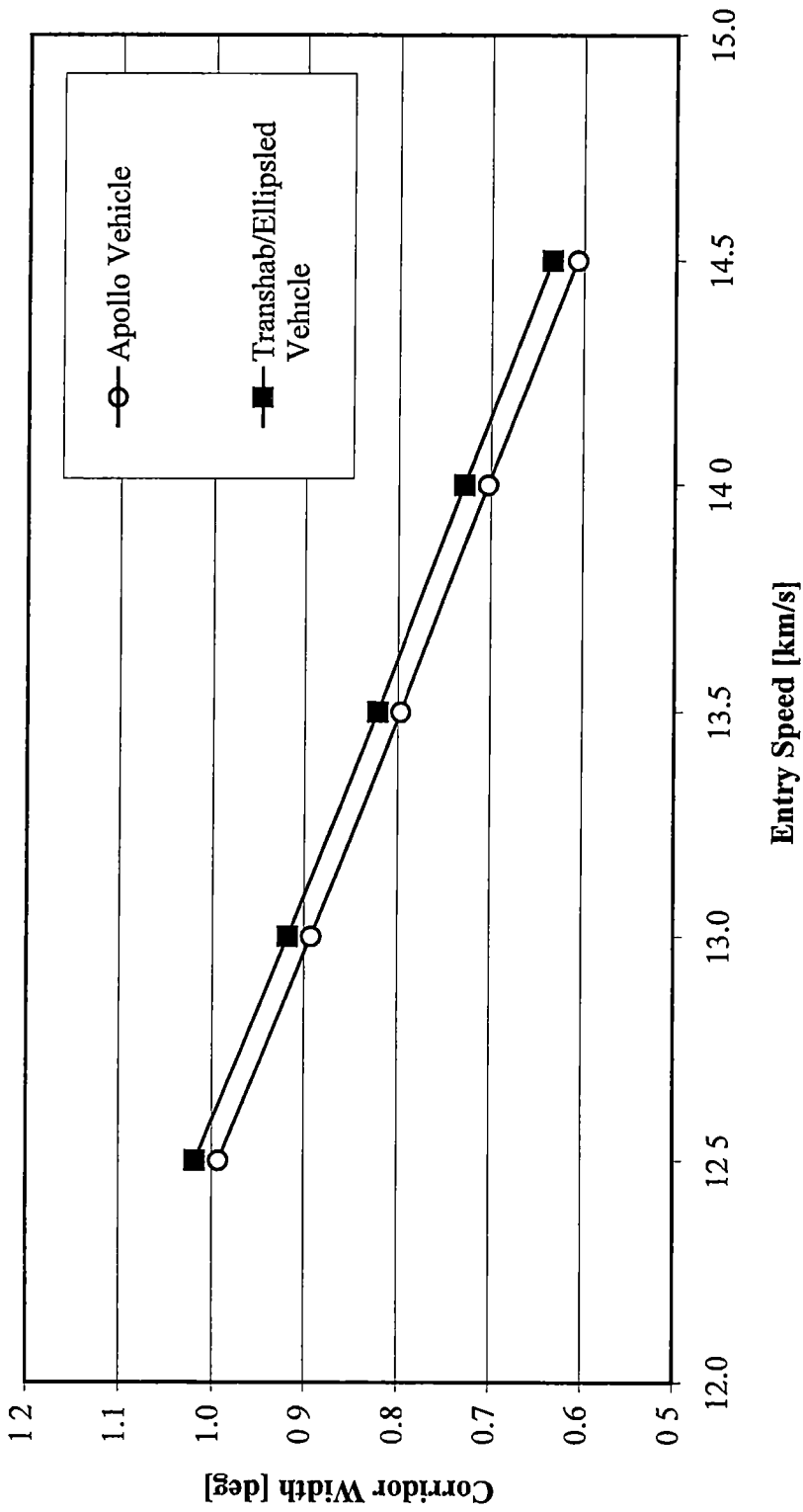
Figure 5-2. Entry Corridor Width for the Apollo Derived Vehicle

Chapter 6

Conclusions and Recommendations

Section 6-1.   Conclusions

After a study of several aspects of the Earth return aerocapture, some brief summarizing comments and conclusions can be made. First, it appears that the Transhab/Ellipsled vehicle has adequate L/D and control to possess a corridor width within the 0.5 - 0.7 degree standard for trajectories with entry speeds ranging from 12.5 to 14.5 km/s using a nominal atmospheric density profile.

Secondly, the simple atmospheric dispersions considered in this study did not seem to affect the corridor width significantly. However, a 30% uncertainty in atmospheric density would cause the corridor to shrink by approximately 0.25 degrees This reduction causes the corridor width to drop below 0.5 degrees somewhere between entry speeds of 13.5 km/s and 14.0 km/s.

Next, a deceleration limit of 3.5-g instead of 5-g causes the entry corridor to close at the higher speeds. Therefore, if a 3.5-g deceleration limit was imposed for the Earth return, the entry speed of the vehicle would have to be limited to approximately 13.5 km/s.

The ballistic coefficient analyses completed for this research shows that although the entry corridor width is not significantly affected by ballistic coefficient, the values of the entry angles for the corridor boundaries are in fact changed when the ballistic coefficient is altered. The entry angle will have some effect on heating rate and integrated heat loads and this needs further study.

The Apollo comparison study showed that the Transhab/Ellipsled has a wider entry corridor over the range of entry speeds considered. This is due primarily to the slightly greater L/D of the Transhab/Ellipsled when compared to the Apollo derived capsule. Therefore, from a purely aerodynamic point of view, the Transhab/Ellipsled vehicle appears to be better suited for the aerocapture procedure than the Apollo competitor.

A preliminary heating rate analysis showed that the dominant form of atmospheric heating is radiative heating and accounts for 75% of the peak stagnation point heating rate. Convective heating, as calculated with the Chapman heating equation, contributes 25% to the total peak heating rate. The total stagnation point heating rates range from 280 W/cm^2 to 1124 W/cm^2 which indicates that the TPS for the Transhab/Ellipsled should be of the ablator type. The integrated heat loads were calculated to be in the range of 37,000 to 85,000 J/cm^2, indicating that a significant amount of TPS will be needed to withstand the extreme heating conditions of the Earth return.

Finally, studies focusing on the circularization and inclination minimization indicate that the ΔV needed to circularize the orbit is made up almost entirely of the velocity increment required to raise the periapse (approximately 85 m/s). In contrast, the

velocity increment needed to correct the apoapse is only on the order of 5 m/s. The ΔV needed to correct the inclination change for the undershoot trajectories is approximately 200 - 235 m/s depending on the entry speed in question. The total post-aerocapture ΔV, which includes the velocity increments needed to both circularize the orbit and correct the inclination, was estimated to be about 325 m/s. A ΔV of 325 m/s translates into a total propellant requirement of 2200 kg if an I_{sp} of 370 sec is assumed. Further studies of the post-aerocapture ΔV showed that savings of around 185 m/s could be realized with some simple changes to the bank angle modulation scheme and following a mid-corridor trajectory.

Section 6-2.   Recommendations for Future Work

The major driving factor for Mars missions is the overall mission mass needed to be placed into Earth orbit for departure. This is also known as the initial mass in low Earth orbit (IMLEO). To reduce IMLEO, several approaches should be made to obtain mass savings. First, further studies should refine the total heat load calculations to determine the TPS thickness needed to protect the vehicle during atmospheric entry. These studies should include refinement in the radiative heating calculations and studies for turbulent convection heating rates as well as an evaluation of centerline heating rates. Stagnation temperatures should also be determined to aid in TPS selection and sizing.

The largest mass savings could potentially come from reductions in the required propellant. Therefore, additional studies are needed to try to reduce the inclination change using aerodynamic methods. Studies of Mars arrival aerocaptures have shown that the

inclination change can be reduced to 0.1 degrees or less [7]. An evaluation of the propellant requirements for roll maneuvers will also be needed. In addition, propellant savings might be realized by raising the periapse altitude during the aerocapture procedure. The final goal of such analyses should be to reduce the overall post-aerocapture ΔV, thereby minimizing the propellant requirements, and subsequently mission cost.

Further studies must be conducted on the effects of atmospheric perturbations such as horizontal density waves, winds, and other phenomena. Improvement should also be made in aerodynamic modeling. All of the simulations completed for this research used a continuum model of the atmosphere. However, at high altitudes the atmosphere follows the "free molecular" model more closely. In between the continuum and free molecular regions is a transition region. The Knudsen number determines where the transition and free-molecular flow regimes are located. Figure 6-1 shows the continuum, transition, and free-molecular regimes by plotting Knudsen number versus altitude. Both the free molecular region and transition region of the upper atmosphere might have significant effects on the vehicle aerodynamics and the ability of the vehicle to target the desired orbit. Therefore, some work should first be done to develop a "fairing" equation to link the continuum regime and the free molecular regime. Then, an analysis of the vehicle aerodynamics in the free molecular and transition regions should be completed, and trajectories should be calculated using this updated aerodynamic data

The next logical step would be development of a guidance algorithm to insure the vehicle can safely navigate the entry corridor given any combination of the possible
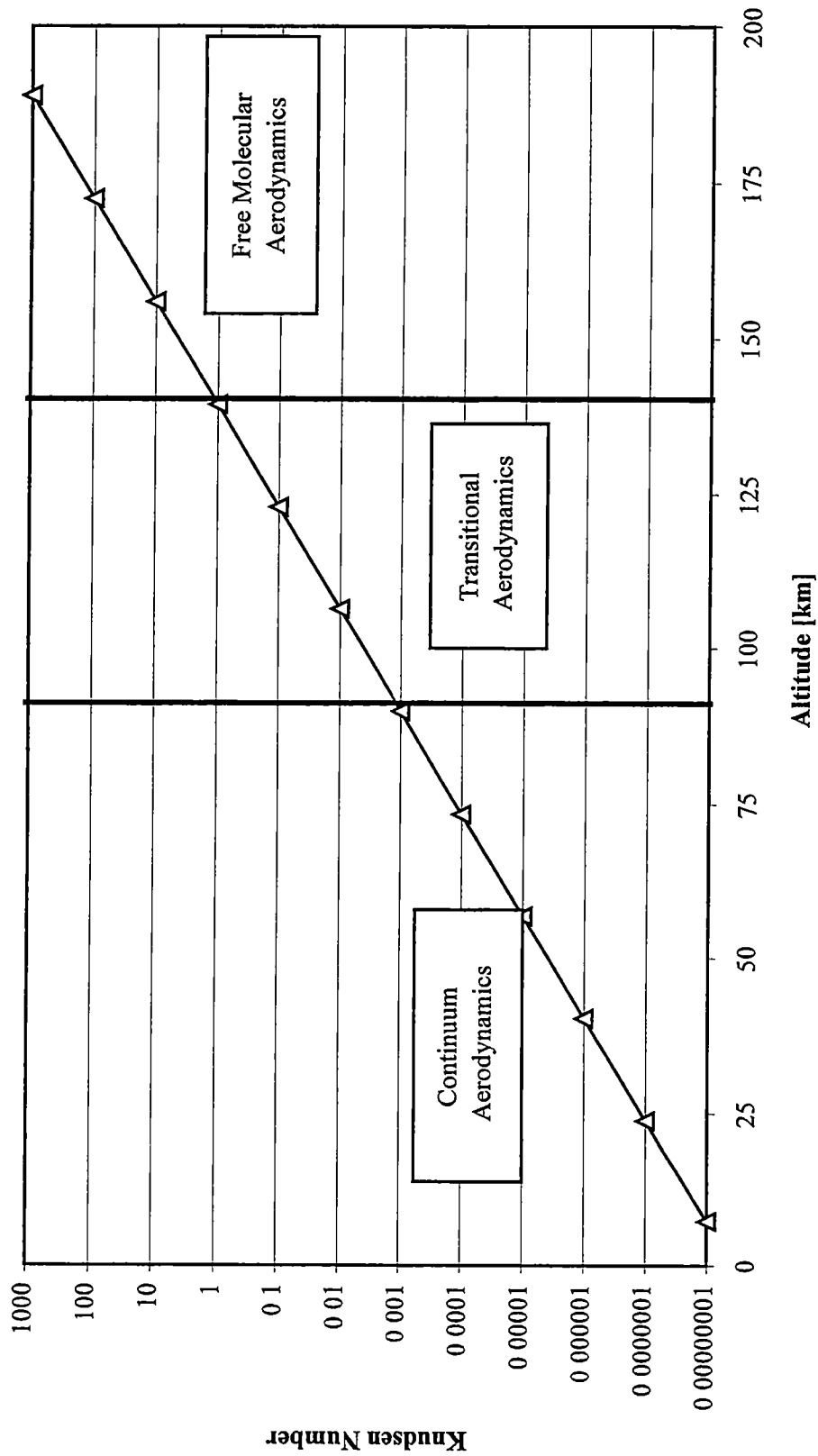
Figure 6-1. Flow Regimes of Earth's Atmosphere as Determined by the Knudsen Number

atmospheric or aerodynamic uncertainties. The guidance algorithm could implement a blended control system like that developed by Jits & Walberg at North Carolina State University [7].

Future studies should also refine the post-aerocapture ΔV and propellant calculations for all three engine types (I_{sp} values) and make a recommendation of which engine is best suited for the mission. These recommendations should be based on minimizing the post-aerocapture ΔV and reducing overall mission mass Attempts should be made to minimize the inclination (to within around 0.1 degrees) and raise the periapse using bank angle modulations An examination of propellant needed by the thrusters for the bank angle modulations is also of importance.

Other work in the distant future may involve the analysis of target orbit selection, rendezvous with the International Space Station, alternate vehicle designs, and direct entry scenarios

List of References

List of References

[1] Gladman, Brett, Joseph A. Burns, Martin Duncan, Pascal Lee, and Harold F Levison, "The Exchange of Impact Ejecta Between Terrestrial Planets," *Science*, Vol. 271, March 8, 1996, pp 1387-1392.

[2] Braun, R.D., D.A. Spencer, P.H. Kallemeyn, R.M Vaughan, "Mars Pathfinder Atmospheric Entry Navigation Operations," AIAA 97-3663, GNC, AFM, and MST Conference and Exhibit, New Orleans, LA., August 11-13, 1997.

[3] Hoffman, Stephen J., and David I. Kaplan (editors), "Human Exploration of Mars: The Reference Mission of the NASA Mars Exploration Study Team," NASA Special Publication 6107, Houston, Texas, March, 1997.

[4] Clark, Benton, Scott Geels, Brian Sutter, and Rohan Zaveri, "Advanced Technologies for Nuclear Propulsion," Martin Marietta, Denver, July 1991.

[5] Lyne, James Evans, and Robert D. Braun, "Flexible Strategies for Manned Mars Missions Using Aerobraking and Nuclear Thermal Propulsion," *The Journal of Astronautical Sciences*, Vol. 41, No 3, July-September, 1993, pp. 339-347

[6] Arnold, Jim, and Paul Wercinski, "Aeroassist Summer/Fall Study," Integrated Mars Exploration Mission Team Meeting, Kennedy Space Center, November 1997.

[7] Jits, R. and G Walberg, "A Blended Two-Axis Control Scheme for Use in the Aerocapture of Vehicles at Mars," Graduate Seminar, University of Tennessee, Knoxville, TN, December 2, 1999

[8]   Lyne, J. Evans, M.E Tauber, and Robert D. Braun, "Parametric Study of Manned Aerocapture Part I Earth Return from Mars," *Journal of Spacecraft and Rockets*, Vol. 29, No. 6, November-December, 1992, pp. 808-813.

[9]   Wercinski, P.F., and J.E. Lyne, "Mars Aerocapture: Extension and Refinement," Journal of Spacecraft and Rockets, Vol. 31, No. 4, March, 1993, pp.703-705.

[10]   Lyne, James Evans, "The Effect of Parking Orbit Selection on Manned Aerocapture at Mars," AAS/AIAA Spaceflight Mechanics Meeting, Colorado Springs, CO, February 24-26, 1992.

[11]   Braun, Robert D., Richard W. Powell, and J. Evans Lyne, "Earth Aerobraking Strategies for Manned Return from Mars," *Journal of Spacecraft and Rockets*, Vol 29, No. 3, May-June, 1992, pp. 297-304.

[12]   Rasky, D.J., H.K. Tran, and D.B. Leiser, "Thermal Protection Systems," *Launchspace*, Vol. 3, No. 3, June/July, 1998, pp. 49-54

[13]   Petro, A., "Transhab Vehicle Ellipsled Configuration," taken from a compilation of vehicle information provided by NASA Langley Research Center, November 16, 1997.

[14]   Graves, Claude A., and Jon C. Harpold, "Re-Entry Targeting Philosophy and Flight Results from Apollo 10 and 11," AIAA Paper No. 70-28, AIAA 8th Aerospace Sciences Meeting, New York, January 19-21, 1970.

[15]   Powell, R.W., S.A. Striepe, P.N. Desai, and R D. Braun, "Program to Optimize Simulated Trajectories (POST) Utilization Manual," NASA Langley Research Center, Hampton, VA, September 1996.

[16] Brauer, G.L., D E. Cornick, D.W. Olson, F.M. Peterson, and R Stevenson, "Program to Optimize Simulated Trajectories (POST) Formulation Manual," Martin Marietta, Denver, CO, September 1990.

[17] Wilcockson, W H., "OTV Aeroassist with Low L/D," *Acta Astronautica*, Vol. 17, No. 3, 1988, pp.277-301.

[18] Powell, Richard W., and Robert D. Braun, "Six-Degree-of-Freedom Guidance and Control Analysis of Mars Aerocapture," *Journal of Guidance, Control, and Dynamics*, Vol. 16, No. 6, November-December 1993, pp. 1038-1044.

[19] Anderson, John D., Jr., *Hypersonic and High Temperature Gas Dynamics*. McGraw-Hill, New York, 1989.

[20] Sutton, Kenneth, and Lin C. Hartung, "Equilibrium Radiative Heating Tables for Earth Entry," NASA Technical Memorandum 102652, NASA Langley Research Center, Hampton, VA, May 1990.

[21] Bate, Roger R., Donald D. Mueller, and Jerry E. White, *Fundamental of Astrodynamics*. Dover Publications, New York, 1971.

[22] Wiesel, William E , *Spaceflight Dynamics* McGraw-Hill, New York, 1989.

Appendix

Input Decks

The following pages contain samples of the input decks used in some of the POST simulations completed during this research. It is important to keep in mind that these are only samples and may contain program flags or variables that were not actually used in any simulation. Anyone wishing to implement these input decks in future simulations should be familiar with POST and the input deck structure. The user should carefully check over the input decks and modify them to fit their own needs. The input decks contain comments next to most of the program flags and variables to aid the user in understanding the input deck structure. However, it is important that the user verifies (using the POST user's manual) the various flags and options. The user should not rely on the comments to fully explain what each variable means or that the program options are set correctly in the sample input decks for any particular simulation.

The following is an example of the POST input used to determine the undershoot boundaries. ("c" or "/" indicates comments that POST does not actually use)

```
cccccccccccccccccccccccccccccc
c       Mars Return Mission     c
c       Undershoot Boundary     c
c           Donny Muth          c
c            Spring 99          c
cccccccccccccccccccccccccccccccc
l$search
 srchm  = 4,                    / projected gradient targeting
 ioflag = 3,                    / SI units
 ipro   = 1,
 maxitr = 20,                   / set maximum # of iterations
 irscl  = 3,
 isens  = 1,
c
c   Optimization Variable
c
 opt    = -1,                   / minimize optimization variable
 optvar = 'gammai',             / optimization variable name
 optph  = 1,                    / phase at which to optimize variable
c
c   Constraint Variables
c
 ndepv  = 2,                    / the # of dependent variables (constraints)
c
 depvr(1) = 'xmax1',            / 1st constraint name
 depph(1) =  100,               / phase at which to satisfy 1st constraint
 depval(1) = 5.0,               / desired value of 1st constraint
 deptl(1) = 0.02,               / tolerance (+/-) on 1st constraint value
 idepvr(1) = 1,                 / 1=upper bound, 0=equality, -1=lower bound constraint
c
 depvr(2) = 'malta',
 depph(2) = 100,
 depval(2) = 407.0,
 deptl(2) = 15.0,
 idepvr(2) = 1,
c
c   Control Variables
c
 nindv  = 2,                            / # of independent variables (controls)
c
```

```
indvr = 'gammai','critr',              / names of controls
indph  = 1,50,                         / phases at which controls occur
u = -6.444471019983,49.5698929957,     / initial guesses for controls
pert = 1.0E-3,1.0E-3,                  / perturbations for targeting routine
c
c
$
l$gendat
    title='Earth Return from Manned Mars Mission',
    prnt(1)= 'time','veli','gdalt','asmg','gammai','dens',    / variables to print in output
             'bnkang','banki','energy','cd','cl','malta',
             'maltp','xmax1','dynp','period','alpha',
             'beta','dragw','pstop',
    event=1,                           / current event number
    fesn=100,                          / final event number
    npc(1)=3,                          / Keplerian conic calc flag
    npc(2)=1,                          / Runge Kutta integration
    dt=1.0,                            / integration step size
    pinc=20.,                          / print interval
    prnca=1,                           / ascii plotting interval
    prnc=1,                            / binary plotting interval
    monx(1) = 'asmg',                  / monitor g-load maximum
c
c state vector
c
    npc(3)=2,                          / velocity spherical coordinates
c   gammai=-6.058,                     / initial flight path angle
    azveli=90.0,                       / inertial azimuth angle
    veli=13500.0,                      / inertial velocity
    npc(4)=2,                          / position spherical coordinates
    gdalt=121900.0,                    / initial geodetic altitude
    long=0.00,                         / initial longitude
    gclat=0.00,                        / initial geocentric latitude
    npc(12)=1,                         / calculate downrange, crossrange
c
c atmospheric parameters
c
    npc(5)=5,                          / 1976 US stand atm model
    npc(8)=3,                          / aero coefficient flag
c
c gravity model
c
    npc(16)=0,                         / oblate planet with harmonic
values
        j2 = 1.0826271e-03,
        j3 = -2.5358868e-06,
```

```
        j4 = -1.6246180e-06,
        j5 = -2.2698599e-07,
        j6 = 5.4518572e-07,
        j7 = -3.6319255e-07,
        j8 = -2.0772554e-07,
c
    omega = 7.29212e-05,                    / rotation rate (rad/s)
    mu = 3.986009e+14,                      / gravitational constant (m^3/s^2)
    re = 6378165.8568,                      / equatorial radius (m)
    rp = 6356783.832,                       / polar radius  (m)
c
c vehicle geometry parameters
c
    wgtsg=250108.0,                         / weight (N) =mass (kg)*Earthg (m/s^2)
    sref=84.348528,                         / reference area (m^2)
    rn=6.7,                                 / nose radius (m)
    lref=16.79448,                          / reference length (m)
c
c guidance initialization
c
    iguid(1)=0,                             / aero angles  alpha, beta, bank
    iguid(2)=0,                             / same steering opt all angles
    iguid(3)=0,                             / const poly term = input value
    alppc(1)=45.0,                          / initial alpha (constant poly term)
    bnkpc(1)=0 0,                           / initial bank  (constant poly term)
c
 $
l$tblmlt
 $
l$tab
 table='denkt',0,1.0,                       / density multiplier table
 $
l$tab table='cdt',1,'mach',8,1,1,1,         / Cd vs. Mach # table
    2.00, 1.5760,
    3.00, 1.5576,
    5 00, 1.5128,
   10.00, 1.4676,
   15.00, 1.4623,
   24.00, 1 4445,
   30.00, 1.4445,
   35.00, 1.4445,
 $end
 $
l$tab table='clt',1,'mach',8,1,1,1,         / Cl vs  Mach # table
    2 00, 0 6899,
    3 00, 0.6317,
```

```
   5 00, 0.5658,
  10.00, 0.5476,
  15.00, 0.5493,
  24.00, 0.5636,
  30.00, 0.5636,
  35.00, 0.5636,
 endphs=1,
 $
l$gendat                                    / new event
 event=50,critr='tdurp',                    / event #, criterion variable
 bnkpc(2)=5.0,                              / control (roll rate)
 endphs=1,                                   / end event
 $
l$gendat
 event=75,critr='bnkang',value=180.0,
 bnkpc(1)=180.0,
 bnkpc(2)=0.0,
 endphs=1,
 $
l$gendat                                    / final event
 event=100,critr='gdalt',value=407000.00,   /  event #, criterion variable, value
 endphs=1,                                   / end event
 endprb=1,                                   / end problem
 endjob=1,                                   / end job
 $
```

111

The following is an input deck set up so that the user must find the overshoot boundary "manually". That is to say, the user must (by hand) alter the entry angle until the shallowest angle that allows the orbit to be targeted is found. ("c" or "/" denote commmments that POST does not actually use)

```
ccccccccccccccccccccccccccccc
c       Mars Return Mission    c
c         Overshoot Boundary    c
c              Donny Muth        c
c                Spring 99       c
ccccccccccccccccccccccccccccccc
l$search
  srchm  = 0,                / no targeting
  ioflag = 3,                / SI units
$
l$gendat
    title='Earth Return from Manned Mars Mission',
    prnt(1)= 'time','veli','gdalt','asmg','gammai',      / variables to print in output
            'dens','bnkang','energy','cd','cl',
            'period','malta','maltp','dynp',
            'xmax1','pstop',
    event=1,                    / current event number
    fesn=100,                   / final event number
    npc(1)=3,                   / Keplerian conic calc flag
    npc(2)=1,                   / Runge Kutta integration
    dt=1 0,                     / integration step size
    pinc=1,                     / print interval
    prnca=1,                    / ascii plotting interval
    prnc=1,                     / binary plotting interval
    monx(1) = 'asmg',           / monitor maximum g-load
c
c state vector
c
    npc(3)=2,                       / velocity spherical coordinates
    azveli=90.0,                    / inertial azimuth angle
    gammai=-5.62254132491,          /inertial entry angle
    veli=13500 0,                   / inertial velocity
    npc(4)=2,                       / position spherical coordinates
    gdalt=121900 0,                 / initial geodetic altitude
    long=0.00,                      / initial longitude
    gdlat=0.00,                     / initial geodetic latitude
    npc(12)=1,                      / calculate downrange, crossrange
c
c atmospheric parameters
```

112

```
c
      npc(5)=5,                        / 1976 US stand atm model
      npc(8)=2,                        / aero coefficient flag
c
c gravity model
c
      npc(16)=0,                       / oblate planet with harmonic values
         j2 = 1.0826271e-03,
         j3 = -2.5358868e-06,
         j4 = -1.6246180e-06,
         j5 = -2.2698599e-07,
         j6 = 5.4518572e-07,
         j7 = -3.6319255e-07,
         j8 = -2.0772554e-07,
c
      omega = 7.29212e-05,             / rotation rate (rad/s)
      mu = 3.986009e+14,               / gravitational constant (m^3/s^2)
      re = 6378165.8568,               / equatorial radius (m)
      rp = 6356783.832,                / polar radius  (m)
c
c vehicle geometry parameters
c
      wgtsg = 250108.0,                / weight (N) = mass (kg) *Earthg (m/s^2)
      sref  = 84.348528,               / reference area (m^2)
      rn = 6.7,                        / nose radius (m)
      lref = 16.79448,                 / reference length (m)
c
c guidance initialization
c
      iguid(1) =  0,                   / aero angles: alpha, beta, bank
      iguid(2) =  0,                   / same steering opt all angles
      iguid(3) =  1,                   / const poly term = input value
      alppc(1) =  45.0,                / initial alpha
      bnkpc(1) =  180.0,               / initial bank
c
      $
l$tblmlt  $
l$tab
 table='denkt',0,1.0,$                 / density multiplier table
      $
l$tab table='cdt',1,'mach',8,1,1,1,   / Cd vs. Mach # table
      2.00, 1.5760,
      3.00, 1.5576,
      5.00, 1.5128,
      10.00, 1.4676,
      15.00, 1.4623,
```

```
    24.00, 1.4445,
    30.00, 1.4445,
    35.00, 1 4445,
  $
l$tab table='clt',1,'mach',8,1,1,1,          / Cl vs. Mach # table
    2.00, 0.6899,
    3.00, 0.6317,
    5.00, 0.5658,
    10 00, 0.5476,
    15.00, 0.5493,
    24.00, 0.5636,
    30.00, 0.5636,
    35 00, 0.5636,
  endphs=1,
  $
l$gendat                                      / final event
  event=100,critr='gdalt',value=407000 00,    / event #, criterion variable, value
  endphs=1,endprb=1,endjob=1,                  / end event, problem, and job
  $
```

This is an example of the input deck used to find the overshoot boundary automatically using POST's targeting/optimization routine. ("c" or "/" denote comments that POST does not actually use)

```
ccccccccccccccccccccccccccccc
c      Mars Return Mission    c
c      Overshoot Boundary     c
c          Donny Muth         c
c           Spring 99         c
ccccccccccccccccccccccccccccc
l$search
 srchm   = 4,                 / Projected Gradient targeting
 ioflag  = 3,                 / SI units
 ipro    = 1,
 maxitr  = 20,                / maximum # of iterations
 irscl   = 3,
 isens   = 1,
c
c   Optimization Variable
c
 opt     = 1,                 / maximize optimization variable
 optvar  = 'gammai',          / variable to optimize
 optph   = 1,                 / phase at which to optimize variable
 wopt    = -0 1735,           / weight of the optimized variable (wopt=1/expected
value)
c
c   Constraint Variables
c
 ndepv   = 1,                 / # of constraints
c
 depvr(1) = 'malta',          / 1st constraint variable name
 depph(1) =  300,             / phase at which to satisfy 1st constraint
 depval(1) = 407.0,           / desired value of 1st constraint
 deptl(1) =  15.0,            / tolerance (+/-) on 1st constraint
 idepvr(1) = 1,               / upper bound constraint
c
c   Control Variables
c
 nindv   = 1,                 / # of controls
c
 indvr = 'gammai',            / names of controls
 indph = 1,                   /  phases at which controls occur
 u = -5.766047176749,         / initial guess for controls
 pert = 1.0E-12,              / perturbation sizes for targeting routine
```

```
c
c
 $
l$gendat
    title='Earth Return from Manned Mars Mission',
    prnt(1)= 'time','veli','gdalt','asmg','gammai',          / variables to print in output
             'dens','bnkang','banki','energy','cd',
             'cl','malta','maltp','xmax1','dynp',
             'period','alpha','beta','dragw','pstop',
c
    event=1,                    / current event number
    fesn=100,                   / final event number
    npc(1)=3,                   / Keplerian conic calc flag
    npc(2)=1,                   / Runge Kutta integration
    dt=1.0,                     / integration step size
    pinc=20.,                   / print interval
    prnca=1,                    / ascii plotting interval
    prnc=1,                     / binary plotting interval
    monx(1) = 'asmg',           / monitor maximum g-load
c
c state vector
c
    npc(3)=2,                    / velocity spherical coordinates
    azveli=90.0,                 / inertial azimuth angle
    veli=13500.0,                / inertial velocity
    npc(4)=2,                    / position spherical coordinates
    gdalt=121900 0,              / initial geodetic altitude
    long=0.00,                   / initial longitude
    gclat=0.00,                  / initial geocentric latitude
    npc(12)=1,                   / calculate downrange, crossrange
c
c atmospheric parameters
c
    npc(5)=5,                    / 1976 US stand atm model
    npc(8)=3,                    / aero coefficient flag
c
c gravity model
c
    npc(16)=0,                   / oblate planet with harmonic values
        j2 = 1.0826271e-03,
        j3 = -2.5358868e-06,
        j4 = -1.6246180e-06,
        j5 = -2.2698599e-07,
        j6 = 5 4518572e-07,
        j7 = -3.6319255e-07,
        j8 = -2.0772554e-07,
```

116

```
c
    omega = 7.29212e-05,          / rotation rate (rad/s)
    mu = 3.986009e+14,            / gravitational constant (m^3/s^2)
    re = 6378165.8568,            / equatorial radius (m)
    rp = 6356783.832,             / polar radius  (m)
c
c vehicle geometry parameters
c
    wgtsg=250108 0,               / weight(N) =mass(kg)*Earthg(m/s^2)
    sref=84.348528,               / reference area (m^2)
    m=6.7,                        / nose radius (m)
    lref=16.79448,                / reference length (m)
c
c guidance initialization
c
    iguid(1)=0,                   / aero angles: alpha, beta, bank
    iguid(2)=0,                   / same steering opt all angles
    iguid(3)=1,                   / const poly term = input value
    alppc(1)=45.0,                / initial alpha
    bnkpc(1)=180.0,               / initial bank
c
 $
l$tblmlt
 $
l$tab
  table='denkt',0,0.7,           /density multiplier table
 $
l$tab table='cdt',1,'mach',8,1,1,1,    / Cd vs. Mach # table
    2.00, 1 5760,
    3.00, 1.5576,
    5 00, 1.5128,
    10.00, 1.4676,
    15.00, 1.4623,
    24.00, 1 4445,
    30.00, 1.4445,
    35.00, 1.4445,
 $end
 $
l$tab table='clt',1,'mach',8,1,1,1,        / Cl vs. Mach # table
    2.00, 0 6899,
    3.00, 0 6317,
    5.00, 0.5658,
    10.00, 0 5476,
    15.00, 0 5493,
    24.00, 0.5636,
    30.00, 0.5636,
```

```
   35.00, 0.5636,
endphs=1,
$
l$gendat                              / new event (final event)
event=100,critr='gdalt',value=407000.00,   / event #, criterion variable, value
endphs=1,                             / end event
endprb=1,                             / end problem
endjob=1,                              / end job
                                    $
```

Vita

Wiliam Donald (Donny) Muth was born in Lake City, Florida on May 20, 1975. He spent the first five years of his life growing up on a racing greyhound farm in Lake City. Then, his family moved their greyhound operations to Orange Park, Florida where he attended the first through third grades. After that, the family's business headquarters was relocated to Memphis, Tennessee. Donny attended Auburndale private school for fourth through sixth grades. In seventh grade he once again changed schools. Finally, he graduated from Houston High School in Germantown, Tennessee in May of 1993. During the early years of his education, Donny showed an aptitude for science, history, and art. Upon graduating from high school, he had decided to enter college in one of four fields: Aerospace Engineering, Genetic Engineering, Chemical Engineering, or Art. He chose Aerospace Engineering because he felt that was the field where he could make the biggest impact on society In August of 1993, he began his undergraduate studies at the University of Tennessee in Knoxville, Tennessee. He graduated Summa Cum Laude and received his Bachelor of Science with a major in Aerospace Engineering, and a minor in Business Administration, from the University of Tennessee in December of 1997. He immediately decided to remain at the University of Tennessee to pursue a Master of Science degree and do Mars mission research under Dr Evans Lyne. The acceptance of this thesis will complete the graduation requirements and he will receive his Master of Science in Aerospace Engineering in August of 2000. After finishing the thesis requirements, Donny will begin work with Military Technology, Inc. in Huntsville, Alabama as a Junior Engineer.